MODELING OF AGITATED BUNSEN REACTOR FOR IODINE SULFUR THERMOCHEMICAL PROCESS FOR PRODUCTION OF HYDROGEN WITH EXPERIMENTAL VALIDATION

By

A SHRINIWAS RAO

ENGG01200904025

Bhabha Atomic Research Centre,
Mumbai – 400085
INDIA

A thesis submitted to the
Board of Studies in Engineering Sciences
In partial fulfillment of requirements For the Degree of

DOCTOR OF PHILOSOPHY
of
HOMI BHABHA NATIONAL INSTITUTE

August, 2016

HOMI BHABHA NATIONAL INSTITUTE

Recommendations of the Viva Voce Board

As members of the Viva Voce Board, we certify that we have read the dissertation prepared by **A Shriniwas Rao** entitled **“Modeling of Agitated Bunsen Reactor for Iodine Sulfur Thermochemical Process for production of hydrogen with experimental validation”** and recommend that it may be accepted as fulfilling the dissertation requirement for the award of Degree of Doctor of Philosophy.

Chairperson: Prof.(Smt) S. B. Roy **Date:**

Guide & Convenor: Prof. P. K. Tewari **Date:**

Examiner: Prof A. Mani **Date:**

Member 1: Prof. D. Srivastava **Date:**

Member 2: Prof. (Smt) Sulekha Mukhopadhyay **Date:**

Member 3: Prof. R.Kapoor **Date:**

Final approval and acceptance of this dissertation is contingent upon the candidate’s submission of the final copies of the dissertation to HBNI.

I hereby certify that I have read this dissertation prepared under my direction and recommend that it may be accepted as fulfilling the dissertation requirement.

Date: 05/08/2016

Place: Mumbai **Guide:** Prof. P. K. Tewari

STATEMENT BY AUTHOR

This dissertation has been submitted in partial fulfillment of requirements for an advanced degree at Homi Bhabha National Institute (HBNI) and is deposited in the Library to be made available to borrowers under rules of the HBNI.

Brief quotations from this dissertation are allowable without special permission, provided that accurate acknowledgement of source is made. Requests for permission for extended quotation from or reproduction of this manuscript in whole or in part may be granted by the Competent Authority of HBNI when in his or her judgment the proposed use of the material is in the interests of scholarship. In all other instances, however, permission must be obtained from the author.

Date : 05/08/2016 A Shriniwas Rao

DECLARATION

I, hereby declare that the investigation presented in the thesis has been carried out by me. The work is original and has not been submitted earlier as a whole or in part for a degree/diploma at this or any other Institution/University.

Date : 05/08/2016 A Shriniwas Rao

Dedicated to
My

Parents
&
Parents-in-law

List of Publications from this Work

Journals

1. “Study of effect of high Pressures and elevated Temperatures on Bunsen reaction of Iodine-Sulfur thermo-chemical process” A Shriniwas Rao, S. Sujeesh, V. Nafees Ahmed, H Z Fani, P K Tewari, L M Gantayet, International Journal of Hydrogen Energy, 2015, 40 pp 5025-5033.
2. “Study of Bunsen reaction in Agitated reactor operating in counter current mode for Iodine-Sulfur thermo-chemical process” A Shriniwas Rao, S Sujeesh, V Nafees Ahmed, H Z Fani, A Sanyal, P K Tewari, L M Gantayet, International Journal of Nuclear Hydrogen Production and Applications, Vol. 3, No. 1, 2016, pp 12-31.
3. “Effect of agitation speed & fluid velocity on heat transfer performance in agitated Bunsen Reactor of Iodine-Sulfur thermo chemical cycle” A Shriniwas Rao, S Sujeesh, A Sanyal, P K Tewari, L M Gantayet, International Journal of Nuclear Hydrogen Production and Applications, Vol. 3, No. 1, 2016, pp 65-79.

Date : 05/08/2016 A Shriniwas Rao

ACKNOWLEDGEMENTS

This thesis would not have been accomplished without the support and encouragement of numerous people including my well wishers, my friends and colleagues who contributed in many ways to the successful completion of this thesis.

First and Foremost, I would like to express my sincere gratitude to my research guide **Dr. P. K. Tewari** for the continuous support, patience, motivation, and enthusiasm. His encouragement, immense knowledge and experience helped me in overcoming all the hurdles not only during the course of my Ph.D but in all spheres of life. I would also thank **Dr. L. M. Gantayet** who gave his guidance and shared his deep knowledge of various subjects. I owe my deep sense of gratitude for his unimaginable support and inspiration. I could not have imagined having a better mentor for my Ph.D. study.

Besides my advisors, I would like to thank members of the doctoral committee; for their encouragement, thoughtful ideas and critical evaluation during the course of this work. My sincere thanks are due to ***Shri S Sujeesh, Shri Nafees Ahmed and Shri Hunaid Fani*** for all their precious help, stimulating discussions and cooperation.

I would like to thank my colleagues ***Shri S. B. Menon, Shri Wankhede, Shri Chavda, Shri Paulose, Smt Indira, Shri Kanchan Garai,*** with ***Shri A. Sanyal, Head ChTD*** in particular, ***Shri S. Sarkar, AD, ChTG*** for their help, encouragement and support during the course of the research work. I thank ***Kaushal, Vishal, Riyaz, Vamsi Bhusan, Sandeep Singh, Sandeep Sinku, Anant, Shashikant, Kamaruzzaman, Dattu Rao, Chavan, Parera, Dashrath, Ajit, Neelesh*** and ***all members of ChTD,*** for their help and co-operation during experiments.

I am blessed to have friends who are constant source of laughter, joy and support. I would like to thank all my friends ***Soumitra, Aishwarya, Mahesh, Jayashree, P. Nimbulkar*** who always stood by me and lend constant encouragement and support. I

would also like to thank all ***my training school batch mates*** for their warm friendship which helped in sailing through all hardships.

I would like to acknowledge all the ***teachers***; I learnt from since my childhood, I would not have been here without their guidance, blessings and support.

Finally, I would like to acknowledge the people who mean the world to me, ***my family***. I would like to thank ***my parents Shri A S Satyanarayana and Smt A S Lakshmi*** for their unconditional love, support, faith, encouragement and confidence in me. They have been my driving force and inspiration in all pursuits of life. I owe all my accomplishments to them. My ***brothers (Raman and Vasu)*** and ***sister (Neeraja)*** have been constant source of love and confidence and their belief helped in overcoming all hurdles of my life. I would like to thank my ***parents in law Shri P Gopalam and Smt P Jayanthi*** for their unconditional support and faith. I would also like to thank my ***sisters in law (Manju and Aruna)*** and ***brother in law (Srinivas)*** for constant encouragement and support. I run short of words in expressing my gratitude towards my **wife** ***Nagavani*** who always stood by me and encouraged me up at every step of life. She has faith in me and my intellect which helped me to keep things in perspective. She is everything for me, without her love and understanding I would not have been able to make it. I would like to express thanks to my ***daughters Ms Sayesha and Ms Saistuti*** who in their own way geared me up to reach the goal.

Lastly, I would like to thank everybody who was important in the successful realization of this thesis, as well as apologize that I could not mention everyone personally.

A Shriniwas Rao

List of Abbrevations

ABR	Agitated Busen Reactor
atm	atmosphere
BARC	Bhabha Atomic Research Center
CANDU	CANada Deuterium Uranium
CB&H	Carbon black & hydrogen process
CEA	Commissariat à l'énergie atomique
CSP	Concentrated Solar Power
CSTR	Continuous stirred tank reactor
Cu–Cl	Copper–chlorine cycle
DLR	German Aerospace Center
DOE	Department of Energy, USA
EIA	Energy Information Administration
g	Gauge
GA	General Atomics
GHG	Green house gas
GIF	Generation IV International Forum
G/L	Gas liquid interface
gps	Grams per second
HI	Hydriodic acid
HIx	Hydriodic acid with iodine
HIXΦ	Hydriodic acid phase
H_2O	Water
H_2SO_4	Sulfuric acid
HyS	Hybrid sulfur cycle
I_2	Iodine
IAEA	International Atomic Energy Agency
ID	Internal Diameter
IEA	International Energy Agency
I-S	Iodine Sulfur cycle

INERI	International Nuclear Energy Research Initiative
InP	Indium phosphide
IPCC	Intergovernmental Panel on Climate Change
Ipsos	Innovative, entrepreneurial, client-focused organization
JAEA	Japan Atomic Energy Agency
KOH	Potassium hydroxide
LLE	Liquid-liquid equilibrium
lpm	Litres per minute
M	Motor
MASCOT	Model Apparatus for the Study of Cyclic Operation in Tokyo
mlpm	Milli litre per minute
MOC	Material of construction
N_2	nitrogen
NaCl	Sodium chloride
NGCC	Natural gas combined cycle
no	Number
Nu	Nusselt number
OD	Outside Diameter
PEC	Photo electrochemical cell
PFR	Plug flow reactor
PLC	Programmable Logic Controler
PSDVB	Poly-styrene-*co*-divinylbenzene
PT	Pressure transmitter
PTFE	Polytetra fluoro ethylene
PV	Photo Voltaics
Re	Renolds number
RTD	Residence Time Distribution
REN21	Renewable Energy Policy Network for the 21st Century
RPM	Rotations/revolutions per minute
SA	Sulfuric acid
SAΦ	Sulfuric acid phase
SNL	Sandia National Laboratories
SCADA	Supervisory control and data acquisition
SO_2	Sulfur dioxide

SP	Sampling point
TE	Temperature element
Temp	Temperature
USA	United States of America
UT-3	University of Tokyo, Ca-Br-Fe cycle
VOC	Volatile organic compounds

CONTENTS

CHAPTER-I

CHAPTER-II

CHAPTER-III

CHAPTER-IV

CHAPTER-V

Heat transfer studies in agitated Bunsen reactor 104

CHAPTER-VI

Phase Separation studies in agitated Bunsen reactor 116

CHAPTER VII

Reaction and layer separation studies in agitated Bunsen reactor 128

CHAPTER VIII

CHAPTER IX

SYNOPSIS

In today's depleting energy scenario, hydrogen is perceived as future alternate energy carrier. When the source of hydrogen is renewable such as water, and process with no emission of green house gases, is established; it can become the large scale deployable practical method of producing hydrogen. Thermo-chemical process [1] accomplishes the splitting of water into hydrogen and oxygen. It is an efficient and environmentally cleaner way to produce hydrogen without use of fossil fuels. It is one of the potential processes for commercialization because of its capability to be coupled to a high temperature nuclear reactor [2] or by hybrid solutions including both.

Iodine-Sulfur (I-S) thermochemical process is one of such processes having the potential for commercialization. General Atomic (GA) company, USA was the first to start working on I-S process and was first described in the open literature by Russell [3] in the 1st World Hydrogen Energy Conference, March 1976. GA has worked on bench-scale unit [3], performed catalysis work for sulphuric acid decomposition and hydriodic acid decomposition [4].

The work on I-S process was started in Japan as early as 1978. I-S process is reviewed including experimental data obtained at JAERI on the chemistry of each reaction step, product separations and corrosion resistance of structural materials [5].

The French "Commissariat a` l'Energie Atomique" (CEA) has been involved in the I-S process in a research programme through theoretical and laboratory studies and through the development of a laboratory scale hydrogen production loop [6], which is currently performed within the framework of an international collaboration (I-NERI project with DOE) with two American partners: Sandia National Laboratories (SNL) and General Atomics.

Bunsen reaction

In Iodine-Sulfur (I-S) thermo-chemical cycle [7,8], water is decomposed via chemical reactions using intermediates I_2 and SO_2, which are recycled. In this process Bunsen reaction is the prime reaction [9] as shown below.

Bunsen reaction: $SO_2 + I_2 + 2H_2O \rightarrow 2HI + H_2SO_4$ 293K - 393K (1)

Bunsen reaction is an exothermic reaction producing two immiscible acid phases viz. sulfuric acid and hydriodic acid, at high iodine concentration [10]. The sulfuric acid decomposition step is an endothermic two stage reaction: first sulfuric acid dehydration to produce sulfur trioxide, then sulfur trioxide catalytic decomposition [11] to produce sulfur dioxide and oxygen. Hydrogen iodide is decomposed in vapour phase producing hydrogen [12], which is also an endothermic reaction.

Bunsen reaction is a gas-liquid reaction system. Reactants iodine, water and sulfur dioxide (SO_2) form products sulfuric acid and hydriodic acid [13]. Reaction stoichiometry is given by reaction (1). Bunsen reaction is fast in the range 293K - 393K. At higher temperature the reaction is reversible. However, in this temperature range conversion is not equilibrium limited, so complete conversion is possible. By operating at non-stoichiometric conditions and using a large excess of iodine and water, the conversion is greatly improved according to reaction (2). The excess iodine shifts Bunsen reaction equilibrium forward to produce more acids. Excess iodine also helps the two acids produced to spontaneously separate into two aqueous solutions. The phase separation occurs due to the formation of the poly-hydriodic acid [14]. Excess of water also causes the equilibrium to shift forward to produce more acids, but it also causes a substantial increase in the reaction enthalpy due to acid dilution. This modified Bunsen reaction is thermodynamically favorable.

$$9I_{2(l)} + SO_{2(g)} + 16H_2O_{(l)} = (H_2SO_4 + 4H_2O)_{(aq)} + (2HI + 10H_2O + 8I_2)_{(aq)} \qquad (2)$$

This is a heterogeneous (gas-liquid) reaction system, in which sulfur dioxide first dissolves in the reaction liquid (water) and then reacts with other reactants [15].

Bunsen reaction is crucial step in the Iodine-Sulfur cycle since the optimization of H_2O and I_2 excesses determines a good separation between the two acid solutions, and a favorable reaction rate for controlling hydrogen production rate, and a low energy consumption for separating and recycling H_2O and I_2 excesses. So far, most efforts have been focused mainly on the thermodynamic performance of the Bunsen section.

The thermodynamic and kinetics for Bunsen reaction have been studied using the SO_2/N_2 gas mixtures fed into the I_2/H_2O aqueous solution in a jacketed stirred reactor. A fundamental kinetic model is proposed to explain the kinetics of the Bunsen reaction, ignoring the effect of mass transfer and diffusion between SO_2 and reactant solution, and the dilution effect of H_2O.

The effects of operating parameters, including reaction temperature, I_2 and H_2O concentrations, and H_2SO_4/HI molar ratio, on the liquid-liquid equilibrium (LLE) phase separation characteristics were investigated. It was found that an increase in I_2 concentration and a decrease in H_2O concentration improved the LLE phase separation [16, 17].

An increase in the molar ratio of H_2SO_4/HI favoured the separation and resulted in a dehydration of the HIx phase [18].

The allowable bound of I_2 content for phase separation was widened with an increase in the reaction temperature [19, 20].

An optimal operating window of 4-6 mol excess iodine and 11-13 mol excess water within a temperature range of 330-350 K has been proposed by Lee et al. according to collating experimental data from literature as well as conducting their own experiments.

A thermodynamic model has been proposed to understand the chemo-physical behaviour of the Bunsen reaction system and the chemicals equilibrium in terms of iodine and sulfur species separation [21].

The addition of a precipitation agent has been proposed to separate the two acids [22]. Although a significant reduction in I_2 excess was obtained, large amounts of solid handling would be required in this process.

The use of solvents, such as TBP, PSDVB, toluene and ionic liquids in the Bunsen reaction was considered as a method to release HI from the reaction [23]. However, further solvents need to be investigated to find one that both has the ability to extract HI and is stable to hot HI to allow recovery.

In I-S process, side reactions from HI, H_2SO_4 and I_2 mixture solution were investigated experimentally in the operating temperature range [24].

Bunsen Reactor:

The reactants sulfur dioxide, water and iodine; can be added to the reactor either co-currently or counter-currently. In co-current reactor, chemicals are added to one end of the reactor and products are removed from other end. The product acids are separated in subsequent separation column. In counter-current reactor both reaction and acid separation take place in the same reactor. Reactants iodine and water are fed from the top; sulfur dioxide is fed from the bottom. The lighter product viz. sulfuric acid is removed from the top, while heavier product, hydriodic acid is removed from the bottom most part of the reactor.

There are different reactor alternative to carry out Bunsen reaction in continuous mode; for acid production and/or separation such as stirred tank reactor, packed tubular reactor (co-current & counter-current), electrochemical reactor etc.

The concept of a concurrent heat exchange Bunsen reactor was demonstrated by GA in 1981, and subsequently by JAERI in 2003.

GA constructed a staged counter-current flow reactor column to enrich 50% H_2SO_4 to 57% H_2SO_4 with liquid iodine as feed from top and 50% H_2SO_4 as bottom feed. Several experiments were run with this equipment; most were to establish flow control information. The apparatus was operated so that meaningful data with fully describable flow and stirring parameters were available.

Use of an electrochemical membrane cell for the Bunsen reaction has a large potential to reduce the excess I_2 and H_2O [25-28]. However, the significant cross-contamination of the two acids was still seen. There is a serious problem when scaling these electrochemical membrane cells to a plant size.

The Bunsen reactor is sized by CEA, as counter-current liquid-liquid contactor (extraction equipment) with mechanical stirring, as using different correlations described by Godfrey & Slater. An alternative flow sheet is currently being considered by CEA involving a counter-current multiphase reactor [29]. Aside from SO_2, the chemical system includes two solvents (excess water and excess iodine) and two solutes (H_2SO_4 and HI). Water and iodine being almost immiscible, allows the operation to be considered a reactive liquid-liquid extraction in which water is the solvent for H_2SO_4 and iodine the solvent for HI. In counter-current streams, circulating phases are never at chemical equilibrium, theoretically, resulting in a possible increase in reaction rate by modifying the reactants amounts (particularly SO_2).

Republic of Korea carried out Bunsen reaction using counter-current flow reactor [30, 31]. Ceramic packing material of Raschig ring was introduced in the reactor to avoid channelling of SO_2 gas. Solid I_2 was introduced from the top at intervals and gaseous SO_2 and water were fed continuously from the bottom. In the study composition variation of discharged at top and bottom are studied by varying SO_2 feed rate, temperature and I_2/H_2O ratio and it's concluded that the composition of each phase collected are similar irrespective of SO_2 flow rate and there is an increase in purity with increase in I_2/H_2O ratio.

Kinetic study in semi-batch reactor was carried out in BARC, India [32].

Design of tubular flow reactor with concurrent operation is discussed by Sandia National Laboratories, USA [33].

Motivation for this work: Information on Bunsen reaction and simultaneous phase separation in single equipment, thereby, integrating one unit process and one unit operation, is not available in literature. Study of such a kind of equipment for Bunsen reaction and phase separation on continuous operation mode, and modeling of the equipment, would be initial step towards realizing the I-S process on a large scale.

A new counter-current reactor concept has been proposed to implement the Bunsen reaction and phase separation. Agitated tubular Bunsen reactor (ABR), operating in counter-current mode, is one of the reactor alternatives to carry out Bunsen reaction in continuous mode. In this reactor, both, reaction as well as phase separation occurs in single equipment. Thus, process integration is the possibility by combining reaction as well as acids separation in single equipment. Also, it has the potential importance as Bunsen reactor in Iodine-Sulfur thermo-chemical cycle because of its improved heat and mass transfer characteristics. An attempt has been made, in this study, to model the reactor, accounting, all the controlling resistances of heterogeneous Bunsen reaction.

Chapter 1: In this chapter, the historical background of energy, energy perspective, energy production by developed, developing and other nations is presented. The nature of energy source such as primary viz. wind, water, solar, wood, coal, oil, nuclear and secondary viz. electricity, gas, for power plants is presented. According to energy reserves of source used and regeneration capacity grouping can be renewable and non-renewable. Fossil fuels, nuclear energy and different renewable energy are discussed. Hydrogen economy is proposed and supporters of it advocate hydrogen as potential fuel for the future. Hydrogen production by different processes such as biological, electrolysis of various types, photo electrochemical water splitting, thermo-chemical production and as by-product of other chemical processes is discussed. Thermochemical cycles such as iron oxide cycle, cerium oxide cycle, copper-chlorine cycle, hybrid sulfur cycle, UT-3 cycle and one of the most researched iodine-sulfur cycle is discussed.

Most of the research has been to study the kinetics of Bunsen reaction. Work has been presented on separation of hydriodic acid and sulfuric acid with excess iodine and also with other solvents as TBP etc. Bunsen reaction is studied in batch reactors under different conditions of sulfur dioxide flow, temperature, water content and iodine content. Different types of reactors such as batch and co-current reactors have been studied. Information on reactors used by General Atomics, USA; JAERI, Japan; Republic of Korea and CEA, France is presented.

To accomplish the objective, initially semi-batch Bunsen reaction experiments have been carried out. It was followed by counter-current Bunsen reaction experiments in agitated type Bunsen reactor. Prior to reaction experiments, to study the reactor flow pattern, Residence Time Distribution was studied. To carry out reaction at isothermal conditions, the data on heat transfer was generated. As phase separation of products is also critical, experiments on phase separation with available product solutions were conducted. Finally, counter-current Bunsen reaction experiments were carried out.

Chapter 2: In this chapter, Experimental techniques and methods are discussed. Semi-batch experiments at moderately high temperature and high pressure, in metallic reactor was planned. Accordingly, jacketed tantalum tube reactor with static mixers inside was fabricated and system was made ready. ABR in glass MOC, with agitator, baffles and flat blades of PTFE and provision for temperature measurement and nozzles for inlet and outlet streams was fabricated. The systems of feeding, scrubbing, cooling and agitation have been built with adequate safety. Analytical methods for different species of feed and product have been described.

Chapter 3: In this chapter, Reaction studies in semi-batch mode in static mixer reactor and modeling of the reactor are discussed. Experiments have been carried out with pure sulfur dioxide and mixture of SO_2 and nitrogen. The effect of pressure and temperature on reaction length for the given SO_2 flow is discussed.

Chapter 4: In this chapter, results of residence time distribution studies in agitated Bunsen reactor are presented. Axial dispersion has been calculated for different flows of water and different agitator speed. The range of agitator speed for minimal dispersion is understood.

Chapter 5: In this chapter, heat transfer studies in ABR with different flow rates of reactor fluid i.e. water, cooling fluid and agitator speed are presented. Modified heat transfer correlation for the reactor side/shell side, which accounts for both fluid flow as well as mixing, has been suggested which is applicable for the range of experimental conditions. The same is validated with the heat data of Bunsen reaction experiments.

Chapter 6: In this chapter, phase separation studies in ABR is presented. Bunsen reaction products mixture, phase separation behaviour was studied using a counter-current reactor at different flow rates and different agitation speeds. It was observed that the best phase separation is achieved when there is no agitation and as the agitation speed is increased the impurity levels increase and the inter-phase layer broadens for Bunsen reaction products mixture; the optimum agitation speed has been arrived at.

From the experiments, it can be concluded that higher agitation intensities lead to undesirable scenarios such as broadening of the inter-phase layer, cross contamination of the two phases. Lower agitation intensities are desirable as it gives stable interphase layer.

From the studies, it is concluded that process integration of Bunsen reaction and separation of phases in single equipment is feasible.

Chapter 7: In this chapter, reaction studies in ABR in counter-current mode of operation described and analysis of product samples is presented. The conversion of sulfur dioxide was found out experimentally for pure and diluted SO_2, at different flow rates, different temperatures. Layer separation i.e. top phase sulfuric acid and bottom phase hydriodic acid was observed when iodine to water ratio in the production stream is above 0.3.

Chapter 8: In this chapter, modeling and validation of ABR is presented. The model 'Tanks-in-series' is proposed. Equations have been proposed and are given in Annexure 1, to estimate gas phase mass transfer coefficient, diffusivity, bubble diameter, gas hold up, gas-liquid interfacial area, gas diffusivity, and liquid phase mass transfer coefficient. Proposed model predictions are within 11 % compared to experimental results for all the cases studied. It can be safely concluded that the assumptions are valid and are applicable to the studied reactor. This approach can be useful for the design and scaling up of agitated reactor.

Chapter 9: In this chapter Conclusions and recommendations are presented.

ABR has been sized taking into consideration mixing of reactants, stages for mixing, size and type of impeller blades, cooling coil located inside the reactor and provision for input and output of reactants and products.

The reaction and acids separation experiments have been carried out successfully. Experiments were carried out in continuous counter-current fashion. The feasibility of Bunsen reaction as well as acids separation in single equipment is established.

A mathematical model has been proposed for Bunsen reaction system and model has been validated with experimental results.

It is concluded that the proposed Agitated Bunsen reactor with rotating blades on the axial shaft can be used as integrated equipment in iodine-sulfur thermo-chemical process for combining Bunsen reaction as well as acids separation. The proposed mathematical model can be used for scale up of reactor.

Recommendations for future work are:

1) High pressure, high temperature experiments in metallic agitated Bunsen reactor and validating/improving the proposed model.
2) Mixing of reactants in each stage and flow behaviour can be understood using CFD (computational fluid dynamics) software for better understanding of inside of the reactor.

References:

1. Dokiya M., Kameyama T., Fukuda K. Thermochemical hydrogen preparation-Part V. A feasibility study of the Sulfur-Iodine cycle [1-4]. International Journal of Hydrogen Energy 1979; Vol 4, 267-277.
2. Charles W Forsberg. Hydrogen, nuclear energy, and the advance high-temperature reactor. International Journal of Hydrogen Energy 2003; 28: 1073-1081.
3. O'Keefe D., Allen C., Besenbruch G., Brown L., Norman J., sharp R., McCorkle K. Preliminary results from bench-scale testing of a sulfur-iodine thermochemical Water-Splitting cycle. International Journal of Hydrogen Energy 1982; Vol 7, No. 5, 381-392.
4. Norman J. H., Mysels K. J., Sharp R., Williamson D**.** Studies of the Sulfur-Iodine thermochemical water–splitting cycle. International Journal of Hydrogen Energy 1982; Vol 7, No. 7, 545-556.

5. IS process for thermochemical hydrogen production. JAERI-Review 94-006.

6. Leybros J, Carles P, Jean-Marc Borgard. Counter current reactor design and flow sheet for sulfur-iodine thermochemical water splitting process. International Journal of Hydrogen Energy 2009; 34, 9060-9075.
7. Zhang P, Chen S Z., Wang L J., Yao T Y, Xu J M. Study on lab-scale hydrogen production by closed cycle thermo-chemical iodine sulfur process. International Journal of Hydrogen Energy 2010; 35: 10166-10172.
8. Seiji Kasahara, Shinji Kubo, Ryutaro Hino, Kaoru Onuki, Mikihiro Nomura, Shin-inchi Nakao. Flow sheet study of the thermochemical water-splitting iodine-sulfur process for effective hydrogen production. International Journal of Hydrogen Energy 2007; 32: 489-496.
9. Shinji Kubo, Hayato Nakajima, Seiji Kasahara, Syunichi Higashi, Tomoo Masaki, Hiroyoshi Abe, Kaoru Onuki. A demonstration study on a closed-cycle hydrogen production by the thermochemical water-splitting iodine-sulfur process. Nuclear Engineering and Design 2004; 233: 347-354.
10. Saeed Dehghani, Hoseyn Sayyaadi. Energy and exergetic evaluations of Bunsen section of the sulfur-iodine thermochemical hydrogen production plant. International Journal of Hydrogen Energy 2013; 38: 9074-9084.
11. Banerjee A M, Pai M R, Bhattacharya K, Tripathi A K, Kamble V S, Bharadwaj S R, Kulshreshtha S K. Catalytic decomposition of sulfuric acid on mixed Cr/Fe oxide samples and its application in sulfur-iodine cycle for hydrogen production. International Journal of Hydrogen Energy 2008; 33: 319-326.
12. Laijun Wang, Daocai Li, Ping Zhang, Songzhe Chen, Jingming Xu. The HI catalytic decomposition for the lab-scale Hydrogen producing apparatus for the iodine-sulfur thermochemical cycle. International Journal of Hydrogen Energy 2012; 37: 6415-6421.

13. Daniel M, Ginosar, Lucia M, Petkovic, Kyle C, Burch. Commercial activated carbon for the catalytic production of hydrogen via sulfur-iodine thermochemical water splitting cycle. International Journal of Hydrogen Energy 2011; 36: 8908-8914.
14. Qiaoqiao Zhu, Yanwei Zhang, Zhi Ying, Shujie Wang, Zhihua Wang, Junhu Zhou, Kefa Cen. Kinetic and thermodynamic studies of the Bunsen reaction in the sulfur-iodine thermochemical process. International Journal of Hydrogen Energy 2013; 38: 8617-8624.
15. Mohamed Kamel Hadj-Kali, Vincent Gerbaud, Patrick Lovera, Olivier Baudouin, Pascal Floquet, Xavier Joulia, Jean-Marc Borgard, Philippe Carles. Bunsen section thermodynamic model for hydrogen production by the sulfur-iodine cycle. International Journal of Hydrogen Energy 2009; 34: 6625-6635.
16. Lee BJ, No HC, Yoon Hj, Kim SJ, Kim ES. An optimal operating window for the Bunsen process in the I-S thermochemical cycle. International Journal of Hydrogen Energy 2008; 33:2200-10.
17. Guo H, Zhang P, Lan S, Chen s, Wan L, Xu J. Study on the phase separation characteristics of $HI.I_2$ - $H_2SO_4.H_2O$ mixtures at 20^0 C. Fluid Phase Equilibria 2012;324:33-40.
18. Colete-Maatouk s, Brijou-Mokrani N, Tabarant M, Fleche JL, Carles P. Study of the miscibility gap in $H_2SO_4/HI/$ I_2 /H_2O mixtures produces by the Bunsen reaction –part I : preliminary results at 308 K. International Journal of Hydrogen Energy 2009; 37:7155-61.
19. Sakurai M, Nakajima H, Onuki K, Shimizu S. Investigation of 2 liquid phase separation characteristics on the Iodine-Sulfur thermochemical hydrogen production process. International Journal of Hydrogen Energy 2000; 25:605-11.

20. Zhu QQ Zhang YW, Zhou C, Wang ZH, Zhou JH, Cen KF, Optimization of liquid–liquid phase separation characteristics in the Bunsen section of the sulfur–iodine hydrogen production process International Journal of Hydrogen Energy 2012;37:6407-14.
21. Hadj-Kali MK, Gerbaud V, Lovera P, Baudouin O, Floquet P, Joulia X, et al. Bunsen section thermodynamic model for hydrogen production by the sulfur-iodine cycle. International Journal of Hydrogen Energy 2009; 34:6625-35.
22. Sau S, Giaconia A, Caputo G, Prosini PP. Decrease the rate of recycling agents in the sulfur-iodine cycle by solid phase separation. International Journal of Hydrogen Energy 2008; 33:6439-44
23. Giaconia A, Caputo G, Sau S, Prosini PP, Pozio A, De Francesco M, et al. Survey of Bunsen reaction routes to improve the sulfur-iodine thermochemical water-splitting cycle. International Journal of Hydrogen Energy 2009; 34:4041-8
24. Sakurai M, Nakajima H, Amir R, Onuki K, Shimizu S. Experimental study on side-reaction occurrence condition in the iodine-sulfur thermochemical hydrogen production process. International Journal of Hydrogen Energy 2000; 25:613-619.
25. Nomura Nakao SI, Okuda H, Fujiwara S, Kasahara S, Ikenoya K, et al. Development of an electrochemical cell for efficient hydrogen production through the IS process. AICHE J 2004; 50; 1991-8.
26. Nomura M, Fujiwara S, Ikenoya K, Kasahara S, Nkajima H, Kubo S, et al. Application of an electrochemical membrane reactor to the thermochemical water splitting IS process for hydrogen production Journal of Membrane Science 2004; 240:221-226
27. V. Immanuel, K. U. Gokul, Anupam Shukla. Membrane electrolysis of Bunsen reaction in the iodine-sulfur process for hydrogen production. International Journal of Hydrogen Energy 2012; 37: 3595-3601.

28. Zhi Ying, Yanwei Zhang, Qiaoqiao Zhu, Pingan Peng, Zhihua Wang, Junhu Zhou, Jianzhong Liu, Kefa Cen. Electro chemical investigation of the Bunsen reaction in the sulfur-iodine cycle. International Journal of Hydrogen Energy 2013; 38: 14391-401.
29. Leybros J, T. Gilardi, Saturnin A., Mansilla C., Carles P. Plant sizing and evaluation of hydrogen production costs from advanced processes coupled to a nuclear heat source. Part I: Sulfur-iodine cycle. International Journal of Hydrogen Energy 2010; 35, 1008-1018.
30. Hyo Sub Kim, Young Ho Kim, Sang Jin Han, Chu Sik Park, Ki Kwang Bae, Jong Gyu Lee. Continuous Bunsen reaction and simultaneous separation using a counter-current flow reactor for the sulfur-iodine hydrogen production process. International Journal of Hydrogen Energy 2010; 35, 1008-1018.
31. Young-Ho Kim, Hyo-Sub Kim, Sang-Jin Han, Chu-Sik Park, Ki-Kwang Bae and Jong-Gyu Lee. Bunsen Reaction using a counter-current flow reactor in Sulfur-Iodine hydrogen production process: Effects of reactor shape and temperature. Advanced Materials Research Vols, 347-353 (2012) pp 3238-3241
32. C. S. R. Prasad, H. Z. Fani, S. B. Menon, “Heterogeneous Bunsen reaction analysis & experimental study of chemical absorption of sulfur dioxide and dissolution of iodine into aqueous reacting system”. IAEA-CN-152-18 (2007) held in Japan.
33. Rober C. Moore “Design options for a Bunsen reactor” Sandia Report, SAND2012-9318.

LIST OF FIGURES

LIST OF TABLES

NOTATIONS

a	Gas − Liquid interfacial area per unit volume of contactor, $m^2\ m^{-3}$
A	Parameter in equatioin A.6
A_O	*Outside heat transfer area*, m^2
b	Stoichiometric coefficient of B, *moles*
B	Parameter in equatioin A.6
C	Parameter in equatioin A.6
C_A	Concentration of A in the bulk liquid phase, *moles of A* m^{-3}
C_{Ai}	Concenration of A at the interface in equlibrium with P_{Ai}, *moles of A* m^{-3}
C_B	Concentration of liquid reactant, B, *moles of B* m^{-3}
C_{Bi}	Concentration of B at the interface, *moles of B* m^{-3}
C_{P_c}	*Specific heat at constant pressure of cold water*, $J\ kg^{-1}\ K^{-1}$
d	*Impeller diameter of agitator*, m
d_b	Bubble diameter, *mm*
d_i	*Inner diameter of tube*, m
d_{LM}	*Logarithmic mean diameter of tube* $\left(\frac{d_o - d_i}{\ln\left({}^{d_o}/_{d_i}\right)}\right), m$
d_o	*Outer diameter of tube*, m
D	Dispersion/Diffusivity coefficient, $m^2\ s^{-1}$ or Equivalent diameter of reactor,m
D_e	*Equivalent diameter*, m
D_H	*Average diameter of helix*, m
$^{D}/_{u\,L}$	Vessel dispersion number, *Dimenionless*
E	Enhancement factor for mass transfer with reaction
E_i	Enhancement factor for an infinitely fast reaction
f_l	Liquid hold up
F_{Ain}	Molar flow rate of A at the inlet of the reactor, *moles of A* s^{-1}
F_{Aout}	Molar flow rate of A at the outlet of the reactor, *moles of A* s^{-1}

F_{N_2}	Molar flow rate of N_2 in reactor, $moles\ of N_2\ \ s^{-1}$
$F_{\text{Total in}}$	Molar flow rate of $(A+N_2)$at inlet of reactor, $moles\ of (A+N_2)\ \ s^{-1}$
$F_{\text{Total out}}$	Molar flow rate of $(A+N_2)$at outlet of reactor, $moles\ of (A+N_2)\ \ s^{-1}$
g	Acceleration due to gravity, $m.s^{-2}$
h_i	$Heat\ transfer\ coefficient\ in\ cold\ water\ side\ or\ tube\ side$ $(std\ notation), Wm^{-2}K^{-1}$
h_{ic}	$Heat\ transfer\ coefficient\ in\ cold\ water\ side\ for\ helical$ $coil\ tube, Wm^{-2}K^{-1}$
h_O	$Heat\ transfer\ coefficient\ in\ hot\ water\ side\ or\ reactor(shell)$ $side\ (std\ notation), Wm^{-2}K^{-1}$
H_A	Phase distribution coefficient or Henry's law constant; for gas phase system, $m^3\ atm\ mole^{-1}$
K_{Al}	Liquid phase mass transfer coefficient, $m^3 of\ liquid\ (m^2 of\ surface)^{-1}\ s^{-1}$
K_{Ag}	Gas phase mass transfer coefficient, $moles\ of\ A\ (m^2 of\ surface)^{-1}\ atm^{-1}$
k	Reaction rate constant, s^{-1}
k	$Thermal\ conductivity\ of\ tube\ material, W\ m^{-1}K^{-1}$
L	Reactor length, m
m_c	$Mass\ flow\ rate\ of\ cold\ water, kg\ s^{-1}$
m_h	$Mass\ flow\ rate\ of\ hot\ water, kg\ s^{-1}$
N	$Agitation\ speed, s^{-1}$
Nu_i	$Nusselt\ number\ in\ cold\ water\ side\ or\ tube\ side\ (std\ notation)$
Nu_O	$Nusselt\ number\ in\ hot\ water\ side\ or\ reactor(shell)side\ (std\ notation)$
M_A	Molecular weight of 'A' reactant
M_B	Molecular weight of 'B' reactant
M_H	Hatta modulus

P_A	Partial pressure of A in the bulk gas phase, atm
P_{Ai}	Partial pressure of A at the interface, atm
$P_{A\,in}$	Partial pressure of A at inlet of reactor, atm
$P_{A\,out}$	Partial pressure of A at outlet of reactor, atm
Pr	$Prandtl\ number(standard\ notation)$
Pr_c	$Prandtl\ number\ in\ cold\ water\ side\ or\ tube\ side$
Pr_h	$Prandtl\ number\ in\ hot\ water\ side\ or\ reactor(shell)side$
q	$heat\ flux, Wm^{-2}$
Q	$heat\ duty\ of\ the\ equipment, W$
Q_c	$heat\ energy\ gained\ by\ cold\ fluid, W$
Q_h	$heat\ energy\ lost\ by\ hot\ fluid, W$
$-r_1, -r_2 \ldots$	Rate of reaction per unit volume of 1^{st}, 2^{nd} … CSTR, $moles.m^{-3}\ s^{-1}$
$-r''_A$	Rate of reaction per unit gas-liquid interfacial area, $moles.m^{-2}.s^{-1}$
$-r''''_A$	Rate of reaction per unit volume of contactor, $moles.m^{-3}\ s^{-1}$
$-r''''_i$	Rate of reaction per unit volume of i^{th}CSTR, $moles.m^{-3}\ s^{-1}$
Re	$Reynolds'number(standard\ notation)$
$Re_{impeller}$	$Mixing\ Reynolds'number\ in\ hot\ water\ side\ or\ reactor(shell)side$
$R_{film}c$	$Resistance\ offered\ by\ cold\ water\ film, K\ W^{-1}$
$R_{film}h$	$Resistance\ offered\ by\ hot\ water\ film, K\ W^{-1}$
Re_{flow}	$Flow\ Reynolds'number\ in\ hot\ water\ side\ or\ reactor(shell)side$
R_{Wall}	$Resistance\ offered\ by\ solid\ cylindrical\ wall, K\ W^{-1}$
t_m	Mean residence time, s
T	Temperature, K

T_c	Bulk temperature of cold water at any point, K
$T_c(i)$	Inlet temperature of cold water, K
$T_c(o)$	Outlet temperature of cold water, K
T_{cw}	Temperature at innerwall or cold water side of cylindrical tube at any point, K
T_h	Bulk temperature of hot water at any point, K
$T_h(i)$	Inlet temperature of hot water, K
$T_h(o)$	Outlet temperature of hot water, K
T_{hw}	Temperature at outerwall or hot water side of cylindrical tube at any point, K
ΔT_C	Temperature rise of cold water $(T_C(o) - T_C(i))$, K
ΔT_h	Temperature drop of hot water $(T_h(i) - T_h(o))$, K
ΔT_{LM}	Logarithmic mean temperature difference, K
u	Fluid (water) velocity through the reactor, $m\ s^{-1}$
u_{SG}	Gas velocity, $m.s^{-1}$
U_O	Overall heat transfer coefficient based on A_O (standard notation), $Wm^{-2}K^{-1}$
V	Reactor volume, m^3
V	Molar volume, $m^3.mole^{-1}$
V	Velocity of the fluid , $m\ s^{-1}$
V_c	Volumetric flow rae of cold water, m^3s^{-1}
V_h	Volumetric flow rae of hot water, m^3s^{-1}
V_r	Volume of the reactor, m^3

V_i	Volume of i^{th}CSTR, m^3
x	$Thickness\ of\ the\ tube, m$

Greek symbols

σ^2	Variance, s^2
σ_L	Surface tension of liquid, $N.m^{-1}$
σ_θ^2	Dimensionless variance
ε	Gas holdup
ρ	$Density\ of\ fluid\ (Standard\ notation), kgm^{-3}$
ρ_L	Density of liquid, $kg.m^{-3}$
μ	$Viscosity\ of\ fluid\ (Standard\ notation), Pa\ s^{-1}$
μ_L	Viscosity of liquid, $Pa.s$
μ_w	$Viscosity\ of\ fluid\ at\ wall\ temperature\ (Standard\ notation), Pa\ s^{-1}$
ϑ	Volumetric flow rate, $m^3 s^{-1}$

Chapter I

Introduction

1.1. Energy perspective:

The world is entirely dependent on energy for all its needs. Therefore energy development is the key issue. Fig 1.1 shows total world energy consumption by the source of energy such as fossil fuels, renewables and nuclear. Renewable Energy Policy Network for the 21st Century, REN21, is a global renewable energy policy network which provides international leadership for the speedy transition to renewable energy. The network was launched in June 2005 as an outcome of the International Conference for Renewable Energies in Bonn, Germany.

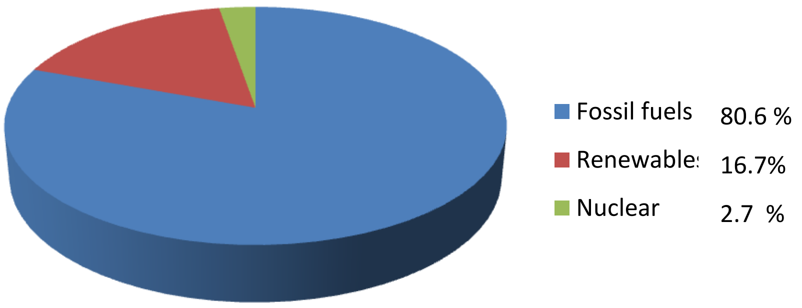

Renewable energy can be further represented as

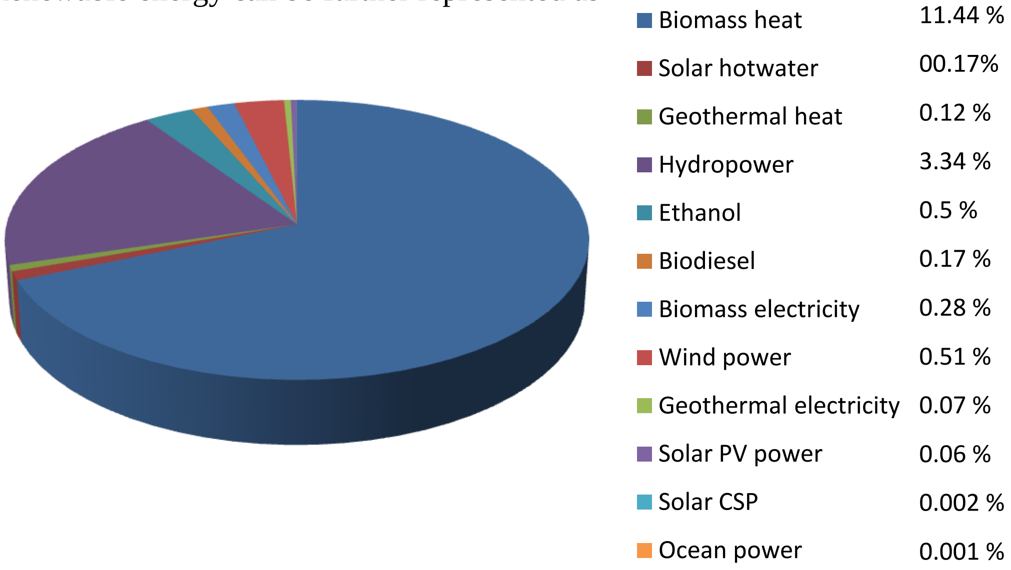

Fig 1.1: Total world energy consumption by Source (2010) [1]

Energy development [2,3] is primarily focused on making available sufficient primary energy sources [4] and secondary energy forms to meet the needs [5-9]. Energy development include production of conventional, alternative and renewable sources of energy, and the recovery and reuse of energy that would otherwise be wasted. Energy conservation and efficiency measures reduce the requirement of energy development. It can have benefits to society with respect to economic cost and environmental effects.

World total primary energy production is shown in Fig 1.2 till 2010.

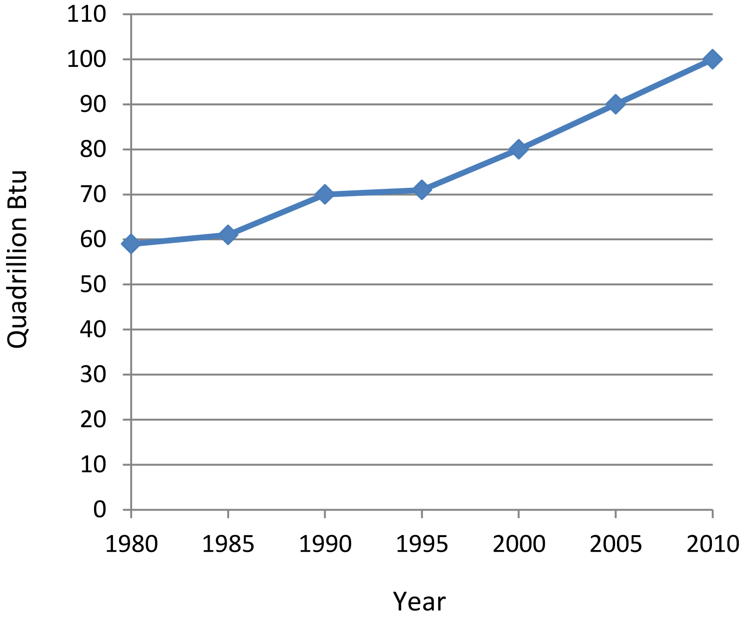

Fig 1.2: World total primary energy production

Developed countries and industries use primary and secondary energy sources for transportation and production of innumerable manufactured items.

Large industrial hubs have variety of generation and delivery methods for energy distribution and end-user utilization. Level of use of external energy sources differs across societies, according to availability of domestic energy sources and the requirement. The conventional industry comprises the petroleum industry, the gas industry, the coal industry, and the nuclear power industry. New energy industries include the renewable energy industry, comprising alternative and sustainable manufacture, distribution, and sale of alternative fuels. Also efforts to develop sources of alternative and renewable energy are underway with the focus on mitigating climate change.

According to their nature, the power plants can be classified into:

- Primary: wind, water, solar, wood, coal, oil, nuclear (they are found in nature).
- Secondary: electricity, gas (are obtained from primary energy sources).

According to energy reserves of source used and regeneration capacity grouping can be:

- Renewable: Renewable energy is the energy sources freely regenerated in a short period and have practically limitless reserves. Renewable energies are:
  - original solar, from sun
  - natural wind (atmospheric flows)
  - natural geothermal
  - oceanic tidal
  - natural waterfall (hydraulic flows)
  - natural plant: paper, wood
  - natural animal: wax, grease, pack animals and sources of mechanical energy
- Nonrenewable: Nonrenewable energy is energy coming from limited sources on Earth in quantity and, so exhaustible. These energy sources include, non-exclusively:

- fossil source: petroleum, natural gas, coal
- original mineral/chemical: uranium, shale gas

The principle on the conservation of matter applies to energy development: "nothing is created." Thus any energy "production" is actually a recovery transformation of the forms of energy whose origin is that of the universe.

1.2. Fossil fuels:

Fossil fuels (primary non-renewable fossil) are the remains of the decomposition of plants and animals. There are three main types of fossil fuels: coal, petroleum, and natural gas. These fuels are based on the carbon cycle; thus allow stored (historic solar) energy to be reused in today’s time. Almost 81% of the world's energy needs were met from fossil sources in 2005 [11]. Biomass is also derived from wood and other organic wastes and modern remains.

The bulk of the world's current primary energy sources are fossil fuels. The technology and infrastructure already are developed for the use of fossil fuels. As far as energy density in terms of volume and mass is concerned, Petroleum ranks currently above that of alternative energy sources (or energy storage devices, like a battery). Fossil fuels are currently economical, and as they are distributed all over, are suitable for decentralized energy use.

The fossil fuels are mainly based on organic carbon compounds. They are, according to the Intergovernmental Panel on Climate Change (IPCC), the causes of the global warming [12]. Greenhouse gas emissions result from fossil fuel-based electricity generation. A typical coal plant generates billions of kilowatt hours per year [13]. Emissions from such fossil fuel power station include carbon dioxide, sulfur dioxide, small particulates, nitrogen oxides, smog with high levels of ozone, carbon monoxide (CO), hydrocarbons, volatile organic compounds (VOC), mercury, arsenic, lead, cadmium, other heavy metals, and traces of uranium [14,15].

1.3. Nuclear energy:

Nuclear energy is the energy of exothermic nuclear processes [16], used to generate useful heat and electricity. Nuclear processes include nuclear fission, nuclear decay and nuclear fusion. Presently the nuclear fission of elements in the actinide series of the periodic table, produce the vast majority of nuclear energy in the direct service of humankind, with nuclear decay processes, primarily in the form of geothermal energy, and radioisotope thermoelectric generators. Nuclear (fission) power stations, excluding the contribution from naval nuclear fission reactors, provided about 5.7% of the world's energy and 13% of the world's electricity in 2012 [17]. In 2013, the International Atomic Energy Agency (IAEA) report that there are 437 operational nuclear power reactors[18], in 31 countries [19], although not every reactor is producing electricity [20].

Along with other sustainable energy sources, nuclear power is a low carbon power generation method of producing electricity, with an analysis of the literature on its total life cycle emission intensity finding that it is similar to other renewable sources in a comparison of greenhouse gas (GHG) emissions per unit of energy generated [21].

Fig 1.3 shows Global public support for energy sources such as solar, wind, hydroelectric, natural gas, coal and nuclear. This indicates whether strongly support, somewhat support, somewhat oppose or strongly oppose, particular way of producing energy. Strongly supported is solar, followed by wind, next is hydroelectric, all having more than 90% support. Coal and nuclear are the least supported.

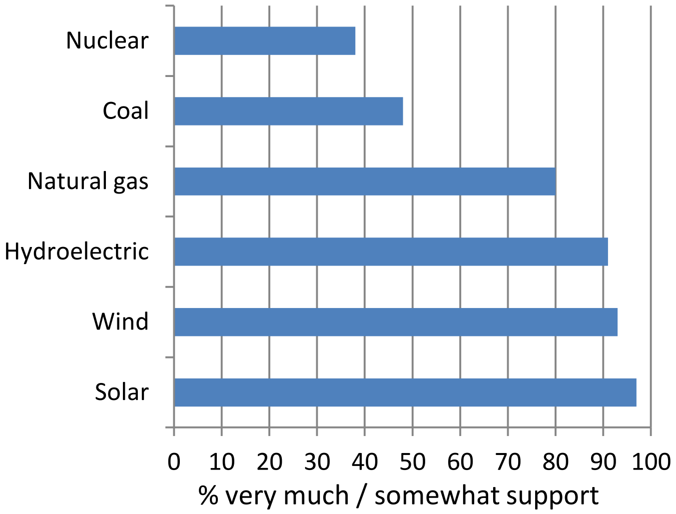

Fig 1.3: Global public support for energy sources, based on a survey by Ipsos (2011) [22].

1.4. Renewable energy:

Renewable energy is the energy that comes from resources which are naturally replenished on a human time scale such as sunlight, wind, rain, tides, waves and geothermal heat [23]. Renewable energy replaces conventional fuels in four distinct areas viz. electricity generation, hot water/space heating, motor fuels and rural (off-grid) energy services [24].

About 16% of global energy consumption presently comes from renewable resources, with 10% [25] of all energy from traditional biomass, mainly used for heating, and 3.4% from hydroelectricity. New renewables (small hydro, modern biomass, wind, solar, geothermal, and biofuels) account for another 3% and are growing rapidly [26]. At least 30 nations around the world already have renewable energy contributing more than 20% of energy supply. National renewable energy markets are projected to continue to grow strongly in the coming decades [27]. Wind power, is growing at the rate of 30% annually, with a worldwide installed capacity of 282,482 megawatts (MW) at the end of 2012.

Renewable energy resources are available over wide geographical areas, in contrast to other energy sources, which are concentrated in a limited number of regions/countries. Rapid deployment of renewable energy and energy efficiency is resulting in significant energy security, climate change mitigation, and economic benefits [28]. In international public opinion surveys there is strong support for promoting renewable sources such as solar power and wind power [29].

Many renewable energy projects should be large-scale, renewable technologies in smaller scale are also suited to rural and remote areas and developing countries, where energy is very crucial in human development [30]. United Nations' Secretary-General Ban Ki-moon has said that renewable energy has the ability to lift the poorest nations to new levels of prosperity [31].

1.4.1. Hydroelectricity:

Hydroelectricity is electricity generated by hydropower; the production of electrical power through the use of the gravitational force of falling or flowing water. It is the most widely used form of renewable energy, accounting for 16 % of global electricity generation i.e. 3,427 terawatt-hours of electricity production in 2010 [32] and is expected to increase about 3.1% each year for the next 25 years.

Hydropower is produced in 150 countries, with the Asia-Pacific region generating 32 % of global hydropower in 2010. China is the largest hydroelectricity producer, with 721 terawatt-hours of production in 2010, representing around 17 % of domestic electricity use. There are now three hydroelectricity plants larger than 10 GW namely; the Three Gorges Dam in China, Itaipu Dam across the Brazil/Paraguay border, and Guri Dam in Venezuela [32].

The cost of hydroelectricity is relatively low, making it a competitive source of renewable electricity. However, damming interrupts the flow of rivers and can harm local ecosystems, and building large dams and reservoirs often involves displacing people and wildlife [32]. Once a hydroelectric complex is constructed, the project produces no direct waste, and has a considerably lower output level of greenhouse gas carbon dioxide than fossil fuel powered energy plants [33].

1.4.2. Wind power:

Wind (primary renewable natural) power harnesses the power of the wind to propel the blades of wind turbines. These turbines cause the rotation of magnets, which creates electricity. Wind towers are usually built together on wind farms. There are offshore and onshore wind farms. Global wind power capacity has expanded rapidly to 336 GW in June 2014, and wind energy production was around 4% of total worldwide electricity usage and is growing rapidly [34].

Many of the world's largest onshore wind farms are located in the United States, China, and India. Most of the world's largest offshore wind farms are located in Denmark, Germany and the United Kingdom.

1.4.3. Solar PV systems and concentrated solar power:

Radiant light and heat from the sun, is harnessed as solar energy; using a range of ever-evolving technologies such as solar heating, solar photovoltaics, solar thermal electricity, solar architecture and artificial photosynthesis [35,36].

Solar technologies are broadly characterized as either passive solar or active solar depending on the way they capture, convert and distribute solar energy. Active solar techniques include the use of photovoltaic panels and solar thermal collectors to harness the energy. Passive solar techniques include orienting a building to the Sun, selecting materials with favorable thermal mass or light dispersing properties, and designing spaces that naturally circulate air.

In 2011, the International Energy Agency (IEA) said that "the development of affordable, inexhaustible and clean solar energy technologies will have huge longer-term benefits. It will increase countries' energy security through reliance on an indigenous, inexhaustible and mostly import-independent resource, enhance sustainability, reduce pollution, lower the costs of mitigating climate change, and keep fossil fuel prices lower than otherwise. These advantages are global.

Photovoltaics (PV) is a method of generating electrical power by converting solar radiation into direct current electricity using semiconductors that exhibit the photovoltaic effect. Photovoltaic power generation employs solar panels composed of a number of solar cells containing a photovoltaic material. Materials presently used for photovoltaics include monocrystalline silicon, polycrystalline silicon, amorphous silicon, cadmium telluride, and copper indium gallium selenide/sulfide. Due to the increased demand for renewable energy sources, the manufacturing of solar cells and photovoltaic arrays has advanced considerably in recent years.

Solar photovoltaic is a sustainable energy source. By the end of 2011, a total of 71.1 GW [37] had been installed, sufficient to generate 85 TWh/year [38]. And by the end of 2012, the 100 GW installed capacity milestone was achieved [39]. Solar photovoltaics is now, after hydro and wind power, the third most important renewable energy source in terms of globally installed capacity. More than 100 countries use solar PV. Installations may be ground-mounted (and sometimes integrated with farming and grazing) or built into the roof or walls of a building (either building-integrated photovoltaics or simply rooftop).

1.4.4. Biofuel and Sustainable biofuel:

A biofuel is a fuel that contains energy from geologically recent carbon fixation. These fuels are produced from living organisms. Examples of this carbon fixation occur in plants and microalgae. These fuels are made by a biomass conversion (biomass refers to recently living organisms, most often referring to plants or plant-derived materials). This biomass can be converted to convenient energy containing substances in three different ways viz. thermal, chemical and biochemical conversion. This biomass conversion can result in fuel in solid, liquid, or gas form. This new biomass can be used for biofuels. Biofuels have increased in popularity because of rising oil prices and the need for energy security.

The International Energy Agency (IEA) has a goal for biofuels to meet more than a quarter of world demand for transportation fuels by 2050 to reduce dependence on petroleum and coal [40].

1.4.5. Geothermal energy:

Geothermal energy is thermal energy generated and stored in the Earth. Thermal energy is the energy that determines the temperature of matter. The geothermal energy of the Earth's crust originates from the original formation of the planet (20%) and from radioactive decay of minerals (80%) [41]. The geothermal gradient, which is the difference in temperature between the core of the planet and its surface, drives a continuous conduction of thermal energy in the form of heat from the core to the surface.

From hot springs, geothermal energy has been used for bathing since Paleolithic times and for space heating since ancient Roman times, but it is now better known for electricity generation. Worldwide, 11,400 megawatts (MW) of geothermal power is online in 24 countries in 2012 [42]. An additional 28 gigawatts of direct geothermal heating capacity is installed for district heating, space heating, spas, industrial processes, desalination and agricultural applications in 2010 [43].

Geothermal power is cost effective, reliable, sustainable, and environmentally friendly [44] but has historically been limited to areas near tectonic plate boundaries. Recent technological advances have dramatically expanded the range and size of viable resources, especially for applications such as home heating, opening a potential for widespread utilization. Geothermal wells release greenhouse gases trapped deep within the earth, but these emissions are much lower per energy unit than those of fossil fuels. As a result, geothermal power has the potential to help mitigate global warming if widely deployed in place of fossil fuels.

1.5. Energy storage:

Energy storage is accomplished by devices or physical media that store energy to perform useful operation at a later time.

All forms of energy are either potential energy (e.g. Chemical, gravitational, electrical energy, temperature differential, latent heat, etc.) or kinetic energy (e.g. momentum). Some technologies provide only short-term energy storage, and others can be very long-term such as power to gas using hydrogen or methane and the storage of heat or cold between opposing seasons in deep aquifers or bedrock. A wind-up clock stores potential energy (in this case mechanical, in the spring tension), a battery stores readily convertible chemical energy to operate a mobile phone, and a hydroelectric dam stores energy in a reservoir as gravitational potential energy. Ice storage tanks store ice (thermal energy in the form of latent heat) at night to meet peak demand for cooling. Fossil fuels such as coal and gasoline store ancient energy derived from sunlight by organisms that later died, became buried and over time were then converted into these fuels. Even food (which is made by the same process as fossil fuels) is a form of energy stored in chemical form. World energy consumption by the type of fuel is shown in Fig 1.4. Projections till 2040 for various fuels such as liquids (including biofuels), coal, natural gas, renewables and nuclear, for energy consumption show consumption of coal will not increase but remain steady, in terms of share of world total energy consumption. There will be sharp rise for renewables.

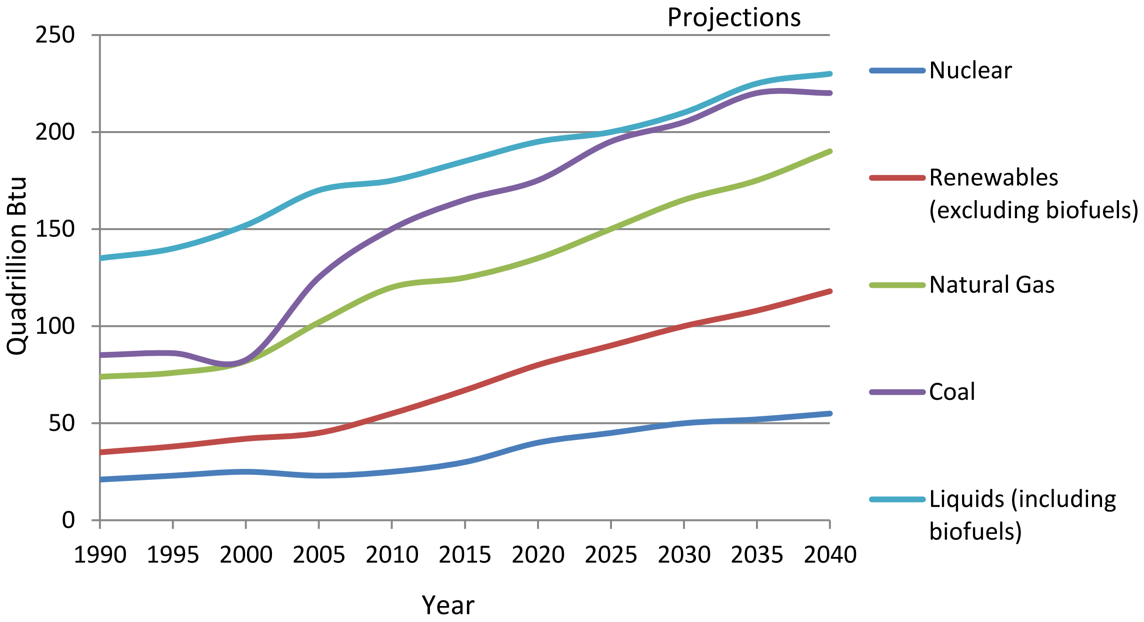

Fig 1.4: World energy consumption by fuel [45]

Increasing share of energy consumption by developing nations is depicted in Fig 1.5.

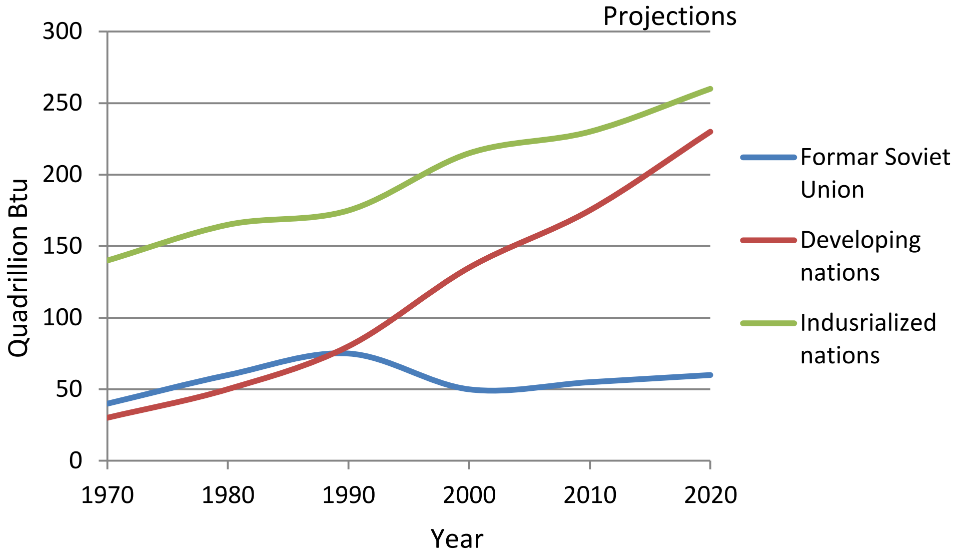

Fig 1.5: Increasing share of energy consumption by developing nations [46].

1.6. Hydrogen economy:

The hydrogen economy is a proposed system of delivering energy using hydrogen. The term hydrogen economy was coined by John Bockris during a talk he gave in 1970 at General Motors (GM) Technical Centre [47].

Supporters of a hydrogen economy advocate hydrogen as a potential fuel for motive power (including cars and boats) and on-board auxiliary power, stationary power generation (e.g., for the energy needs of buildings), and as an energy storage medium (e.g., for inter conversion from excess electric power generated off-peak). Molecular hydrogen of the sort that can be used as a fuel does not occur naturally in convenient reservoirs; nonetheless it can be generated by steam reformation of hydrocarbons, water electrolysis or by other methods [48]. As shown in Fig 1.6, elements of hydrogen economy are production, storage, delivery, safety and codes & standards.

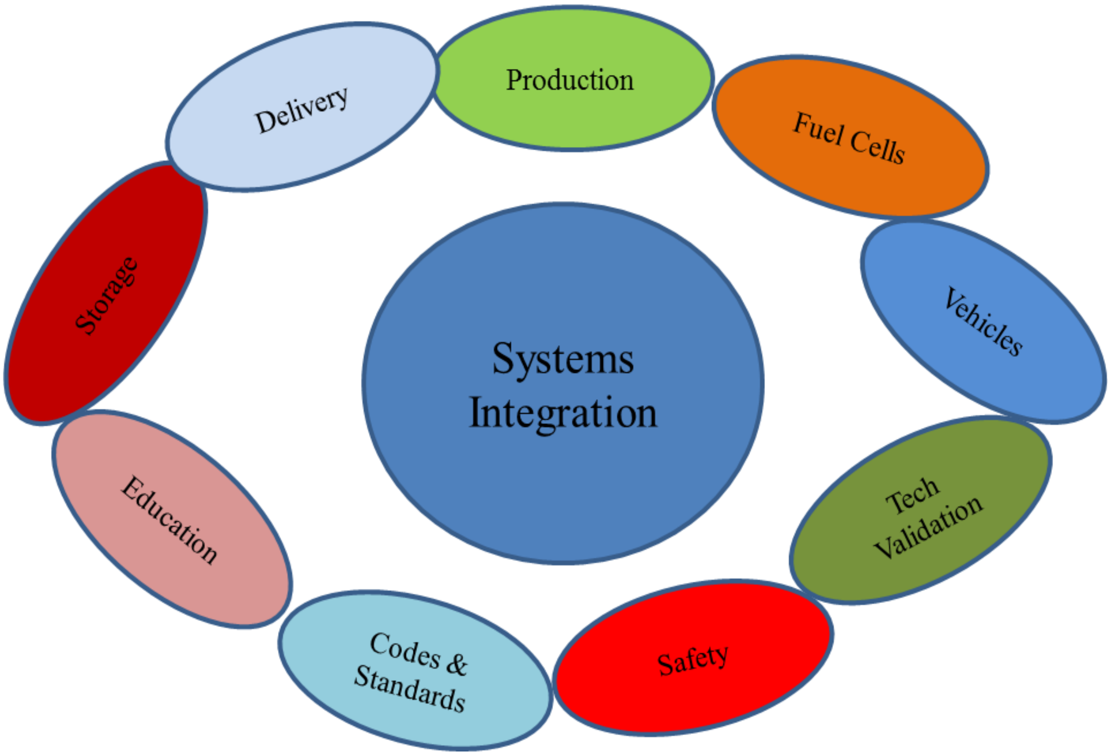

Fig 1.6: Elements of the hydrogen economy (Source: Wikipedia)

In the current hydrocarbon economy, transportation is fueled primarily by petroleum. Burning of hydrocarbon fuels emits carbon dioxide and other pollutants. The supply of economically usable hydrocarbon resources in the world is limited, and the demand for hydrocarbon fuels is increasing, particularly in China, India, and other developing countries.

Supporters of a world-scale hydrogen economy argue that hydrogen can be an environmentally cleaner source of energy to end-users, particularly in transportation applications, without release of pollutants or carbon dioxide at the point of end use. A 2004 analysis asserted that "most of the hydrogen supply chain pathways would release significantly less carbon dioxide into the atmosphere than would gasoline used in hybrid electric vehicles" and that significant reductions in carbon dioxide emissions would be possible if carbon capture or carbon sequestration methods were utilized at the site of energy or hydrogen production [49].

Hydrogen has a high energy density by weight but has a low energy density by volume when not highly compressed or liquefied. An Otto cycle internal-combustion engine running on hydrogen is said to have a maximum efficiency of about 38%, 8% higher than a gasoline internal-combustion engine [50].

Other technical obstacles include hydrogen storage issues and the purity requirement of hydrogen used in fuel cells. With current technology, an operating fuel cell requires the purity of hydrogen to be as high as 99.999%. On the other hand, hydrogen engine conversion technology is more economical than fuel cells [51].

1.7. Hydrogen production:

Hydrogen production is a large and growing industry. Globally, some 57 million metric tons of hydrogen [52], equal to about 170 million tons of oil equivalent, were produced in 2004. The growth rate is around 10% per year.

There are two primary uses for hydrogen, about half is used in the Haber process to produce ammonia (NH_3), which is then used directly or indirectly as fertilizer, the other half of current hydrogen production is used to convert heavy petroleum sources into lighter fractions suitable for use as fuels. This latter process is known as hydrocracking. Hydrocracking represents an even larger growth area, since rising oil prices encourage oil companies to extract poorer source material, such as tar sands and oil shale. The scale economies integral in large-scale oil refining and fertilizer manufacture make possible on-site production and "captive" use. Smaller quantities of "merchant" hydrogen are manufactured and delivered to end users as well.

Currently, global hydrogen production is 48% from natural gas, 30% from oil, and 18% from coal; water electrolysis accounts for only 4% [53]. The distribution of production reflects the effects of thermodynamic constraints on economic choices: of the four methods for obtaining hydrogen, partial combustion of natural gas in a NGCC (natural gas combined cycle) power plant offers the most efficient chemical pathway and the greatest off-take of usable heat energy.

The large market and sharply rising prices in fossil fuels have also stimulated great interest in alternate, cheaper means of hydrogen production. As of 2002, most hydrogen is produced on site and the cost is approximately $0.32/lb and, if not produced on site, the cost of liquid hydrogen is about $1.00/lb to $1.40/lb [54].

Today's hydrogen is mainly produced (>90%) from fossil sources [55]. Linking its centralized production to a fleet of light-duty fuel cell vehicles would require the siting and construction of a distribution infrastructure with large investment of capital. Further, the technological challenge of providing safe, energy-dense storage of hydrogen on board the vehicle must be overcome to provide sufficient range between fill-ups.

Molecular hydrogen is not available on Earth in convenient natural reservoirs. Most hydrogen in the lithosphere is bonded to oxygen in water. Manufacturing elemental hydrogen does require the consumption of a hydrogen carrier such as a fossil fuel or water. The former carrier consumes the fossil resource and produces carbon dioxide, but often requires no further energy input beyond the fossil fuel. Decomposing water, the latter carrier, requires electrical or heat input, generated from some primary energy source (fossil fuel, nuclear power or a renewable energy). Hydrogen can also be produced by refining the effluent from geothermal sources in the lithosphere. Hydrogen produced by zero emission renewable energy sources such as electrolysis of water using wind power, solar power, hydro power, wave power or tidal power is referred to as green hydrogen. Hydrogen produced by non-renewable energy sources may be referred to as brown hydrogen. Hydrogen produced as a waste by-product or industrial by-product is sometimes referred to as grey hydrogen.

Hydrogen is industrially produced from steam reforming, which uses fossil fuels such as natural gas, oil, or coal. The energy content of the produced hydrogen is less than the energy content of the original fuel, some of it being lost as excessive heat during production. Steam reforming leads to carbon dioxide emissions, in the same way as a car engine would do.

A small part (4% in 2006) is produced by electrolysis using electricity and water, consuming approximately 50 kilowatt-hours of electricity per kilogram of hydrogen produced.

Various hydrogen production processes are described below.

1.7.1 Kvaerner-process:

The Kvaerner-process or Kvaerner carbon black & hydrogen process (CB&H) [55] is a method, developed in the 1980s by a Norwegian company of the same name, for the production of hydrogen from hydrocarbons (CnHm), such as methane, natural gas and biogas. Of the available energy of the feed, approximately 48% is contained in the hydrogen, 40% is contained in activated carbon and 10% in superheated steam.

1.7.2. Biological hydrogen production (Algae):

Fermentative hydrogen production is the fermentative conversion of organic substrate to bio-hydrogen established by a diverse group bacteria using multi enzyme systems involving three steps similar to anaerobic conversion. Dark fermentation reactions do not require light energy, so they are capable of constantly producing hydrogen from organic compounds throughout the day and night. Photo-fermentation differs from dark fermentation because it only proceeds in the presence of light. For example photo-fermentation with Rhodobacter sphaeroides SH2C can be employed to convert small molecular fatty acids into hydrogen [26]. Electrohydrogenesis is used in microbial fuel cells where hydrogen is produced from organic matter (e.g. from sewage, or solid matter [56]) while 0.2 - 0.8 V is applied.

Biological hydrogen can be produced in an algae bioreactor. In the late 1990s it was discovered that if the algae is deprived of sulfur it will switch from the production of oxygen, i.e. normal photosynthesis, to the production of hydrogen.

Biological hydrogen can be produced in bioreactors that use feed stocks other than algae, the most common feedstock being waste streams. The process involves bacteria feeding on hydrocarbons and excreting hydrogen and CO_2. The CO_2 can be sequestered successfully by several methods, leaving hydrogen gas. A prototype hydrogen bioreactor using waste as a feedstock is in operation at Welch's grape juice factory in North East, Pennsylvania.

1.7.3. Biocatalysed electrolysis:

Besides regular electrolysis, electrolysis using microbes is another possibility. With biocatalysed electrolysis, hydrogen is generated after running through the microbial fuel cell and a variety of aquatic plants can be used. These include reed sweet grass, cord grass, rice, tomatoes, lupines, and algae.

1.7.4. Electrolysis of water:

Hydrogen can be prepared via high pressure electrolysis, low pressure electrolysis of water or a range of other emerging electrochemical processes such as high temperature electrolysis or carbon assisted electrolysis [57]. Current best processes have an efficiency of 50% to 80% [58], so that 1 kg of hydrogen (which has a specific energy of 143 MJ/kg, about 40 kWh/kg) requires 50 to 79 kWh of electricity. At 0,08 $/kWh, that's $4.00/kg, which is with traditional methods 3 to 10 times the price of hydrogen from steam reformation of natural gas [54]. The price difference is due to the efficiency of direct conversion of fossil fuels to produce hydrogen, rather than burning fuel to produce electricity. Hydrogen from natural gas, used to replace e.g. gasoline, emits more CO_2 than the gasoline it would replace, and so is no help in reducing greenhouse gases [60].

1.7.4.1. High-pressure electrolysis:

High pressure electrolysis is the electrolysis of water by decomposition of water into oxygen and hydrogen gas by means of an electric current being passed through the water. The difference with a standard electrolyzer is the compressed hydrogen output around 120-200 Bar (1740-2900 psi). By pressurising the hydrogen in the electrolyser, through a process known as chemical compression, the need for an external hydrogen compressor is eliminated [48], The average energy consumption for internal compression is around 3%.

1.7.4.2. High-temperature electrolysis:

Hydrogen can be generated from energy supplied in the form of heat and electricity through high-temperature electrolysis (HTE). Because some of the energy in HTE is supplied in the form of heat, less of the energy must be converted twice (from heat to electricity, and then to chemical form), and so potentially far less energy is required per kilogram of hydrogen produced.

While nuclear-generated electricity could be used for electrolysis, nuclear heat can be directly applied to split hydrogen from water. High temperature (950–1000 °C) gas cooled nuclear reactors have the potential to split hydrogen from water by thermochemical means using nuclear heat. Research into high-temperature nuclear reactors may eventually lead to a hydrogen supply that is cost-competitive with natural gas steam reforming. General Atomics predicts that hydrogen produced in a High Temperature Gas

Cooled Reactor (HTGR) would cost $1.53/kg. In 2003, steam reforming of natural gas yielded hydrogen at $1.40/kg. At 2005 natural gas prices, hydrogen costs $2.70/kg.

High-temperature electrolysis has been demonstrated in a laboratory, at 108 megajoules (thermal) per kilogram of hydrogen produced [61], but not at a commercial scale. In addition, this is lower-quality "commercial" grade Hydrogen, unsuitable for use in fuel cells [62].

1.7.5. Photo electrochemical water splitting:

Using electricity produced by photovoltaic systems offers the cleanest way to produce hydrogen. Water is broken into hydrogen and oxygen by electrolysis—a photo electrochemical cell (PEC) process which is also named artificial photosynthesis. William Ayers at Energy Conversion Devices demonstrated and patented the first multi junction high efficiency photo electrochemical system for direct splitting of water in 1983 [63]. This group demonstrated direct water splitting now referred to as an "artificial leaf" or "wireless solar water splitting" with a low cost thin film amorphous silicon multi junction sheet immersed directly in water. Hydrogen evolved on the front amorphous silicon surface coated with various catalysts while oxygen evolved off the back metal substrate. A Nafion membrane above the multi junction cell provided a path for ion transport. Research continues towards developing high-efficiency multi-junction cell technology at universities and the photovoltaic industry. If this process is assisted by photo-catalysts suspended directly in water instead of using photovoltaic and an electrolytic system, the reaction is in just one step, which can improve efficiency [64,65].

1.7.6. Photo electrocatalytic production:

A method studied by Thomas Nann and his team at the University of East Anglia consists of a gold electrode covered in layers of indium phosphide (InP) nanoparticles.

They introduced an iron-sulfur complex into the layered arrangement, which when submerged in water and irradiated with light under small electric current, produced hydrogen with an efficiency of 60% [66].

1.7.7. Thermochemical production:

There are more than 353 [67] thermochemical cycles which can be used for water splitting, around a dozen of these cycles such as the iron oxide cycle, cerium(IV) oxide-cerium(III) oxide cycle, zinc zinc-oxide cycle, sulfur-iodine cycle, copper-chlorine cycle and hybrid sulfur cycle are under research and in testing phase to produce hydrogen and oxygen from water and heat without using electricity. These processes can be more efficient than high-temperature electrolysis, typical in the range from 35% - 49% LHV efficiency. Thermochemical production of hydrogen using chemical energy from coal or natural gas is generally not considered, because the direct chemical path is more efficient.

Thermochemical hydrogen production processes have to reach demonstration at production levels, though several have been demonstrated in laboratories.

1.8. Hydrogen as a byproduct of other chemical processes:

The industrial production of vinyl by electrolysis, like other chlorine industries generates a sizeable amount of Hydrogen byproduct. In the port of Antwerp a 1MW fuel cell power plant is powered by such byproduct. This unit has been operational since late 2011. The excess hydrogen is often managed with a hydrogen pinch analysis.

1.9. Thermochemical cycles:

Thermochemical cycles combine solely heat sources (thermo) with chemical reactions to split water into its hydrogen and oxygen components. The term cycle is used because apart from water, hydrogen and oxygen, the chemical compounds used in these processes are continuously recycled.

If work is partially used as an input, the resulting thermochemical cycle is defined as a hybrid one.

This concept was first postulated by Funk and Reinstrom (1966) as a reflexion about the most efficient way to produce fuels (e.g. hydrogen, ammonia) from stable and abundant species (e.g. water, nitrogen) and heat sources [68]. Although fuel availability was scarcely considered before the oil crisis era, these researches were justified by niche markets. As an example, in the military logistics field, providing fuels for vehicles in remote battlefields is a key task. Hence, a mobile production system based on a portable heat source (a specific nuclear reactor was strongly considered) was being investigated with the highest interest. Following the crisis, many programs (Europe, Japan, USA) were set-up to design, test and qualify such processes for more peaceful purposes such as energy independence. High temperature (1000K) nuclear reactors were still considered as the heat sources. However, the optimistic expectations of the first thermodynamics studies were quickly moderated by more pragmatic analysis based on fair comparisons with standard technologies (thermodynamic cycles for electricity generation, coupled with the electrolysis of water) and by numerous practical issues (not high enough temperatures with nuclear reactors, slow reactivities, reactor corrosion, significant losses of intermediate compounds with time) [69]. Hence, the interest for this technology was fading away during the next decades [70], or at least some tradeoffs (hybrid versions) were being considered with the use of electricity as a fractional energy input instead of only heat for the reactions (e.g. Hybrid sulfur cycle). A rebirth in the year 2000 can be explained by both new energy crisis and the rapid pace of development of concentrated solar power technologies whose potentially very high temperatures are ideal for thermochemical processes [71], while the environmentally friendly side of these researches attracts funding in a period with the peak oil shadow.

Single step thermolysis of water requires temperatures above 3000K, which make reactor design and operation extremely challenging [72]. As shown by Funk and Reinstrom [73], multiple reactions (e.g. k steps) provide additional means to allow spontaneous water-splitting with an extra benefit compared with water thermolysis, that oxygen and hydrogen are separately produced, avoiding complex separations at high temperatures. Although practical implications about the minimum number of reactions for such a process; depends upon the maximum process temperature [74]. With solar concentrator temperature of say around 2000K, water splitting can be achieved with only two reactions [75]. This is the goal of the Hydrosol-2 project (Greece, Germany (German Aerospace Center), Spain, Denmark, England) [75] and of the researches of the solar department of the ETH Zurich and the Paul Scherrer Institute (Switzerland) [76]. As shown by Glandt, E.D., Myers, A.L., 1976 [77], the standard thermodynamic values must be unevenly distributed among the reactions.

Hundreds of such cycles have been proposed and investigated. This task has been eased by the availability of computers, allowing a systematic screening of chemical reactions sequences based on thermodynamic databases [78]. The main "families" [79] are based on sulfur and chlorine.

An advantage of the sulfur chemical element is its high covalence. Indeed, it can form up to 6 chemical bonds with other elements such as oxygen (e.g. sulfates), i.e. a wide range of oxidation states. Hence, there exist several redox reactions involving such compounds. This freedom allows numerous chemical steps, with different entropy changes, and thus offers more probabilities to meet the criteria required for a thermochemical cycle (cf. Principles). Most of the first studies were performed in the USA, as an example at the Kentucky University for sulfide-bases cycles [80]. Sulfate-based cycles were studied in the same laboratory [81] and also at Los Alamos National Laboratory [82] and at General Atomics. Significant researches based on sulfates (e.g. $FeSO_4$ and $CuSO_4$) were also performed in Germany [83] and in Japan [84] [85]. However, the cycle which has given rise to the highest interests is probably the (Sulfur-iodine cycle) one (acronym: S-I or I-S) discovered by General Atomics [86].

Few cycles are discussed below.

1.9.1. Iron oxide cycle:

The iron oxide cycle (Fe_3O_4/FeO) is the original two-step thermochemical cycle proposed for use for hydrogen production [87]. It is based on the reduction and subsequent oxidation of iron ions, particularly the reduction and oxidation from Fe^{3+} to Fe^{2+}. The ferrites, or iron oxide, begin in the form of a spinel and depending on the reaction conditions, dopant metals and support material forms either Wüstites or different spinels.

The advantages of the ferrite cycles are: they have lower reduction temperatures than other 2-step systems, no metallic gasses are produced, high specific H_2 production capacity, non-toxicity of the elements used and abundance of the constituent elements.

The disadvantages of the ferrite cycles are: similar reduction and melting temperature of the spinels (except for the hercynite cycle as aluminates have very high melting temperatures), and slow rates of the oxidation, or water splitting, reaction.

1.9.2. Cerium oxide cycle:

The cerium(IV) oxide–cerium(III) oxide cycle or CeO_2/Ce_2O_3 cycle is a two-step thermochemical process that employs cerium(IV) oxide and cerium(III) oxide for hydrogen production. The cerium-based cycle allows the separation of H_2 and O_2 in two steps, making high-temperature gas separation redundant.

The thermochemical two-step water splitting process (thermochemical cycle) uses redox systems:

- Dissociation: $2CeO_2 \rightarrow Ce_2O_3 + 0.5\ O_2$
- Hydrolysis: $Ce_2O_3 + H_2O \rightarrow 2CeO_2 + H_2$

For the first endothermic step, cerium (IV) oxide is thermally dissociated in an inert gas atmosphere at 2,000 °C (3,630 °F) and 100-200 mbar into cerium (III) oxide and oxygen. In the second exothermic step cerium (III) oxide reacts at 400 °C (752 °F)–600 °C (1,112 °F) in a fixed bed reactor with water and produces hydrogen and cerium (IV) oxide.

1.9.3. Copper-chlorine cycle:

The copper–chlorine cycle (Cu–Cl cycle) is a four-step thermochemical cycle for the production of hydrogen. The Cu–Cl cycle is a hybrid process that employs both thermochemical and electrolysis steps. It has a maximum temperature requirement of about 530 degrees Celsius.

The Cu–Cl cycle involves four chemical reactions for water splitting, whose net reaction decomposes water into hydrogen and oxygen. All other chemicals are recycled. The Cu–Cl process can be linked with nuclear plants or other heat sources such as solar and industrial waste heat to potentially achieve higher efficiencies, lower environmental impact and lower costs of hydrogen production than any other conventional technology.

The Cu–Cl cycle is one of the prominent thermochemical cycles under development within the Generation IV International Forum (GIF). Through GIF, over a dozen countries around the world are developing the next generation of nuclear reactors for highly efficient production of both electricity and hydrogen.

The four reactions in the Cu–Cl cycle are listed as follows [88, 89]:

1. $2\ Cu + 2\ HCl\ (g) \rightarrow 2\ CuCl(l) + H_2\ (g)$ (430–475 °C)
2. $2\ CuCl_2 + H_2O(g) \rightarrow Cu_2OCl_2 + 2\ HCl\ (g)$ (400 °C)
3. $2\ Cu_2OCl_2 \rightarrow 4\ CuCl + O_2\ (g)$ (500 °C)
4. $2\ CuCl \rightarrow CuCl_2(aq) + Cu$ (ambient-temperature electrolysis)

Net reaction: $2\ H_2O \rightarrow 2\ H_2 + O_2$

Legend: (g)—gas; (l)—liquid;(aq)—aqueous solution; the balance of the species are in a solid phase. Atomic Energy of Canada Limited has demonstrated experimentally a CuCl electrolyzer in which hydrogen is produced electrolytically at the cathode and Cu(I) is oxidized to Cu(II) at the anode, thereby combining above steps 1 and 4 to eliminate the intermediate production and subsequent transport of solid copper[90].

Approximately 50% of the heat required to drive this reaction can be captured from the reaction itself. The other heat can be provided by any suitable process. Recent research has focused on a cogeneration scheme using the waste heat from nuclear reactors, specifically the CANDU supercritical water reactor [90].

Advantages of the copper–chlorine cycle include lower operating temperatures, the ability to use low-grade waste heat to improve energy efficiency, and potentially lower cost materials. In comparison with other thermochemical cycles, the Cu–Cl process requires relatively low temperatures of up to 530 °C (990 °F). Another significant merit of this cycle is a relatively low voltage (thus low electrical energy expenditure) that is required for the electrochemical step (0.6 to 1.0 V, perhaps even 0.5 if lower current density can be achieved) [91]. The overall efficiency of the Cu–Cl cycle has been estimated to be just over 43% [92], excluding the additional potential gains of utilizing waste heat in the cycle.

Solids handling between processes and corrosive working fluids present unique challenges for the engineering equipment development. Among others, the following materials are being currently used: spray coatings, nickel alloys, glass-lined steel, refractory materials, and other advanced materials [93].

1.9.4. Hybrid sulfur cycle:

The hybrid sulfur cycle (HyS) is a two-step water-splitting process intended to be used for hydrogen production. Based on sulfur oxidation and reduction, it is classified as a hybrid thermochemical cycle because it uses an electrochemical (instead of a thermochemical) reaction for one of the two steps. The remaining thermochemical step is shared with the sulfur-iodine cycle.

The HyS cycle was initially proposed and developed by Westinghouse Electric Corp. in the 1970s [94], so it is also known as the "Westinghouse" cycle. Current development efforts in the United States are being led by the Savannah River National Laboratory.

The two reactions in the HyS cycle are as follows [95]:

$$H_2SO_4(aq) \rightarrow H_2O(g) + SO_2(g) + \frac{1}{2} O_2(g) \qquad \text{(thermochemical, } T > 800\ °C\text{) (1)}$$

$$SO_2(aq) + 2\ H_2O(l) \rightarrow H_2SO_4(aq) + H_2(g) \quad \text{(electrochemical, } T = 80\text{-}120\ °C\text{) (2)}$$

Net reaction: $H_2O(l) \rightarrow H_2(g) + \frac{1}{2} O_2(g)$

Sulfur dioxide acts to depolarize the anode of the electrolyzer. This results in a significant decrease in the reversible cell potential (and, therefore, the electric power requirement) for reaction (2). The standard cell potential for reaction (2) is -0.158 V at 298.15 K, compared to -1.229 V for the electrolysis of water (with oxygen evolution as the anodic reaction) [96].

1.9.5. HYDROSOL:

HYDROSOL (short for Solar Hydrogen via water splitting in advanced monolithic reactors for future solar power plants) is a series of European Union funded projects for the promotion of renewable energy. Its aim is the production of hydrogen using concentrated solar power with a specific thermochemical cycle.

The Fifth Framework Programme for Research and Technological Development (FP5) project HYDROSOL started in December 2002. A pilot-scale solar reactor was designed, built and operated at the German Aerospace Center (DLR) with a solar furnace facility in Cologne (Germany), continuously producing "solar hydrogen".

The FP6 HYDROSOL II a pilot reactor of 100 kW scale for solar thermochemical hydrogen production at the Plataforma Solar de Almería in Spain, which started in November 2005 and has been in operation since 2008.

1.9.6. UT-3 cycle:

The UT-3 (University of Tokyo, Ca-Br-Fe) cycle is a pathway for high temperature hydrogen production. It has been developed by Kameyama and Yoshida [97] and has been studied both theoretically and experimentally since being proposed in 1978.

UT-3 thermochemical cycle is one of the most studied thermochemical hydrogen production cycles in the world [98]. The advantages are easy gas-solid separation and circulation of gases. But it has limited potential for improvement; as already at melting point of Calcium bromide.

The four reactions of UT-3 cycle are as follows.

$CaBr_2(s) + H_2O(g) \rightarrow CaO(s) + 2HBr(g)$ (1)

$CaO(s) + Br2(g) \rightarrow CaBr2(s) + 1/2\ O2(g)$ (2)

$Fe_3O_4(s) + 8HBr(g) \rightarrow 3FeBr_2(s)+ 4H_2O(g) +Br_2(g)$ (3)

$3FeBr_2(s) + 4H_2O(g) \rightarrow Fe_3O_4(s) + 6HBr(g) +H_2(g)$ (4)

The four chemical reactions take place in four adiabatic fixed bed chemical reactors. A bench scale plant was built and operated to produce hydrogen continuously for 200 h [98]. Excess steam and N_2 is used to operate the process in an adiabatic equipment to make sure that membrane separators function as required [99]. Also a reaction model was proposed [100]. The Model Apparatus for the Study of Cyclic Operation in Tokyo (MASCOT) pilot was operated in the late 80's [101]. Nevertheless, the process has the double disadvantage of requiring a reagent preparation unit and increasing the quantity of material by adding an inert phase representing 33-50% of the reactive load [102]. The cycle is improved by adding a recalibration system, and magnetic properties are used to separate the iron loop products within a single reactor [103]. Initially, hydrogen and oxygen were separated by conservative condensation method from the respective gas mixtures [104]. Calcium oxide reactant dispersed and immobilized on a fibrous yttria woven mat [105] was studied. The zirconia-silica composite membranes coated on porous ceramic tubing were durable in the H_2-H_2O-HBr atmosphere at 673 K [106,107]. The cost of hydrogen is variable due to multitude of assumptions for plant sizing. Therefore efficiency of process is best indicator for the prospects of technology [108].

1.9.7. Iodine-Sulfur (I-S) cycle:

I-S cycle was invented at General Atomics in the 1970s [109,110]. The Japan Atomic Energy Agency (JAEA) has conducted successful experiments [111] with the I-S cycle in the Helium cooled High Temperature Test Reactor, a reactor which reached first criticality in 1998, JAEA have the aspiration of using further nuclear high-temperature generation IV reactors to produce industrial scale quantities of hydrogen. Plans have been made to test larger-scale automated systems for hydrogen production. Under an International Nuclear Energy Research Initiative (INERI) agreement, the French CEA, General Atomics and Sandia National Laboratories are jointly developing the iodine–sulfur process. Additional research is taking place at the Idaho National Laboratory, USA as also in Canada, Korea, China, India and Italy.

The iodine–sulfur cycle (I-S cycle) is a three-step thermochemical cycle used to produce hydrogen. I-S cycle consists of three chemical reactions whose net reactant is water and whose net products are hydrogen and oxygen. All other chemicals are recycled. I-S process requires an efficient source of heat.

The three reactions that produce hydrogen are as follows:

$I_2 + SO_2 + 2\ H_2O \rightarrow 2\ HI + H_2SO_4$ (120 °C); (1) Bunsen reaction

The HI is then separated by distillation or liquid/liquid gravity separation.

$2\ H_2SO_4 \rightarrow 2\ SO_2 + 2\ H_2O + O_2$ (850 °C) (2)

The water, SO_2 and residual H_2SO_4 must be separated from the oxygen byproduct by condensation.

$2\ HI \rightarrow I_2 + H_2$ (450 °C) (3)

Iodine and any accompanying water &/or HI are separated by condensation, and the hydrogen product remains as a gas.

Net reaction: $2\ H_2O \rightarrow 2\ H_2 + O_2$

The iodine and sulfur compounds are recovered and reused, hence the consideration of the process as a cycle. This I-S process is a chemical heat engine. Heat enters the cycle in high-temperature endothermic chemical reactions (2) and (3), and heat exits the cycle in the low-temperature exothermic reaction (1). The difference between the heat entering and leaving the cycle exits the cycle in the form of the heat of combustion of the hydrogen produced.

The characteristics of the I-S process can be described as follows:

- All fluid (liquids, gases) process, therefore well suited for continuous operation;
- High utilization of heat predicted (about 50%), but very high temperatures required (at least 850 °C);
- Completely closed system without byproducts or effluents (besides hydrogen and oxygen);
- Corrosive reagents used as intermediaries (iodine, sulfur dioxide, hydriodic acid, sulfuric acid); therefore, advanced materials needed for construction of process equipment;
- Suitable for application with solar, nuclear, and hybrid (e.g., solar-fossil) sources of heat;
- More developed than competitive thermochemical processes (but still requiring significant development to be feasible on large scale).

I-S cycle involves operations with corrosive chemicals at temperatures up to about 1,000 °C (1,830 °F). The selection of materials with sufficient corrosion resistance under the process conditions is of key importance to the economic viability of this process. The materials suggested include the following classes: refractory metals, reactive metals, superalloys, ceramics, polymers, and coatings [112,113]. Some materials suggested include tantalum alloys, niobium alloys, noble metals, high-silicon steels, several nickel-based superalloys, mullite, silicon carbide (SiC), glass, silicon nitride (Si_3N_4), and others. Recent research on scaled prototyping suggests that new tantalum surface technologies may be a technically and economically feasible way to make larger scale installations [114].

The iodine-sulfur cycle has been proposed as a way to supply hydrogen for a hydrogen-based economy. With an efficiency of around 50% it is more efficient than electrolysis, and it does not require hydrocarbons like current methods of steam reforming but requires heat from combustion, nuclear reactions, or solar heat concentrators.

Thermo-chemical process such as I-S cycle [115-119] is an efficient and environmentally cleaner way to produce hydrogen without use of fossil fuels when coupled to a high temperature nuclear reactor [120-122] or solar energy source [123] or by hybrid solutions including both.

I-S cycle is reviewed including experimental data obtained at JAERI on the chemistry of each reaction step, product separations and corrosion resistance of structural materials [124].

The French “Commissariat a` l’Energie Atomique” (CEA) has been involved in the I-S cycle in a research programme through theoretical and laboratory studies and through the development of a laboratory scale hydrogen production loop [125].

1.9.7.1. Bunsen reaction:

Iodine-Sulfur (I-S) process [126-130] is a closed cycle in which water is decomposed via chemical reactions using intermediate elements which are recycled. In this process Bunsen reaction is the prime reaction as shown in (1).

Bunsen reaction is an exothermic reaction producing two immiscible acid phases viz. sulfuric acid and hydriodic acid, at high iodine concentration [131]. The sulfuric acid decomposition step is an endothermic two stage reaction: first sulfuric acid dehydration to produce sulfur trioxide, then sulfur trioxide catalytic decomposition [132-134] to produce sulfur dioxide and oxygen. Hydrogen iodide is decomposed in vapour phase producing hydrogen [135,136], which is also an endothermic reaction.

Bunsen reaction is a gas-liquid reaction system. Reactants iodine, water and sulfur dioxide (SO_2) form products sulfuric acid and hydriodic acid [137]. Reaction stoichiometry is given by reaction (1). Bunsen reaction is fast in the range 293K - 393K. At higher temperature the reaction is reversible. However, in this temperature range conversion is not equilibrium limited, so complete conversion is possible. By operating at non-stoichiometric conditions and using a large excess of iodine and water, the conversion is greatly improved according to reaction (4). The excess iodine shifts Bunsen reaction equilibrium forward to produce more acids. Excess iodine also aids the two acids produced to spontaneously separate into two aqueous solutions. The phase separation occurs due to the formation of poly-hydriodic acid [138]. Excess of water also causes the equilibrium to shift forward to produce more acids, but it also causes a substantial increase in the reaction enthalpy due to acid dilution. This modified Bunsen reaction is thermodynamically favorable.

$$9I_{2(l)}+SO_{2(g)}+16H_2O_{(l)} = (H_2SO_4+4H_2O)_{(aq)} + (2HI+10H_2O+8I_2)_{(aq)} \qquad (4)$$

This is a heterogeneous (gas-liquid) reaction system, in which sulfur dioxide first dissolves in the reaction liquid (water) and then reacts with other reactants [139].

Bunsen reaction is a crucial step in the I-S cycle since the optimization of H_2O and I_2 excesses determines a good separation between the two acid solutions, and a favorable reaction rate for controlling hydrogen production rate, and a low energy consumption for separating and recycling H_2O and I_2 excesses. So far, most efforts have been focused mainly on the thermodynamic performance of the Bunsen section.

The thermodynamic and kinetics for Bunsen reaction have been studied using the SO_2/N_2 gas mixtures fed into the I_2/H_2O aqueous solution in a jacketed stirred reactor. A fundamental kinetic model is proposed to explain the kinetic route of the Bunsen reaction, ignoring the effect of mass transfer and diffusion between SO_2 and reactant solution, and the dilution effect of H_2O [138].

The effect of operating parameters, including reaction temperature, I_2 and H_2O concentrations, and H_2SO_4/HI molar ratio, on liquid-liquid equilibrium (LLE) phase separation characteristics were investigated. It was found that an increase in I_2 concentration and decrease in H_2O concentration improved the LLE phase separation [132,140-142].

An increase in molar ratio of H_2SO_4/HI favored the separation and resulted in dehydration of the HIx phase [141].

The allowable bound of I_2 content for phase separation was widened with an increase in the reaction temperature [143,144].

An optimal operating window of 4-6 mol excess iodine and 11-13 mol excess water within a temperature range of 330-350 K has been proposed by Lee et al. [140] according to collating experimental data from literature as well as conducting their own experiments.

A thermodynamic model has been proposed to understand the chemo-physical behavior of the Bunsen reaction system and the chemicals equilibrium in terms of iodine and sulfur species separation [145].

The addition of a precipitation agent has been proposed to separate the two acids [146]. Although a significant reduction in I_2 excess was obtained, large amounts of solid handling would be required in this process.

The use of solvents, such as TBP, PSDVB, Toluene and ionic liquids for the Bunsen reaction was considered as a method to release HI from the reaction [147]. However, the further solvents need to be investigated to find one that both has the ability to extract HI and is stable to hot HI to allow recovery.

In I-S cycle, side reactions from HI, H_2SO_4 and I_2 mixture solution were investigated experimentally in operating temperature range [148].

1.9.7.2. Bunsen Reactor:

The reactants sulfur dioxide, water and iodine; can be added to the reactor either co-currently or counter-currently. In co-current reactor, chemicals are added to one end of the reactor and products are removed from other end. The product acids are separated in subsequent separation column. In counter-current reactor both reaction and acid separation take place in the same reactor. Reactants iodine and water are fed from the top; sulfur dioxide is fed from the bottom. The lighter product namely sulfuric acid is removed from the top, while heavier product, hydriodic acid is removed from the bottom most part of the reactor.

There are different reactor alternative to carry out Bunsen reaction in continuous mode for acid production and/or separation such as stirred tank reactor, packed tubular reactor (co-current & counter-current), electrochemical reactor etc.

The concept of a concurrent heat exchange Bunsen reactor was demonstrated by GA in 1981 [116], and subsequently by JAERI in 2003 [124].

GA constructed a staged counter-current flow reactor column [117] to enrich 50% H_2SO_4 to 57% H_2SO_4 with liquid iodine as feed from top and 50% H_2SO_4 as bottom feed. Several experiments were run with this equipment; most were to establish flow control information. The apparatus was operated so that meaningful data with fully describable flow and stirring parameters were available.

The use of an electrochemical membrane cell for the Bunsen reaction has a large potential to reduce the excess I_2 and H_2O [149-152]. However, the significant cross-contamination of the two acids was still seen. There is a serious problem when scaling these electrochemical membrane cells to a plant size.

The Bunsen reactor is sized by CEA, as countercurrent liquid-liquid contactor (extraction equipment) with mechanical stirring, using different correlations described by Godfrey & Slater [125]. An alternative flow sheet is currently being considered by CEA involving a countercurrent multiphase reactor [153]. Aside from $SO_{2,}$ the chemical system includes two solvents (excess water and excess iodine) and two solutes (H_2SO_4 and HI)$_.$ Water and iodine being almost immiscible, allow the operation to be considered a reactive liquid-liquid extraction in which water is the solvent for H_2SO_4 and iodine the solvent for HI. In counter-current streams, circulating phases are never at chemical equilibrium theoretically resulting in a possible increase in reaction rate by modifying the reactants amounts (particularly SO_2).

Republic of Korea carried out Bunsen reaction using counter-current flow reactor [154-155]. Ceramic packing material of Raschig ring was introduced in the reactor to avoid channeling of SO_2 gas. Solid I_2 was introduced from the top at intervals and gaseous SO_2 and water were fed continuously from the bottom. In the study composition variation of discharg at top and bottom were studied by varying SO_2 feed rate, temperature and I_2/H_2O ratio and it's concluded that the composition of each phase collected are similar irrespective of SO_2 flow rate and there is an increase in purity with increase in I_2/H_2O ratio.

Kinetic study in semi batch reactor was carried out in BARC, India [156].

Design of tubular flow reactor with concurrent operation is discussed by Sandia National Laboratories, USA [157].

1.10. Motivation for this work:

Information on Bunsen reaction and simultaneous phase separation in single equipment, thereby integrating one unit process and one unit operation, is not available in literature. Study of such a kind of equipment for Bunsen reaction and phase separation on continuous operation mode, and modeling of the equipment, would be initial step towards realizing the I-S process.

A new countercurrent reactor concept has been proposed to implement the Bunsen reaction and phase separation.

Agitated tubular Bunsen reactor (ABR), operating in counter-current mode, is one of the reactor alternatives to carry out Bunsen reaction in continuous mode. In this reactor, both, reaction as well as phase separation occurs in single equipment. Thus, process integration is the possibility by combining reaction as well as acids separatioin in single equipment. Also, it has the potential importance as Bunsen reactor in Iodine-Sulfur thermo-chemical cycle because of its improved heat and mass transfer characteristics.

Chapter II

Experimental Techniques
&
Methods

2.1. Methodology of work:

Experimental techniques and methods to accomplish desired objective have been carried out in two parts viz. semi batch experiments in static mixer reactor and continuous experiments in agitated Bunsen reactor.

2.1.1. Semi-batch Bunsen reaction experiments:

In a small diameter tube with static mixer, semi batch experiments have been carried out. Known quantity of Sulfur dioxide (and nitrogen) was bubbled through the mixture of water and iodine at different temperature and pressure of reactor. Through these experiments overall reaction rate and conversion were be found out and mathematical model was attempted to predict experimental results.

Semi-batch experiments are relatively easy to carry out; therefore they were attempted initially. These experiments gave insight into overall reaction rate and conversion as this information is not available in the literature.

2.1.2. Counter-current Bunsen reaction experiments in agitated type Bunsen reactor:

The plug flow reactor gives the maximum conversion in the minimum reactor volume. Therefore agitated type reactor was constructed to achieve plug flow in the reactor. As exothermic Bunsen reaction was to be studied in counter-current operation mode, the constructed reactor was studied as follows.

2.1.2.1. Residence time distribution (RTD) studies:

RTD studies were carried out for the reactor at different liquid flows and different agitation level. Fluid as water with NaCl solution as tracer was used. The conditions were known, wherein reactor can be operated near to the plug flow behavior.

2.1.2.2. Heat transfer studies:

During Bunsen reaction exothermic heat is to be continuously removed to maintain isothermal conditions in the reactor. Heat removal capacity of the reactor was studied at different liquid flows and agitation level. This was useful in limiting the exothermic reaction heat thereby flow of sulfur dioxide.

2.1.2.3. Phase separation studies:

Product acids viz. sulfuric acid and hydriodic acid once formed should get separated in the reactor which would be operating in counter-current mode. By feeding these acids in counter-current mode, phase separation studies at different flow rates of acids and agitation speed were carried out. This was useful to determine the range of operating conditions where separation of acid phases would be possible.

2.1.2.4. Bunsen reaction studies:

Finally, Bunsen reaction experiments were carried out in counter-current mode of operation. Sulfur dioxide was fed from the bottom portion of the reactor; water and iodine were fed from the top portion of the reactor. The product acids, sulfuric acid and hydriodic acid were collected from top and bottom respectively.

Experiments were carried out at different flow rates of sulfur dioxide (pure as well as diluted), different temperature and different partial pressure. Conversion and reaction rate were obtained experimentally.

The reactor model was proposed and output of mathematical model was validated with experimental results.

2.2. Experimental design and installation:

The basis of experimental design, sizing of apparatus followed by design & installation of experimental set-up for static mixer reactor and agitated Bunsen reactor is discussed below.

2.2.1. Static mixer reactor set-up:

2.2.1.1. Basis of experimental design:

Initial experiments were planned in semi-batch mode of operation, which were relatively easy to perform. Moving parts were avoided and instead, static mixer was used to do the mixing job. Experiments at different temperature, different pressure and dilution of sulfur dioxide were planned.

2.2.1.2. Sizing of equipment:

To limit quantity of reactants, a small diameter (19 mm ID) metal tube in tantalum MOC was chosen. Stainless steel pipe of 40 mm nominal diameter enclosed the tantalum tube, with flanges on both the ends. Flange to flange distance being 270 mm, for one section. The annular space was used for the flow of heating/cooling fluid. Four sections, one above the other were connected with flanges. Each section was provided with set of twisted blade static mixer elements as shown in Fig. 2.1. The details of static mixer chosen are:

MOC : PTFE

OD / Length of twisted blade : 18 mm / 42 mm

Model : 1-KMR-PTFE-6

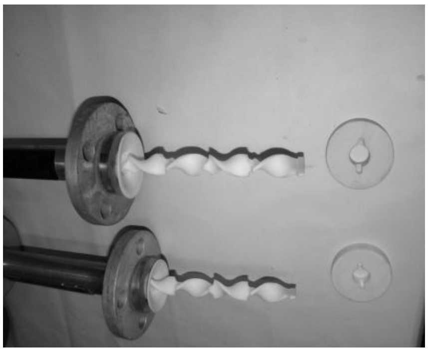

Fig. 2.1: Section of static mixer metallic tubular reactor

2.2.1.3. Design & installation of experimental set-up:

Block diagram of the experimental set-up is shown in the Fig. 2.2. It consists of Bunsen reactor along with pressure and temperature control systems, gaseous reactant (sulfur dioxide) feeding system and un-reacted sulfur dioxide scrubbing system.

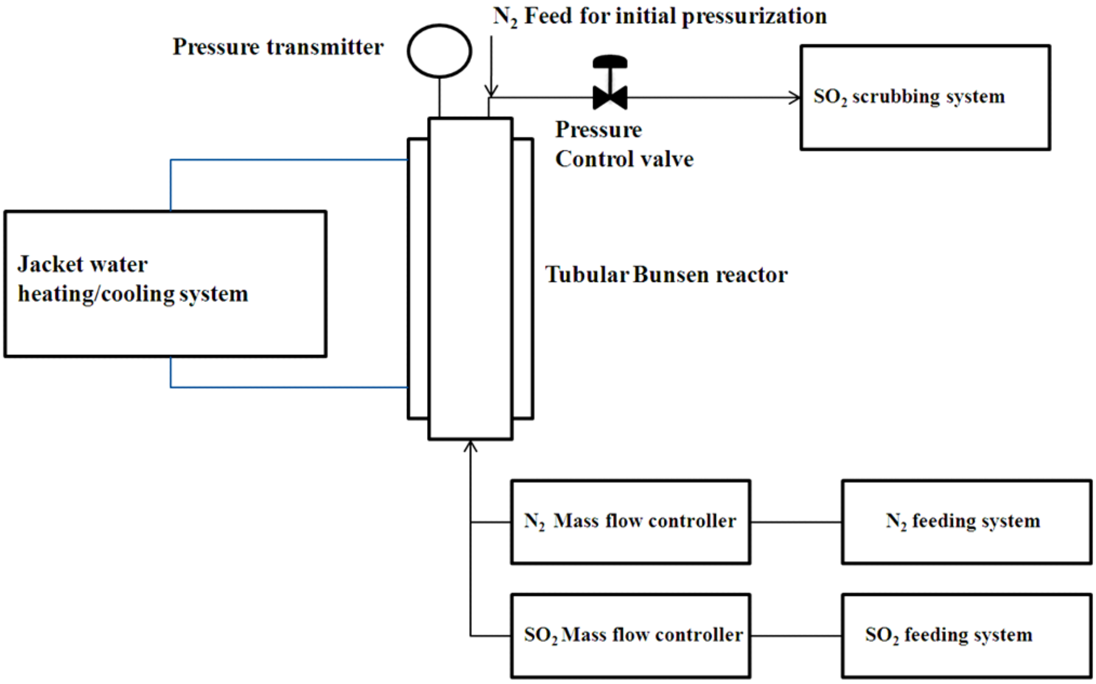

Fig. 2.2: Block diagram of semi-batch experimental set-up

Sulfur dioxide and nitrogen were fed from the cylinder through regulator and flow was controlled by mass flow controller (Bronkhost make). KOH bubbler was used to scrub unreacted sulfur dioxide escaping the reactor. Hot / cold water system circulates hot or cold water through the jacket to bring the reactants to the desired temperature and maintain the temperature. Pressure transmitter was provided on the top gas portion of the reactor. Pressure control loop maintains the desired pressure in the reactor, with the help of control valve and a controller. The provision was given on the top of the reactor to pressurize it with nitrogen. Top flange was used for feeding the initial charge of liquid reactants which was made leak tight before start of the experiment.

2.2.2. Agitated Bunsen reactor set-up:

2.2.2.1. Basis of experimental design:

Agitated Bunsen reactor set-up was designed to carry out all envised experiments such as RTD studies, heat transfer studies, phase separation studies and counter-current Bunsen reaction experiments in the same set-up. Sampling points were provided at various locations in feed lines, reactor, product lines and alkali scrubber. Experiments at different temperature, different partial pressure and dilution of sulfur dioxide with varying flow were planned.

2.2.2.2. Sizing of equipment:

Agitated tubular Bunsen reactor (ABR) is to operate in counter-current and in continuous mode. In this reactor, reaction as well as phase separation is aimed in single equipment.

ABR can be visualized as a set of continuous stirred reactors installed vertically in series. Proposed ABR was a tubular reactor with a long shaft axially provided inside with turbine type mixing blades for good radial mixing of fluids. Mixing blades were within a pair of baffles with openings, thus resembling a CSTR. The shaft with mixing blades was connected to the motor with ‘rpm’ regulator to maintain agitation speed. Reactor was provided with internal helical coil to remove the exothermic heat of reaction. The ABR was provided with many number of nozzles viz. three nos. feed nozzles, three nos. outlet nozzles for acids and gases, two nozzles for cooling water inlet and outlet, two nos of sampling nozzles and openings for incorporating temperature sensors.

Based on concept of rotating disc contactor, ABR has been sized. Impellers chosen were flat blade turbine type with four numbers of blades, to give good radial mixing. Static baffle plates were provided and held together with the help of tie rods. Perforations on the baffle plates allow vertical upward movement of light phase and downward movement of heavy phase. The fractional open cross sectional area for baffle was around 25 % which gave much lower flow constriction.

Taking into consideration above requirement and fabricability, dimensions of the fabricated agitated Bunsen reactor:

Diameter of tubular column : 84 mm

Type and no of blades : Turbine, 4 nos

Diameter of turbine blade : 26 mm

OD/ID of baffle plate : 50 mm / 21 mm

Size and no of perforations on baffle : 3 mm and 12 numbers

Mixing stages : 6 stages

Diameter of helical coil : 76 mm

Cooling tube OD/ID : 6.5 mm / 3 mm

Number of helical turns : 15

Tubular reactor and internal helical coil were made of glass. Turbine blades, baffles and shaft were made of PTFE.

2.2.2.3. Design & installation of experimental set-up:

The block diagram of the agitated Bunsen reactor set-up is shown in Fig 2.3. Elaborate safety was planned as hazardous chemicals would be handled during various Bunsen reaction experiments. Therefore the set-up was installed in glass box with exhaust system and with the provision of adequate air changes. Gas sensors for sulfur dioxide, hydriodic acid and iodine were installed to detect any leakages in the system during operation, so that in case of any eventuality corrective measures could be taken. Sand trays were provided below Bunsen reactor, chemical feed tanks and alkali tank to contain and collect spillages of chemicals, if any. The PLC / SCADA system was connected to the set-up, to control various feed flows and log various data such as flows of feed water, SO_2, nitrogen, Iodine, flow and temperature of heating/cooling water, temperature of reactor.

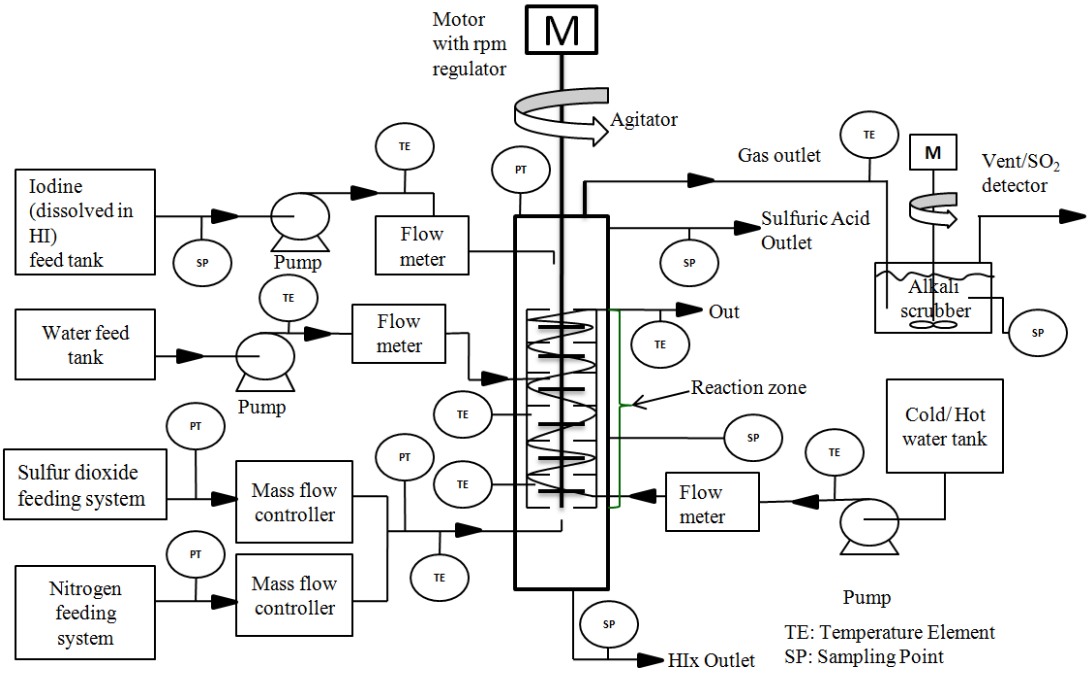

Fig. 2.3: Block diagram of agitated Bunsen reactor experimental set-up

Sulfur dioxide and nitrogen were fed from the cylinder through regulator and flow was controlled by mass flow controller (Bronkhost make). Through metering pump iodine (dissolved in HI) and water were fed to reactor from respective feed tanks. KOH bubbler was used to scrub unreacted sulfur dioxide escaping the reactor. Hot/cold water system circulated hot or cold water through helical coil to bring the reactants to the desired temperature and maintain the temperature. Pressure transmitter was provided on the top gas portion of the reactor. Agitator shaft was connected to the motor with rpm regulator.

Flow measurement error of SO_2, N_2 and iodine were 0.5% of flow rate and that of water was 1% of flow rate. Measurement error of temperature was ±0.5 °C and that of pressure was less than 0.5%.

2.3. Analytical methods:

Analysis of feed solution iodine (dissolved in HI), product acids viz. sulfuric acid and hydriodic acid required to be carried out for various species such as I^-, H^+ and I_2. Alkali solution was to be analysed for KOH. For RTD experiments, NaCl solution was to be analysed.

Analysis of samples for above species was done in potentiometric titration unit (Metrohm, 836 Titrando). Error in analysis of chemicals in potentiometric titration unit was < 1%.

2.3.1. H^+ analysis:

Sulfuric acid analysis was carried out using following standards.

Primary standard	: Potassium Hydrogen Pthalate (KHP) ($KHC_8H_4O_4$)
Secondary standard	: Sodium Hydroxide (NaOH)
Electrode	: pH glass electrode

Secondary standard NaOH was standardised with known concentration of standard primary solution of Potassium Hydrogen Pthalate.

$$KHC_8H_4O_4 + NaOH \rightarrow KNaC_8H_4O_4 + H_2O$$

With the digital pipette, sample was quantified, to it distilled water was added up to sufficient level. pH glass electrode was used to analysis the sample with standardised NaOH solution in automated potentiometric titration unit.

$$2NaOH + H_2SO_4 = Na_2SO_4 + 2H_2O$$

2.3.2. HI (I^-) analysis:

HI acid analysis was carried out using following standards.

Primary standard	: Sodium Chloride (NaCl)
Secondary standard	: Silver Nitrate ($AgNO_3$)
Electrode	: Ag_2S electrode

Secondary standard $AgNO_3$ solution was standardised with known concentration of standard primary solution of Sodium Chloride.

$$NaCl + AgNO_3 \rightarrow AgCl + NaNO_3$$

With the digital pipette, sample was quantified, to it distilled water was added up to sufficient level. Ag_2S glass electrode was used to analysis the sample with standardised NaOH solution in automated potentiometric titration unit.

$$HI + AgNO_3 \rightarrow AgI + HNO_3$$

2.3.3. Iodine (I_2) analysis:

Iodine analysis was carried out using following standards.

Primary standard : Potassium Iodate (KIO_3)

Secondary standard : Sodium thiosulphate pentahydrate ($Na_2S_2O_3.5H_2O$)

Electrode : Pt ring electrode

Secondary standard Sodium thiosulphate pentahydrate solution was standardised by adding known quantities of Potassium iodide salt and Sulfuric acid and then tritrated with known concentration of standard primary solution of Potassium Iodate.

$$KIO_3 + 5KI + 3H_2SO_4 \rightarrow 3I_2 + 3H_2O + 3K_2SO_4$$

$$Na_2S_2O_3 + 2I_2 \rightarrow 2NaI + S_4O_6^{2-}$$

With the digital pipette, sample was quantified, to it distilled water was added up to sufficient level. Pt ring electrode was used to analysis the sample with standardised Sodium thio sulphate solution in automated potentiometric titration unit.

$$Na_2S_2O_3 + 2I_2 \rightarrow 2NaI + S_4O_6^{2-}$$

2.3.4. KOH analysis:

KOH analysis was carried out using following standards.

Primary standard : Standard NaOH solution

Secondary standard : Oxalic Acid $(COOH)_2$

Electrode : pH glass electrode

Secondary standard of Oxalic Acid solution was standardised with known concentration of standard primary solution of NaOH.

With the digital pipette, sample was quantified, to it distilled water was added up to sufficient level. pH glass electrode was used to analyse the sample with standardised Oxalic Acid solution in automated potentiometric titration unit.

$$C_2H_2O_4 + 2KOH \rightarrow K_2C_2O_4 + 2H_2O$$

2.3.5. NaCl analysis:

NaCl analysis was carried out using following standards.

Primary standard : Sodium Chloride (NaCl)

Secondary standard : Silver Nitrate ($AgNO_3$)

Electrode : Ag_2S electrode

Secondary standard of Silver Nitrate solution was standardised with known concentration of standard primary solution of Sodium Chloride.

$$NaCl + AgNO_3 \rightarrow AgCl + NaNO_3$$

With the digital pipette, sample was quantified, to it distilled water was added up to sufficient level. Ag_2S electrode was used to analyse the sample with standardised Silver Nitrate solution in automated potentiometric titration unit.

$$NaCl + AgNO_3 \rightarrow AgCI + NaNO_3$$

2.4. Fluid properties:

Fluid properties of acids and mixture of acids were derived from Chemical process simulation software ‘PROSIM’, France.

Chapter III

Reaction Studies in Static Mixer Reactor and Modeling

3.1. Introduction:

In the present chapter effects of high pressure and elevated temperature on overall Bunsen reaction kinetics is presented. This information is not available in the literature.

3.2. Experimental:

Experiments were carried out in metallic tubular static mixer reactor in semi-batch mode where SO_2 gas (pure SO_2 or SO_2 diluted with nitrogen) was continuously bubbled through a batch of uniform liquid reactant (iodine and water) [158].

Block diagram of the experimental set-up shown in the Fig. 2.2 in chapter II. It consists of Bunsen reactor along with pressure and temperature control systems, gaseous reactant (sulfur dioxide) feeding system and un-reacted sulfur dioxide scrubbing system. Metallic tubular Bunsen reactor having static mixer element inside is shown in Fig. 3.1.

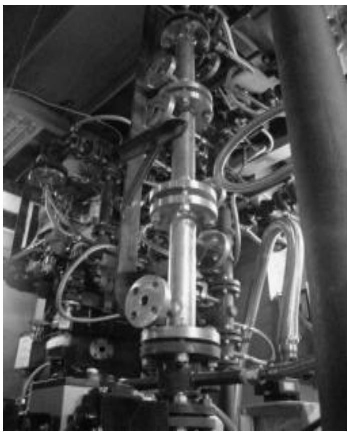

Fig. 3.1: Tubular Bunsen reactor with static mixer element inside

Around 450 ml of liquid reactant (iodine and water) was charged from the top of the reactor. Then the reaction system was purged with nitrogen gas in order to displace the air in the system. Jacket water heating / cooling system was started with a desired temperature set point. Pressure was set as per the requirement. Reaction liquid was brought to the desired temperature with the hot water flowing through the jacket of the reactor. For high pressure experiments (2 and 3.5 bar (g) experiments), pressurization of the system was done with nitrogen gas. Temperature of the jacket water was then reduced to a lower value and then sulfur dioxide (pure or diluted with nitrogen gas) was bubbled continuously from the bottom of the metallic tubular reactor. System pressure was maintained by the control system associated with the outlet of the reactor line. Un-reacted SO_2 was scrubbed continuously in scrubbing system containing potassium hydroxide and the samples were taken at different time intervals for analysis. Experiments were carried out by varying the operating parameters such as pressure (2 bar (g) to 3.5 bar (g)), temperature (40 ^{o}C to 80 ^{o}C) and SO_2 partial pressure (82 % & 100 %).

Flow measurement error of SO_2 was 0.5%. Measurement error of temperature was ±0.5 °C and that of pressure was 0.5%. Analysis of samples for I^-, H^+ and I_2, collected in experimentation, was done in potentiometric titration unit (Metrohm, 836 Titrando). Error in analysis of chemicals in potentiometric titration unit was < 1%.

3.3. Modeling of reaction system:

'Tanks-in-series' model, one of the non ideal reactor models has been chosen to represent reaction system, in order to extract the reactor performance. Tubular reactor, with static mixer element inside and jacket cooling outside, for Bunsen reaction is a complicated reaction system where heat transfer, mass transfer and chemical reaction take place simultaneously. Ideal CSTR has been considered in assumed infinite mixing zones in reactor.

Following are the assumptions for considering non-ideal reactor model for tubular Bunsen reactor:

1. The flow of SO_2 gas through the reactor in plug flow mode i.e. gas assumed to be well mixed in radial direction due to the presence of static mixer element inside a small diameter reactor tube. Static mixer uniformly distributes the fluid flow in radial direction and thereby enhancing the radial mixing.
2. The reaction liquid at uniform temperature.

3. The reaction is first order with respect to SO_2 in presence of excess iodine and water.
4. The reaction system can be modeled as an infinite number of ideal continuous stirred tank reactors (CSTRs) [162-164] in series.

Let the mixing zones be CSTR 1, 2, 3 ….∞ with reaction rate per unit volume of each CSTR ($-r_A''''$) as $-r_1$, $-r_2$, $-r_3$…..$-r_\infty$ as shown in Fig. 3.2. F_{Ain} & F_{Aout} are the molar flow rate of SO_2 in and out of reactor, F_{N2} is the molar flow rate of nitrogen gas, $F_{Total\ in}$ & $F_{Total\ out}$ are the total molar flow rate of gas in and out of the reactor and P_{Ain} & P_{Aout} are the partial pressure of SO_2 gas at inlet and outlet of reactor. Let V_r be the volume of assumed CSTR, then

$$\text{Loss of A from the gas in volume element, } V_r = (F_{Ain} - F_{Aout}) = -r_A''''V_r \quad (3.1)$$

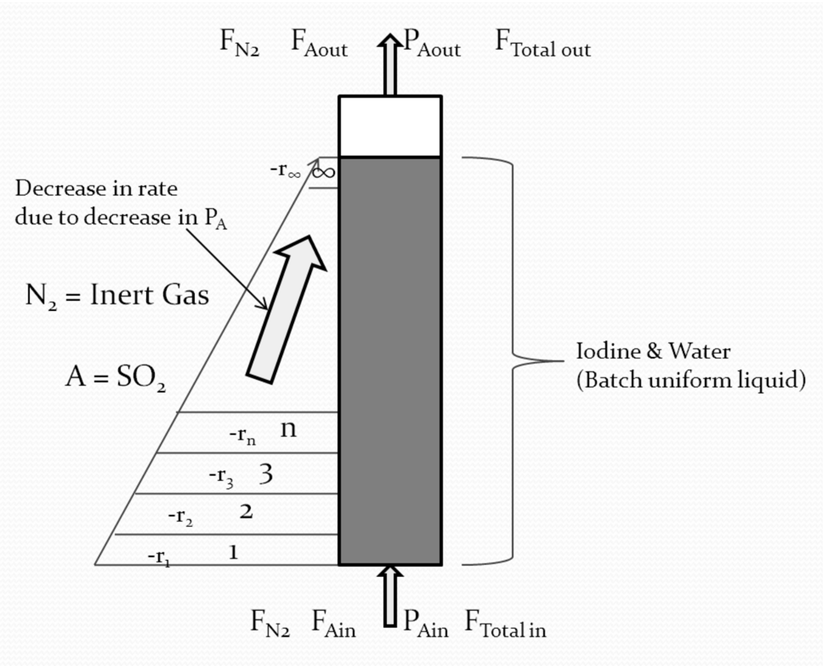

Fig. 3.2: ‘Tanks in series’ model for reactor

The heterogeneous reaction in each CSTR is described based on two film theory wherein the absorption of a diluted gaseous reactant (SO_2 + nitrogen) is taking place in an excess liquid reactant (H_2O) and getting reacted in liquid phase. Fig. 3.3 shows the absorption of a diluted gaseous reactant A (SO_2) in an excess liquid reactant B (H_2O) and getting reacted in liquid phase. Here three resistances are in series; first one is the gas film resistance second one is the liquid film resistance and third is the reaction resistance. Thus the solubility of the gaseous reactant and mass transfer effect from liquid film to the reaction plane should be accounted [159-161].

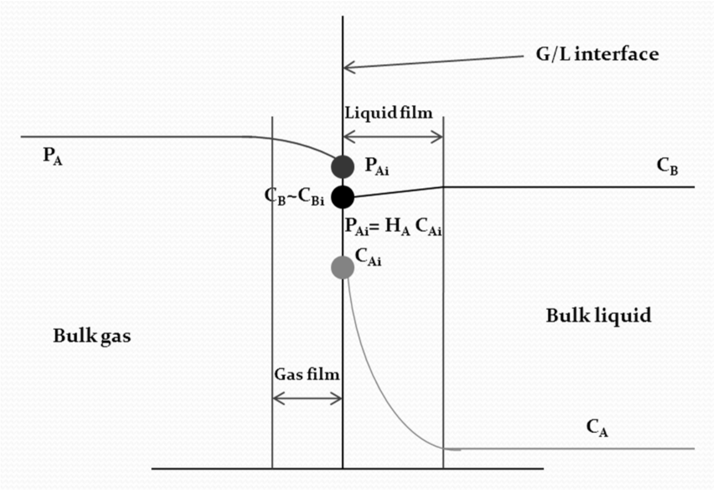

Fig. 3.3: Absorption of A in the liquid and the reaction in the liquid based on two film theory when a diluted reactant gas (A) is reacting with excess liquid reactant

Reaction rate ($-r_A''''$) for the heterogeneous reaction system accounting all three resistances [162] is given by

$$-r_A'''' = \frac{P_A}{\left(\frac{1}{K_{Ag}a} + \frac{H_A}{K_{Al}aE} + \frac{H_A}{kf_l}\right)} \qquad (3.2)$$

Where P_A is the partial pressure of SO_2 gas at any location in the reactor, H_A is the phase distribution coefficient or Henry’s law constant for the gas phase system, K_{Ag} & K_{Al} are the mass transfer coefficients for the gas phase and liquid phase respectively, ‘a’ is the gas-liquid interfacial area per unit volume of contactor, ‘E’ is enhancement factor for mass transfer with reaction, ‘f_l’ is the liquid holdup and ‘k’ is reaction rate constant. Value of ‘k’ reaction rate constant lies between 10^2 – 10^3 s^{-1} [124] and value on lower side i.e. 10^2 s^{-1} has been considered for calculations. Dependent parameters in Equation (3.2) such as K_{Ag} ,

K_{Al} , ‘a’ , E and H_A were calculated by choosing appropriate standard equations and empirical correlations which are given in Annexure 1.

Equations (3.1) & (3.2) describe the reaction system. Equation (3.1) is the material balance for the CSTR system and Equation (3.2) is the kinetic model of Bunsen reaction system which accounts for both reaction kinetics as well as mass transfer kinetics. F_{Aout} from each CSTR is calculated from Equation (3.1) & (3.2), which is the F_{Ain} for the next CSTR. Sulfur dioxide (pure or diluted) enters at the bottom of CSTR 1, where the reaction rate, $-r_1$ is supposed to be the highest as represented in Fig. 3.2. The effect of partial pressure, temperature and velocity of SO_2 gas or SO_2 + N_2 gas mixture which are considered here are the three independent parameters of the system.

3.4. Results and Discussion:

Experimental conversion of SO_2 has been derived from sulfuric acid formed in product solution and SO_2 scrubbed in alkali scrubber and total SO_2 feed as shown in Table 3.1.

Table 3.1 – Experimental conversion of sulfur dioxide 1.125 moles fed for each experiment

Serial No.	H_2SO_4 produced (moles)	% Conversion (Experimental)	SO_2 scrubbed (moles)	SO_2 unaccounted %
1	1.1068	98.38	0.0113	0.61
2	1.1179	99.37	0.000	0.63
3	1.1205	99.60	0.000	0.4
4	1.0903	96.92	0.0337	0.09
5	1.0570	93.95	0.05	1.6
6	0.9	80.00	0.175	4.4
7	0.9394	83.50	0.28125	2.3

Table 3.2 shows the experiments carried out with pure SO_2 and diluted SO_2 (18.6% dilution with N_2) at different temperatures and pressures with various combinations. Experiments were carried out with constant SO_2 flow of 1.5625E-3 moles/s (0.1 g/s). Experiment nos. 1- 5 were carried out with pure SO_2 and experiment nos. 6 & 7 were carried out with diluted SO_2. For the fixed molar flow of SO_2, pressure was varied from 0.3 bar to 3.5 bar, temperature from 40^oC to 80^oC and nitrogen flow for last two experiments was set at 0.3571 milli moles/s. Average reaction rate in 'moles/s', for all the experiments carried out, is calculated experimentally from the moles of sulfuric acid produced in the collected product solution in semi-batch operation time. SO_2 conversion is calculated experimentally by material balance, i.e. SO_2 fed, sulfuric acid produced and SO_2 scrubbed in KOH solution.

'Tanks in series' model calculates reaction rates in each CSTR $(-r_A'''')$ having reactor volumes 'V_r'. Average reaction rate from the model in 'moles/s' was calculated as summation of products of reaction rate and corresponding CSTR volume ($\sum -r_A''''V_r$) for different experiments carried out. There is no gas film resistance for the experiments carried out with pure SO_2 (Experiment nos. 1 - 5). All three resistances were considered for calculation of $-r_A''''$ in each CSTR for the experiments carried out with diluted SO_2 (Experiment nos. 6 & 7).

SO_2 conversion was calculated with the 'Tanks in series' model from the difference between molar flow rate at the inlet of CSTR1 and at the outlet of last CSTR.

Discrepancy in percentage between experimental results and prediction with 'Tanks in series' model are reported in Table 3.2 for all the experiments carried out. From the table, it is seen that introduction of gas film resistance decreases SO_2 conversion significantly. There is a discrepancy of 16% to 20 % when accounting this effect with available correlation for gas film mass transport. For the preliminary Bunsen reaction experimental study at high pressure and elevated temperature and a first attempt to model the reactor using 'Tanks in series' model, this discrepancy is acceptable. Accounting gas film resistance in heterogeneous reaction kinetics with improved correlations needs to be done in further studies.

Table 3.2 - Comparison of the experimental result with the output of Mathematical Model

Serial No.	Operating Condition		Molar flow rate*10^3(moles/s)		% Dilution of SO_2	Average Reaction rate*10^3 (Experimental), moles/s	Average reaction rate*10^3 (Model), moles/s	% discrepancy w.r.t model rate	% Conversion (Experimental)	% Conversion (Model)	% discrepancy w.r.t Model conversion
	P, bar (g)	T, °C	SO_2	N_2							
1	0.3	40	1.5625	0	0	1.41198	1.5372	8.15	98.38	100	1.62
2	2	40	1.5625	0	0	1.48707	1.5527	4.23	99.37	100	0.63
3	3.5	40	1.5625	0	0	1.50023	1.5562	3.60	99.60	100	0.4
4	2	60	1.5625	0	0	1.48481	1.5144	1.95	96.92	100	3.08
5	2	80	1.5625	0	0	1.47992	1.4936	0.916	93.95	100	6.05
6	0.3	40	1.5625	0.3571	18.6	1.2500	1.3800	9.42	80.00	100	20
7	2	40	1.5625	0.3571	18.6	1.3000	1.4000	7.14	83.50	100	16.5

3.4.1. Experiments with pure SO_2

Profile of decrease in reaction rate in moles/s ($-r_A''''V_r$ values in CSTRs) is plotted against the 'Normalized Length' of the reactor for the experiments carried out at different operating conditions. . Normalized length is defined as a fraction of the total length of the reactor. It is the dimensionless length.

The decrease in reaction rate along the length of the reactor for 0.3 bar (g) and 40°C for pure SO_2 experiment is shown in Fig. 3.4. Bunsen reaction rate in first CSTR or at the inlet of the tubular reactor was approximately 8 E-4 moles/s and the rate approached a value closer to zero (1 E-9 moles/s value is taken as zero) within 30% of the total reactor length.

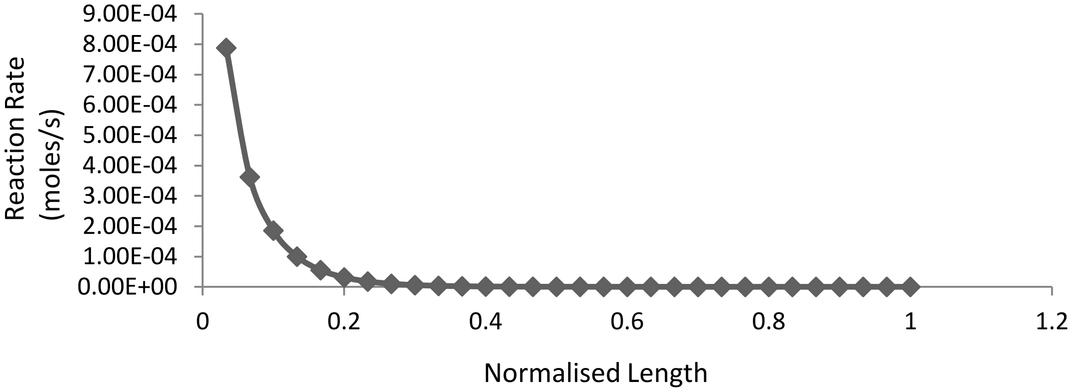

Fig. 3.4: Reaction rate profile along the length of the reactor for 0.3 bar (g) & 40°C experiment

The decrease in reaction rate along the length of the reactor for 2 bar (g) and 40°C for pure SO_2 experiment is shown in Fig. 3.5. Rate at the inlet of the reactor (CSTR 1) was found to be higher at 2 bar (g) experiment than that of 0.3 bar (g), which was due to more solubility of SO_2 in the liquid reactant at elevated pressures. The rate approached a value closer to zero within 20 to 25% of the total reactor length.

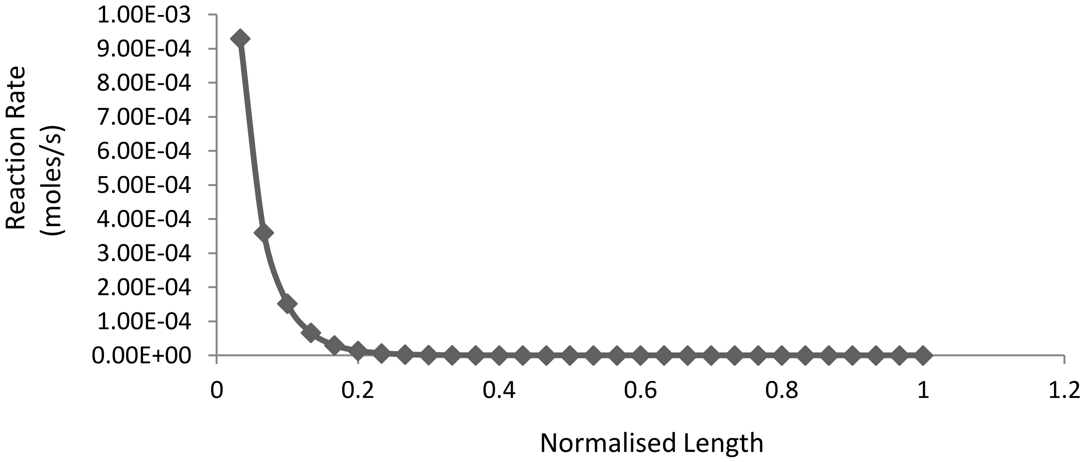

Fig. 3. 5: Reaction rate profile along the length of the reactor for 2 bar (g) & 40°C experiment

Bunsen reaction rates at the inlet of the reactor for 3.5 bar (g) and 40°C experiments for pure SO_2 was approximately 1E-3 moles/s as shown in Fig. 3.6. The rate approached a value closer to zero within 18 to 20% of the total reactor length.

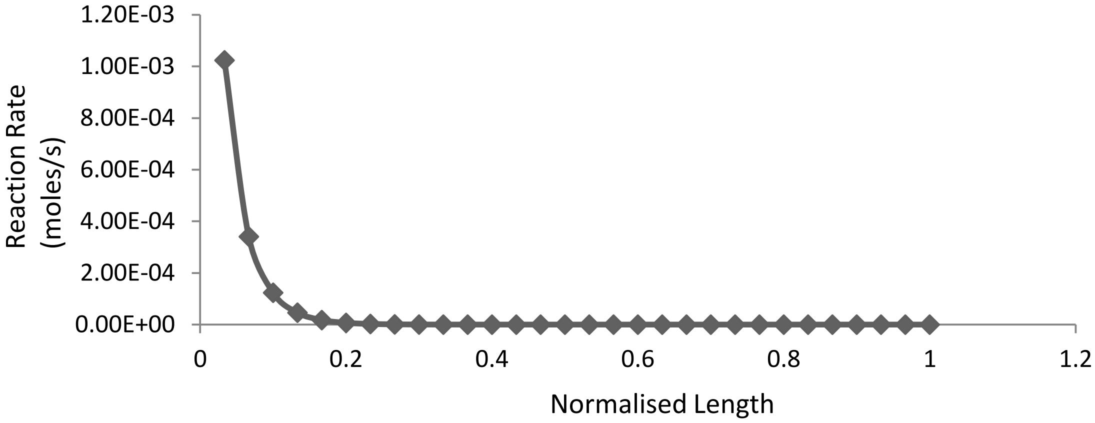

Fig. 3.6: Reaction rate profile along the length of the reactor for 3.5 bar (g) & 40°C experiment

Bunsen reaction rates at the inlet of the reactor for 60°C and 80°C experiments for pure SO_2 at 2 bar (g) were approximately 6E-4 moles/s and 5.5E-4 moles/s as shown in Figs. 3.7 & 3.8 respectively. Here rates at the inlet of the reactor were found to be lesser than that of 40°C experiments. This was because of the decrease in solubility of sulfur dioxide in the reaction liquid with increase in temperature. The rates approach a value closer to zero within 40 to 45% of the total reactor length.

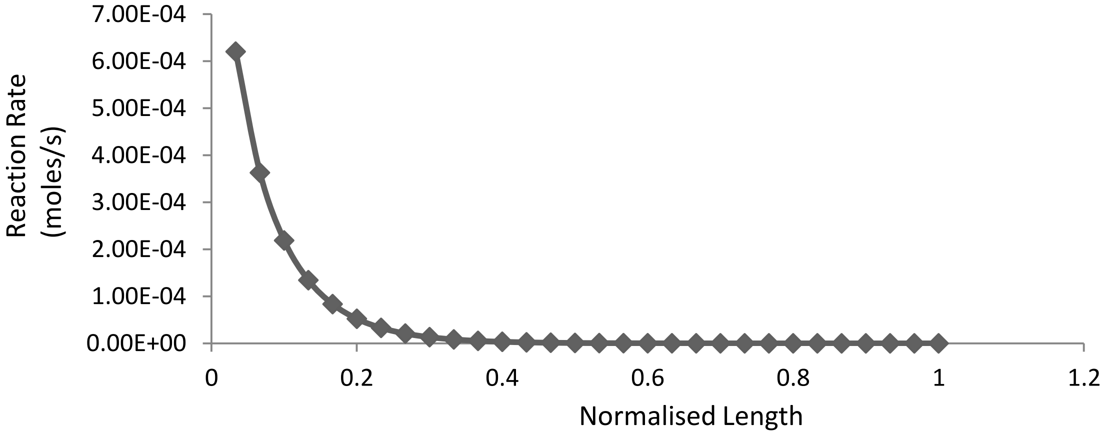

Fig. 3.7: Reaction rate profile along the length of the reactor for 2 bar (g) & 60°C experiment

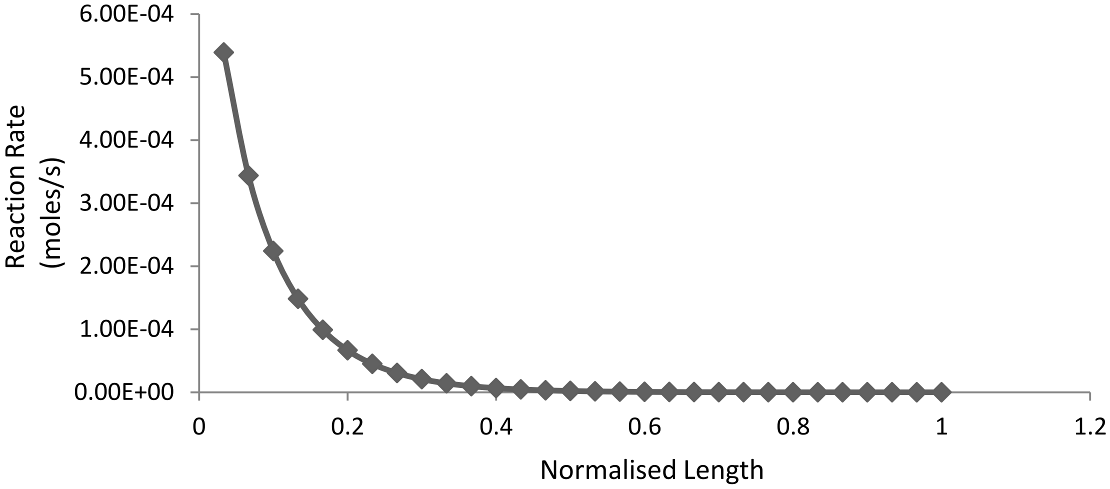

Fig. 3.8: Reaction rate profile along the length of the reactor for 2 bar (g) & 80°C experiment

3.4.1.1. Effect of temperature & pressure on Reaction Length

A new terminology, Reaction length, has been used for better understanding of effect of pressure and temperature. It is defined as the length at which chemical reaction is assumed to be zero or in other way it is defined as the length at which limiting reactant is completely consumed in reaction system. There is an inverse relation between reaction length and average reaction rate. Reactor length required for complete consumption of SO_2 gas will be lesser for a large value of average reaction rate. (Average reaction rate is higher at low temperature and high pressure reaction system). For 2 bar (g) and 80 °C experiment, at the outlet of reactor, reaction rate was of the order of 10^{-9} or molar flow rate of SO_2 was of the order of 10^{-9}, which was taken as zero. This was taken as reference for all other experiments. Full reaction length (100%) was assigned for 2 bar (g) and 80 °C experiment.

Fig. 3.9 & Table 3.3 explain the effect of temperature on reaction length for a fixed operating pressure of 2 bar (g). It was found that the reaction length increases (i.e. average reaction rate decreases) as the temperature of the reaction system increases. This was due to decrease in solubility of SO_2 at higher temperatures. Therefore SO_2 molecules require more length at higher temperature for complete conversion.

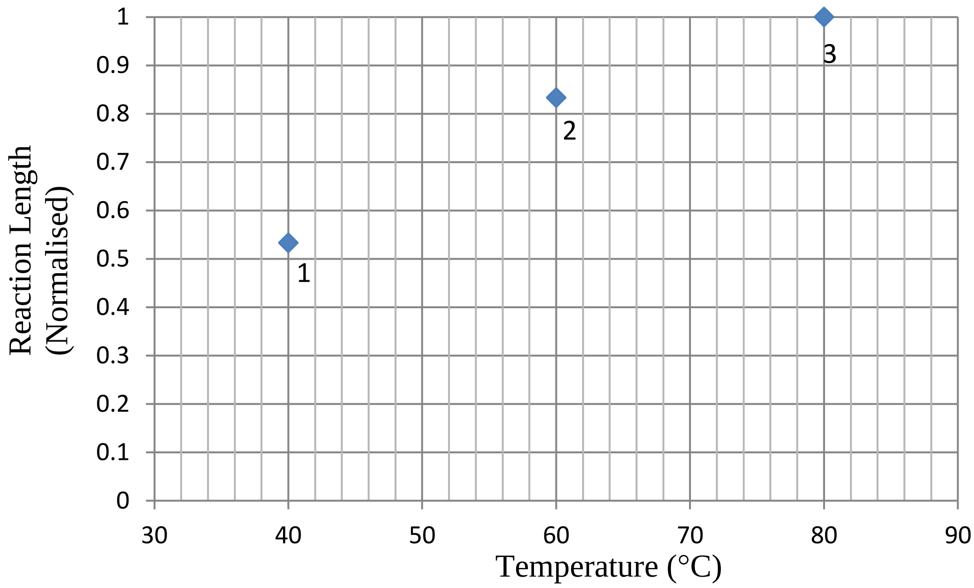

Fig. 3.9: Effect of Temperature on Reaction length for 2 bar (g) experiments

Table 3.3: Effect of Temperature on Reaction length for 2 bar (g) Experiments

Point	T °C	Reaction Length (Normalized)
1	40	0.53
2	60	0.83
3	80	1

Fig. 3.10 & Table 3.4 explain the effect of pressure on reaction length for a fixed operating temperature of 40°C. It was found that the reaction length decreases (i.e. average reaction rate increases) with increase in pressure. i.e. SO_2 molecules require lesser length at higher pressures for complete reaction. This was due to increase in solubility at higher pressures.

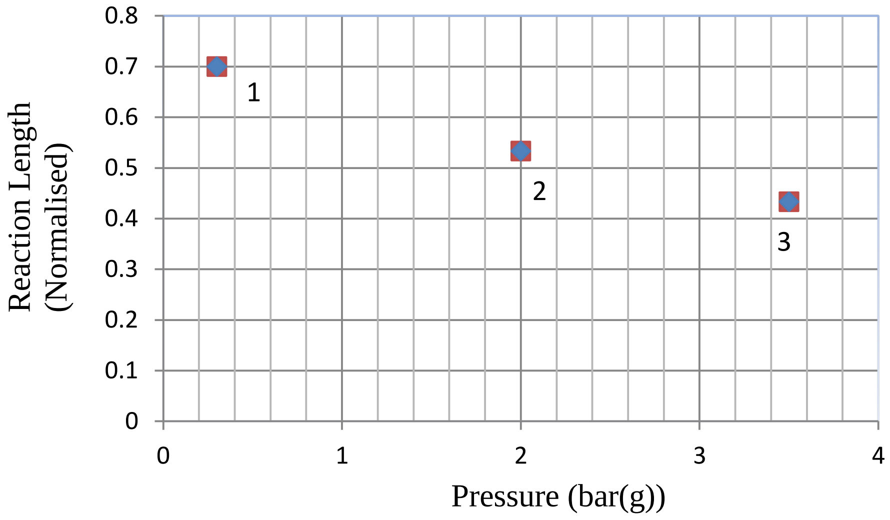

Fig. 3.10: Effect of Pressure on Reaction length for 40°C Experiments

Table 3.4 - Effect of pressure on Reaction length for 40 °C Experiments

Point	P bar(g)	Reaction Length (Normalised)
1	0.3	0.7
2	2	0.53
3	3.5	0.43

3.4.2. Experiments with SO_2 & N_2 mixture: Effect of gas film resistance

Average reaction rate (moles/s) and SO_2 conversion was calculated with the developed model and is compared with the experimental results for sulfur dioxide dilution experiments (Sr. No. 6 & 7) which are as shown in Table 3.2. Percentage dilution of SO_2 is the ratio of molar flow rate of N_2 to the total molar flow rates of N_2+SO_2. Here gas film resistance for the transport of SO_2 gas molecules to the reaction liquid has been accounted in the overall Bunsen reaction rate.

3.4.3. Comparing 0.3 bar (g) & 40 °C experiments: with dilution and without dilution

Profiles of SO_2 partial pressure and reaction rate are plotted against the 'Normalized Length' of the reactor for 18.6 % SO_2 dilution with N_2 are given in Figs. 3.11 & 3.12.

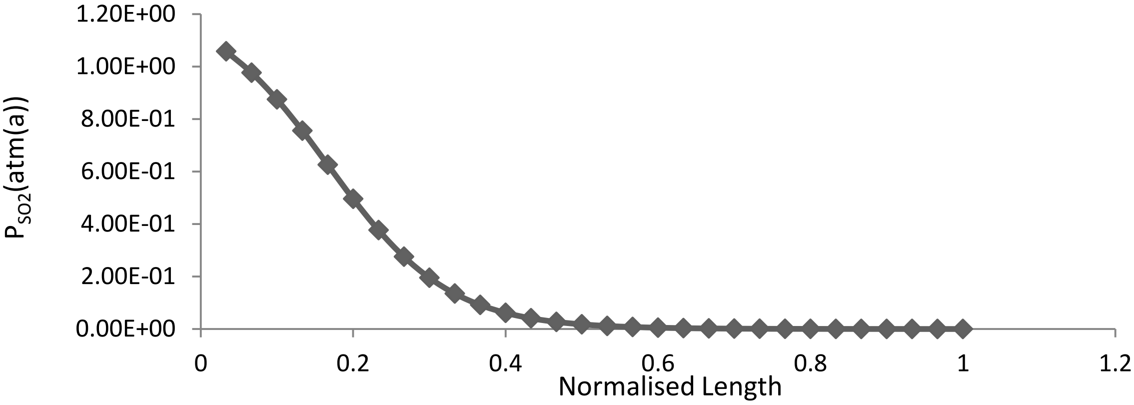

Fig. 3.11: SO_2 partial pressure profile along the length of the reactor for 0.3 bar (g) & 40°C experiment

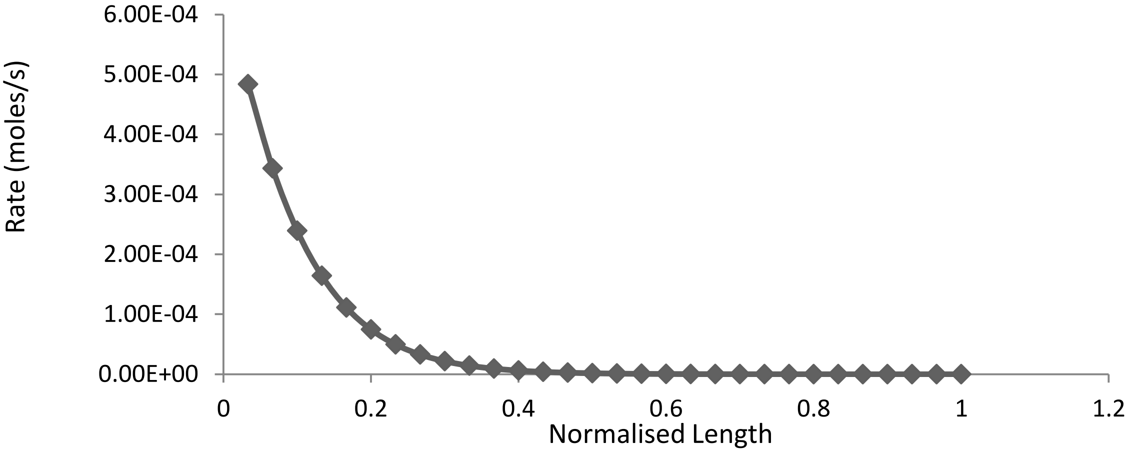

Fig 3.12: Reaction rate profile along the length of the reactor for 0.3 bar (g) & 40°C experiment

Bunsen reaction rate at the inlet of the reactor for 18.6% dilution was approximately 4.9 E-4 moles/s and the rate approached a value closer to zero within 40% of the total reactor length (as seen in Fig. 3.12) and that of pure SO_2 experiment reaction rate at the inlet of reactor was 8 E-4 moles/s and the rate approached a value closer to zero within 30% of the total reaction length (as seen in Fig. 3.4). As seen in Table 3.2, experimental average Bunsen reaction rate decreases by 11.47% for 18.6% SO_2

dilution compared with pure SO_2 and the model predicts decrease in reaction rate by 12.96%. This is because of the effect of gas film resistance to the average Bunsen reaction kinetics.

3.4.4. Comparing 2 bar (g) & 40 °C experiments: with dilution and without dilution

The similar trend can be observed for 2 bar (g) and 40 °C experiments where experimental average Bunsen reaction rate decreases by 12.57% for 18.6% SO_2 dilution compared with pure SO_2 and the model predicts decrease in reaction rate by 11.12%.

Increase in average reaction rate was observed for SO_2 dilution experiments also when the reactor pressure increased from 0.3 bar (g) to 2 bar (g).

For SO_2 dilution experiments, from Table 3.2, it can be seen that actual conversion is 80 to 83.5% against model prediction of complete conversion. This may be attributed to assumption of complete radial mixing of diluted sulfur dioxide.

3.5. Conclusions:

For Iodine-Sulfur thermo-chemical cycle, a detailed study of heterogeneous Bunsen reaction has been carried out through semi-batch experimental studies. It is found that, Bunsen reaction rate increases with increase in pressure for a fixed operating temperature and reaction rate decreases with increase in temperature for a fixed operating pressure. Effect of temperature on reaction length or reaction rate is more predominant compared to the effect of pressure on reaction rate.

Chapter IV

Residence Time Distribution Studies

in

Agitated Bunsen Reactor

4.1. Introduction:

In this chapter the results of RTD studies for ABR are presented.

Residence time distribution (RTD) of a reactor is a distribution function which describes the amount of time a fluid element could spend inside a reactor. The use of RTD is to characterize the mixing and flow within reactors and to compare the behavior of the real reactors to their ideal models. There are different flow models for representing the flow in a real reactor like deviations from plug flow can be explained with either 'dispersion model' or 'tanks-in-series' model [162-164]. The dispersion model has the advantage in that all correlations for flow in real reactors invariably use that model. This model is governed by an analogy to Fick's law of diffusion superimposed on the flow. In this study, the dispersion model is used to represent the flow behavior in Agitated Bunsen Reactor (ABR).

4.2. Theory:

A dimensionless group, '(D/uL)' is convenient to characterize the spread in the whole vessel. The dimensionless group (D/uL) is known as vessel dispersion number. This number measures the extent of axial dispersion. If (D/uL) tending to zero, that means negligible dispersion and hence plug flow. And if (D/uL) tending to infinity, which means large dispersion and mixed flow. The moments of RTD such as mean, t_m and variance, σ^2 are directly linked by theory to D and (D/uL). The mean for the continuous or discrete is defined as

$$t_m = \frac{\int_0^{\propto} t\, C(t)dt}{\int_0^{\propto} C(t)dt} = \frac{\sum t_i C_i \Delta t_i}{\sum C_i \Delta t_i} \quad \text{...}(4.1)$$

The variance is defined as

$$\sigma^2 = \frac{\int_0^{\propto} (t-t_m)^{\,2} C(t)dt}{\int_0^{\propto} C(t)dt} = \frac{\sum (t_i-t_m)^2 C_i \Delta t_i}{\sum C_i \Delta t_i} \quad \text{..}(4.2)$$

The variance represents the square of the spread of the distribution as it passes the vessel exit. It's unit is time^2. From RTD studies mean and the variance can be calculated experimentally. Dispersion coefficient can be calculated as follows.

Fitting dispersion model for small extents of dispersion, D/u.L < 0.01

Equations for t_m and σ^2 representing this family are

$$t_m = \frac{V}{v} = \frac{L}{u} \quad \dots\dots\dots (4.3)$$

$$\sigma_\theta^2 = \frac{\sigma_t^2}{t_m^2} = 2 * \left({}^{D}/_{u\,L} \right) \quad \dots\dots\dots (4.4)$$

Fitting dispersion model for large extents of dispersion, D/u.L > 0.01

Equations for t_m and σ^2 representing this family are

$$t_m = \frac{V}{v} \quad \dots\dots\dots (4.5)$$

$$\sigma_\theta^2 = \frac{\sigma_t^2}{t_m^2} = 2 * \left({}^{D}/_{u\,L} \right) - 2 * \left({}^{D}/_{u\,L} \right)^2 \left(1 - e^{-u\,L/D} \right) \dots\dots\dots (4.6)$$

4.3. Experimental:

The experiments were carried out in ABR with water as reactor fluid and sodium chloride solution as tracer. Experimental set-up is shown in Fig. 4.1.

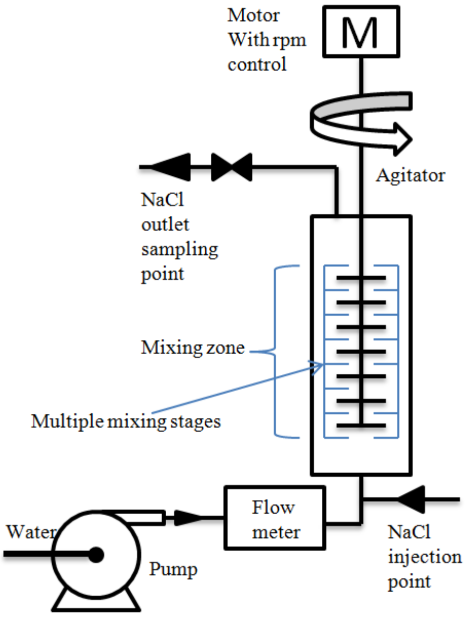

Fig. 4.1: Experimental set-up for RTD studies

It consists of agitated Bunsen reactor (ABR), process water feeding system, tracer injection point, agitation speed control unit and outlet sampling point.

Experiments were carried out by varying the agitation speed at different water flow rate viz 1, 0.5 and 0.25 lpm of water. 20 ml of NaCl solution (5 M) was injected at the inlet of the reactor through which process water flows at fixed flow rate. Samples were collected from the outlet of the reactor periodically and were analyzed potentiometrically for NaCl. Experiments were carried out by varying the agitation speed from 0 rpm to around 700 rpm and analysis was done. The whole procedure was repeated for other water flow rates.

4.4. Results and discussions:

4.4.1. Case A: For 1 lpm water flow rate and different agitation speed

Results obtained from a set of experiments carried out at 1 lpm water flow rate with 20 ml of NaCl tracer of around 5 Molar are explained below. Fig. 4.2 is the C-curve, which shows the plots of exit concentration of NaCl plotted against the sampling time for different agitation speed.

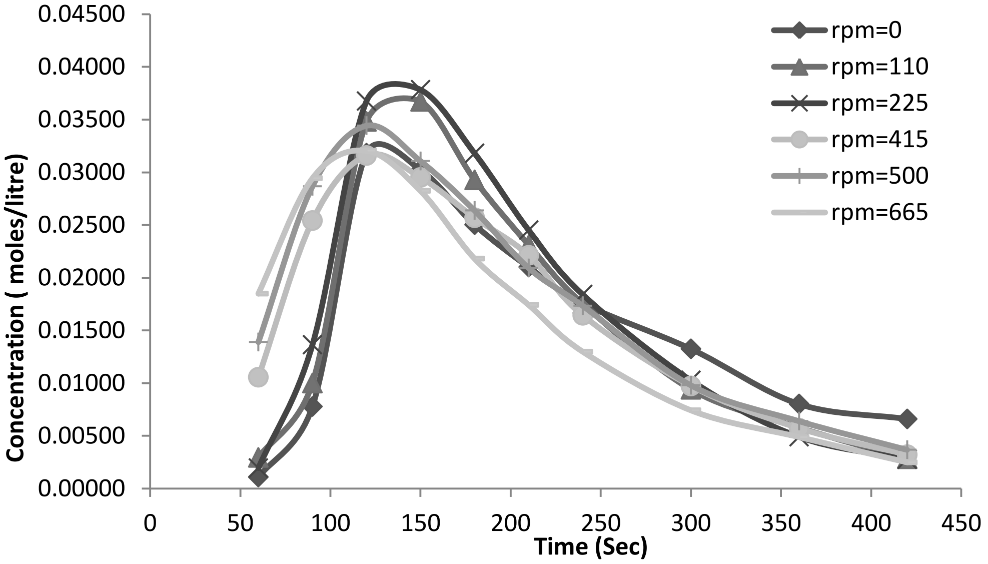

Fig. 4.2: C-curve at different ‘rpm’ for 1*lpm* water flow rate

At zero ‘rpm’, some of the fluid elements leave the reactor ‘early’ than calculated mean time (V/v = 150 seconds) due to channeling/ bypassing through the reactor and some of the fluid elements leave the reactor ‘late’ than calculated mean time due to stagnation region inside the reactor. Channeling and stagnation regions lead to underutilization of reactor volume and insufficient mixing inside the reactor. Higher values of NaCl concentrations even after 300 seconds ($2*t_m$) for 0 rpm and 40 rpm agitation speed, explains the ‘late’ leaving of the fluid elements and stagnation regions. At 665 ‘rpm’, the C-curve is broader and has got shifted towards left compared to other curves. This shows high level of inter-stage mixing and hence approaching CSTR behavior. The C-curve for 315 rpm is having a minimum peak and is broader compared to other higher ‘rpm’ experiments. This is construed as an experimentation error. In order to identify the plug flow regime, two different curves are generated. They are σ^2 Vs rpm and ‘D/uL’ Vs rpm.

Velocity of fluid inside the reactor has been calculated by knowing the volumetric flow rate (1lpm) of water and reactor diameter. Mean residence time, t_m and variance, σ^2 have been calculated from experimentation using Equation (4.1) and (4.2) respectively for different ‘rpm’. σ_θ^2 is evaluated from t_m and σ^2. Deviations from plug flow can be obtained from σ^2 Vs rpm curve. σ^2 indicates the spread of the curve, lesser σ^2 means the flow is plug flow and more value of σ^2 means, the flow is approaching to CSTR condition. As seen in Fig. 3, higher values of σ^2 at lower rpm are due to the deviations from plug flow as a result of stagnant regions or channeling inside the reactor and higher values of σ^2 at very high rpm are due to the deviations from plug flow as a result of inter-stage mixing. Fig. 4.3 shows that the value of σ^2 is minimum corresponding to rpm range between 100 and 250.

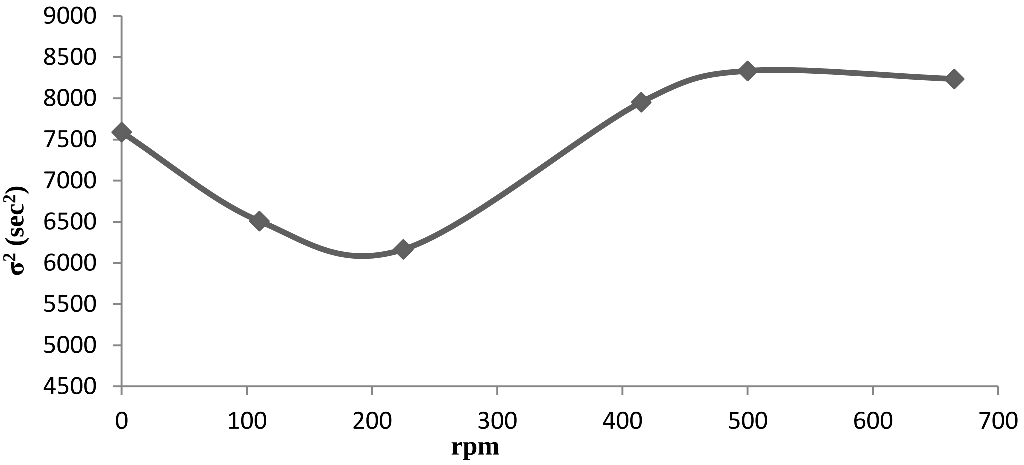

Fig. 4.3: Variation of σ^2 with 'rpm' for 1*lpm* water flow rate

Vessel dispersion number, 'D/uL' is a significant parameter which measures the extent of axial dispersion. The value of 'D/uL' for the 'intermediate dispersion' is 0.02 and for 'large extend of dispersion' is 0.2 [162].

Using Equation (4.6) 'D/uL' is calculated for different 'rpm' experiments and shown in Fig. 4.4. Value of 'D/uL' is 0.092 for no agitation (which is higher than 'D/uL' value for 'intermediate dispersion') and the value remains constant up to around 225 rpm agitation speed. It shows that axial dispersion due to flow dominates compared to that of axial dispersion due to rotating blades in a range of rpm up to around 225. Beyond this rpm, axial dispersion caused by rotating blades dominates over that due to flow.

From Figs. 4.3 & 4.4, for vessel dispersion number of around 0.091, recommended agitation speed is up to 200 rpm and for vessel dispersion number around 0.155 which is also between intermediate and large extent of dispersion, agitation speed of around 500 rpm was identified. 'Large extent of dispersion' observed at around 700 rpm agitation speed.

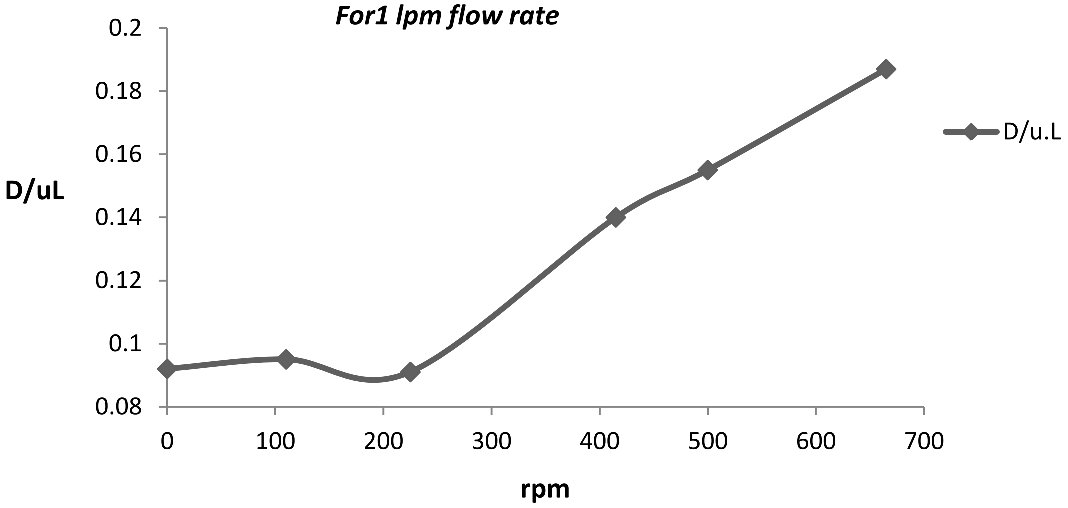

Fig. 4.4: Variation of 'D/uL' with 'rpm' for 1*lpm* water flow rate

4.4.2. Case B: For 0.5 lpm water flow rate and different agitation speed

The results obtained from a set of experiments carried out at 0.5 lpm water flow rate with 20 ml of NaCl tracer of around 5 Molar are explained below. Fig. 4.5 is the C-curve, which shows the plots of exit concentration of NaCl plotted against the sampling time for different agitation speed.

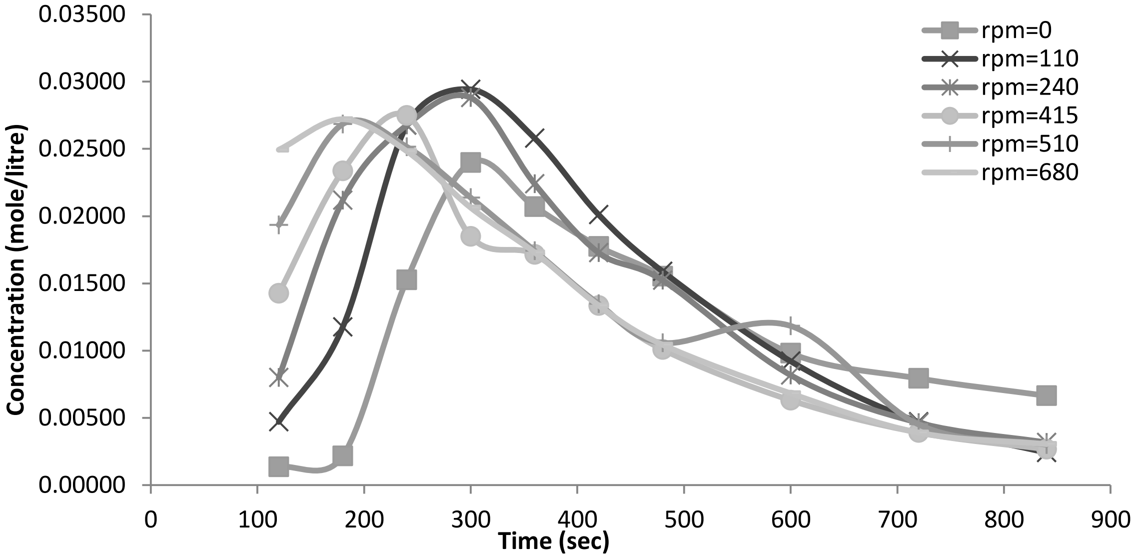

Fig. 4.5: C-curve at different 'rpm' for 0.5*lpm* water flow rate

At zero 'rpm', some of the fluid elements leave the reactor 'early' than calculated mean time (V/v = 300 seconds) due to channeling/ bypassing through the reactor and some of the fluid elements leave the reactor 'late' than calculated mean time due to stagnation region inside the reactor. Higher values of NaCl concentrations even after 600 seconds (2* t_m) for 0 rpm agitation speed, explains the 'late' leaving of the fluid elements and stagnation regions. At 680 'rpm', the C-curve starts at very high concentration and decreases gradually. This is representing the CSTR behavior. In order to identify the plug flow regime, two different curves are generated. They are σ^2 Vs rpm and 'D/uL' Vs rpm.

Velocity of fluid inside the reactor has been calculated by knowing the volumetric flow rate (0.5 lpm) of water and reactor diameter. Mean residence time, t_m and variance, σ^2 have been calculated from experimentation using Equation (4.1) and (4.2) respectively for different 'rpm's. σ_θ^2 is evaluated using t_m and σ^2. As seen in Fig. 4.6, higher values of σ^2 at lower rpm are due to the deviations from plug flow as a result of stagnant regions or channeling inside the reactor and higher values of σ^2 at very high rpm are due to the deviations from plug flow as a result of inter-stage mixing. From Fig. 4.6 it is seen that the value of σ^2 is minimum for agitation speed of around 100 rpm.

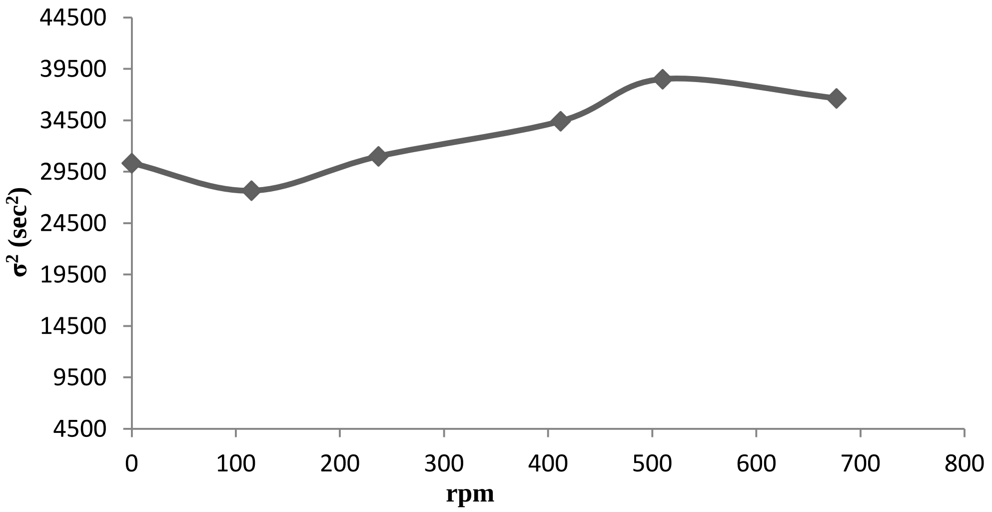

Fig. 4.6: Variation of σ^2 with 'rpm' for 0.5*lpm* water flow rate

Using Equation (4.6) 'D/uL' is calculated for different 'rpm' experiments and shown in Fig. 4.7. . Value of 'D/uL' is 0.081 for no agitation (which is also higher than 'D/uL' value for 'intermediate dispersion'). This vessel dispersion number value at zero rpm is lesser compared to that for 1lpm water flow rate (0.092 for 1lpm). It is observed that 'D/uL' value increases gradually with increase in agitation speed, which shows that axial dispersion due to agitation always dominates compared to that of axial dispersion due to flow.

From Figs. 4.6 & 4.7, for vessel dispersion number of around 0.103, recommended agitation speed is ~100 rpm and for vessel dispersion number around 0.193 which is also between intermediate and large extent of dispersion, agitation speed of around 410 rpm is identified. 'Large extent of dispersion is observed beyond 400 rpm agitation speed.

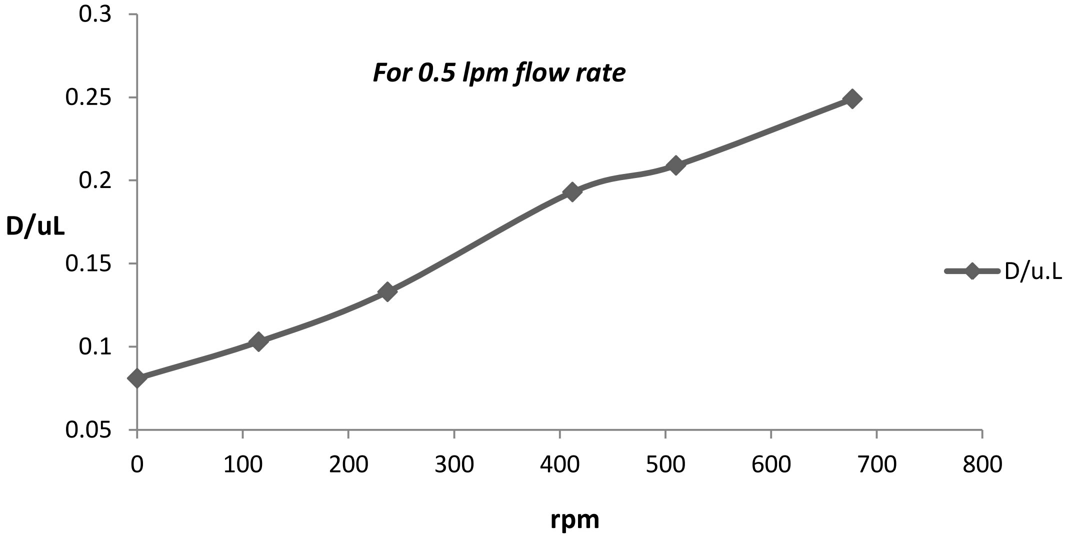

Fig. 4.7: Variation of 'D/u L' with 'rpm' for 0.5*lpm* water flow rate

4.4.3. Case C: For 0.25 lpm water flow rate and different agitation speed

The results obtained from a set of experiments carried out at 0.25 lpm water flow rate with 20 ml of NaCl tracer of around 5 Molar are explained below. Fig. 4.8 is the C-curve, which shows exit concentration of NaCl plotted against the sampling time for different agitation speed.

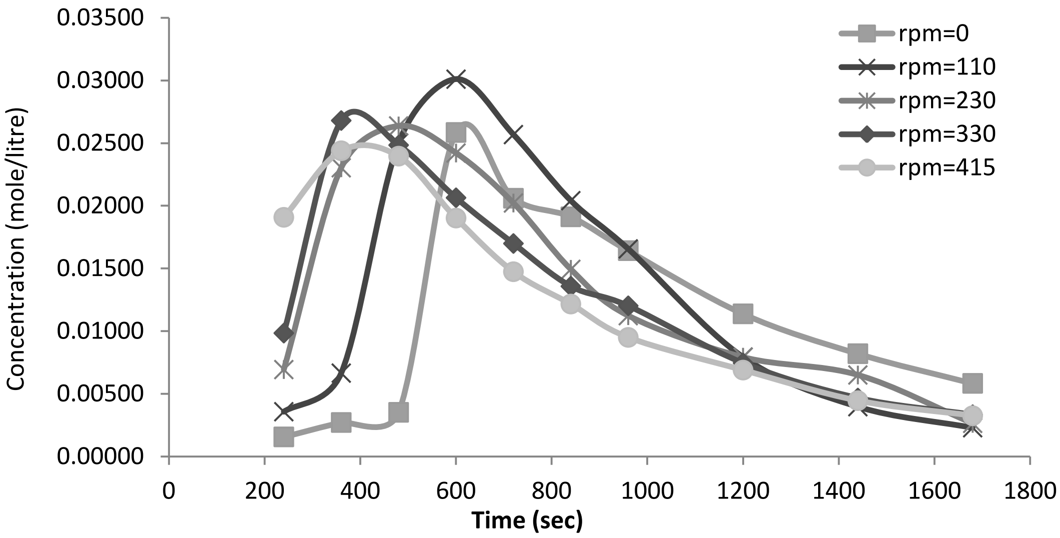

Fig. 4.8: C-curve at different 'rpm' for 0.25*lpm* water flow rate

At zero 'rpm', some of the fluid elements leave the reactor 'early' than calculated mean time (V/v = 600 seconds) due to channeling/ bypassing through the reactor and some of the fluid elements leave the reactor 'late' than calculated mean time due to stagnation region inside the reactor. Higher values of NaCl concentrations even after 1200 seconds (2* t_m) for 0 rpm agitation speed, explains the 'late' leaving of the fluid elements and stagnation regions. Around 415 'rpm' itself, the C-curve starts at very high concentration and decreases gradually. This is representing the CSTR behavior. In order to identify the plug flow regime, two different curves are generated. They are σ^2 Vs rpm and 'D/uL' Vs rpm.

Velocity of fluid inside the reactor has been calculated by knowing the volumetric flow rate (0.25 lpm) of water and reactor diameter. Mean residence time, t_m and variance, σ^2 have been calculated from experimentation using Equation (4.1) and (4.2) respectively for different 'rpm'. σ_θ^2 is evaluated from t_m and σ^2. As seen in Fig. 4.9, high values of σ^2 at lower rpm are due to the deviations from plug flow as a result of stagnant regions or channeling inside the reactor and higher values of σ^2 at very high rpm are due to the deviations from plug flow as a result of inter-stage mixing. From Fig. 4.9 it is seen that the value of σ^2 is minimum corresponding to an agitation speed of around 100 rpm.

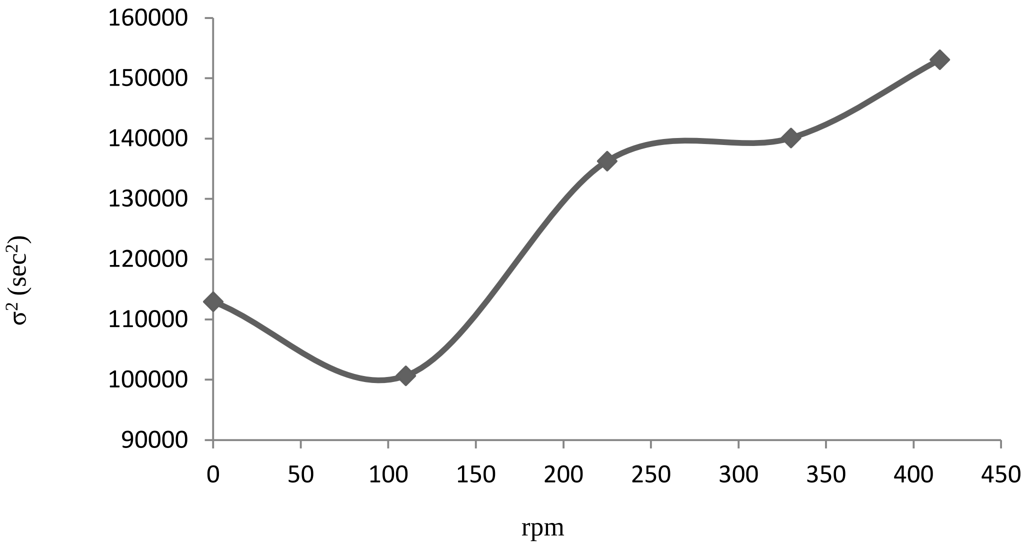

Fig. 4.9: Variation of σ^2 with 'rpm' for 0.25*lpm* water flow rate

Using Equation (4.6) 'D/uL' is calculated for different 'rpm' experiments and shown in Fig. 4.10. Value of 'D/uL' at zero rpm is 0.069, which is also higher than 'D/uL' value for 'intermediate dispersion'. This vessel dispersion number value is lesser compared to that of 1lpm & 0.5 lpm water flow rates. It is observed that 'D/uL' value increases gradually with increase in agitation speed.

From Figs. 4.9 & 4.10, for vessel dispersion number of around 0.091, recommended agitation speed is ~ 100 rpm and for vessel dispersion number around 0.169 which is also between intermediate and large extent of dispersion, agitation speed of around 330 rpm is identified. 'Large extent of dispersion' observed beyond 400 rpm agitation speed.

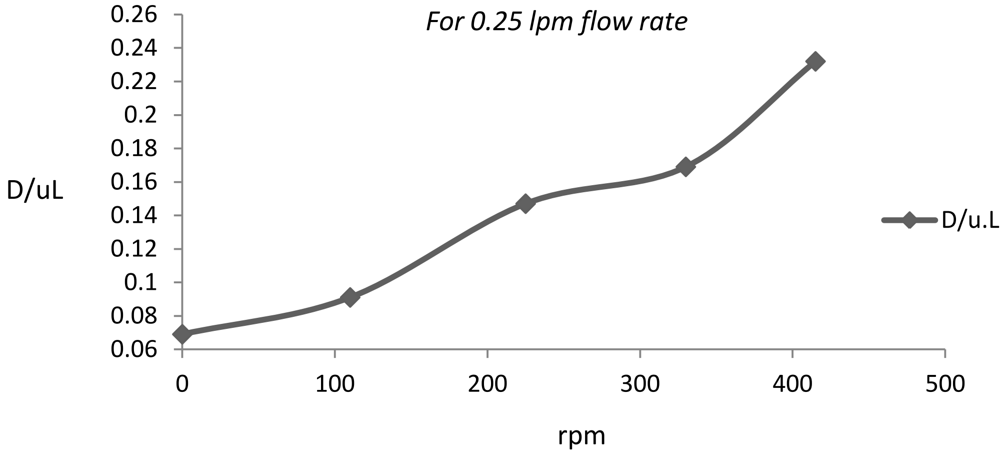

Fig. 4.10: Variation of ‘D/u L’ with ‘rpm’ for 0.25*lpm* water flow rate

For the investigated range of operating flow rates, desired Vessel dispersion number & recommended agitation speed for dispersion between intermediate and large extent of dispersion are given in Table 4.1.

Table 4.1: Desired vessel dispersion number and corresponding ‘rpm’ range

Volumetric flow rate, v *(lpm)*	Desired Vessel dispersion number & recommended agitation speed				Flow condition
	D/u L	‘rpm’ range	D/u L	‘rpm’ range	
1	0.091	Upto 200	0.155	~500	Near to plug flow with dispersion between intermediate and large extent of dispersion
0.5	0.103	~ 100	0.193	~412	
0.25	0.091	~ 100	0.169	~330	

4.5. Conclusions:

Residence Time Distribution (RTD) studies in Agitated Bunsen Reactor (ABR) has the potential importance in identifying the agitation speed for plug flow regime in tubular reactor with an agitator inside. Experiments were carried out in ABR with water as reactor fluid and sodium chloride solution as tracer by varying agitation speed as well as water flow rate. C-curve, variance and vessel dispersion number at different agitation speed range for different flow rates studied have been generated. Agitation speed range for minimal axial dispersion and for vessel dispersion number between intermediate and large extent of dispersion was identified.

Chapter V

Heat Transfer Studies

in

Agitated Bunsen Reactor

5.1. Introduction:

The objective of this study was to analyze the effect of operating parameters on heat transfer and further develop heat transfer correlations or modify existing correlations which are useful for heat transfer based preliminary design of ABR. Objective was also to validate the correlation (developed/ modified with heat transfer study between water-water systems) with the heat transfer between reactor fluid and cooling fluid in actual Bunsen reaction study in ABR.

5.2. Theory:

The correlations are developed from the general and basic equations of heat transfer. In the equation for heat flux, Equation (5.1), the temperature difference is the driving force and the resistance can be either conductive resistance, convective resistance or radiation heat transfer resistance or any combinations of these.

$$Heat\ flux, q = \frac{Driving\ force}{Resistance} \ldots\ldots\ldots\ldots\ldots\ldots\ldots\ldots\ldots\ldots (5.1)$$

Transfer of heat energy from hot fluid to cold fluid is across a solid cylindrical boundary separating them as represented schematically in Fig. 5.1. Here the driving force is 'T_h-T_c' where 'T_h' is the temperature of the hot fluid and 'T_c'is the temperature of the cold fluid. Two convective heat transfer resistances ($R_{film}h$ and $R_{film}c$) due to boundary layer formation and a conductive heat transfer resistance (R_{wall}) due to thermal conductivity of solid boundary and its thickness are present here. The quantity of heat lost by hot fluid, Q_h, the quantity of heat gained by cold fluid, Q_c and quantity of heat transferred through the tube wall (outer heat transfer area, A_O) are represented in Equations (5.2), (5.3) & (5.4) respectively.

$$Q_c = m_c C_{P_c} \Delta T_c \ldots\ldots\ldots\ldots\ldots\ldots\ldots\ldots\ldots\ldots\ldots\ldots\ldots\ldots\ldots\ldots\ldots.. (5.2)$$

$$Q_h = m_h C_{P_h} \Delta T_h \ldots\ldots\ldots\ldots\ldots\ldots\ldots\ldots\ldots\ldots\ldots\ldots\ldots\ldots\ldots\ldots\ldots.. (5.3)$$

$$Q_h = Q_c = Q = U_O A_O \Delta T_{LM} \ldots\ldots\ldots\ldots\ldots\ldots\ldots\ldots\ldots\ldots\ldots\ldots\ldots.. (5.4)$$

Here ΔT_{LM} is the logarithmic mean temperature difference driving force and '$1/U_O A_O$' is the overall resistance accounting for conductive as well as convective resistances. '$1/U_O$' can be calculated using Equation (5.5), where '$1/h_O$' is the convective resistance offered by hot water, $R_{film}h$, '$\frac{d_o}{h_i d_i}$' is the convective resistance offered by cold water, $R_{film}c$ and '$\frac{x d_o}{k\, d_{LM}}$'is the conductive resistance based on outside surface area of the cylindrical geometry, A_o.

$$\frac{1}{U_O} = \frac{1}{h_o} + \frac{d_o}{h_i d_i} + \frac{x d_o}{k d_{LM}} \ldots\ldots\ldots\ldots\ldots\ldots\ldots\ldots\ldots\ldots\ldots\ldots\ldots. \ldots (5.5)$$

'h_o' can be calculated using standard correlations depending up on the situation whether the fluid is experiencing a flow or mixing. In case of flowing system, 'h_o' can be evaluated using Equation (5.6) or (5.7) depending on the degree of turbulence [166,167].

$$\frac{h_o D_e}{k} = 0.6 Re_{flow}^{0.5} Pr^{0.31}, 50 \leq Re_{flow} \leq 10{,}000 \ldots\ldots\ldots\ldots\ldots (5.6)$$

$$\frac{h_o D_e}{k} = 0.36 Re_{flow}^{0.55} Pr^{\frac{1}{3}} (\frac{\mu}{\mu_w})^{0.14}, Re_{flow} \geq 10{,}000 \ldots\ldots..\ldots (5.7)$$

There are number of correlations for the agitated system depending on whether the second fluid is passing through jacket or helical coil or baffle tubes [168] etc.

'h_i' can be calculated using standard flow correlations for internal tube flow as given by Equation (5.8) for laminar flow or Equation (5.9) for turbulent flow.

$$Nu_i = \frac{h_i d_i}{k} = 1.86 \left[\frac{RePr}{L/d_i}\right]^{\frac{1}{3}} \ldots\ldots\ldots\ldots\ldots\ldots\ldots\ldots\ldots\ldots\ldots\ldots\ldots. (5.8)$$

$$Nu_i = \frac{h_i d_i}{k} = 0.023 Re^{0.8} Pr^{0.4} \ldots\ldots\ldots\ldots\ldots\ldots\ldots\ldots\ldots\ldots\ldots\ldots. (5.9)$$

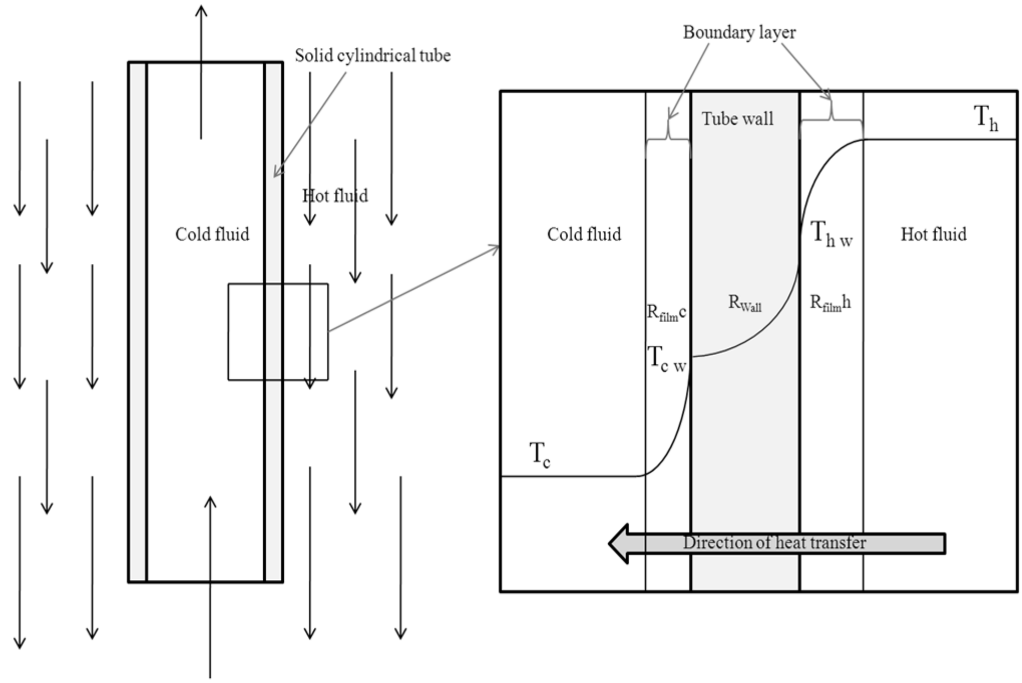

Fig. 5.1: Theory of heat transfer between two fluids separated by a solid cylindrical boundary

5.3 Experimental:

ABR is a tubular reactor with a long shaft axially provided inside with turbine type mixing blades. The shaft with mixing blades is connected to the motor with ‘rpm’ controller to vary agitation speed. Reactor is provided with internal helical coil.

Experiments were carried out in ABR with water as reactor fluid as well as helical coil cooling fluid. Experimental set-up is shown in Fig. 5.2. It consists of agitated Bunsen reactor (ABR) along with hot water circulation system through the reactor side, cooling water circulation system through the helical coil tube side, agitation speed control system and temperature sensors. Hot water circulation system consists of a hot water bath with temperature control unit. Cooling water circulation system consists of a cooling water reservoir (insulated tank).

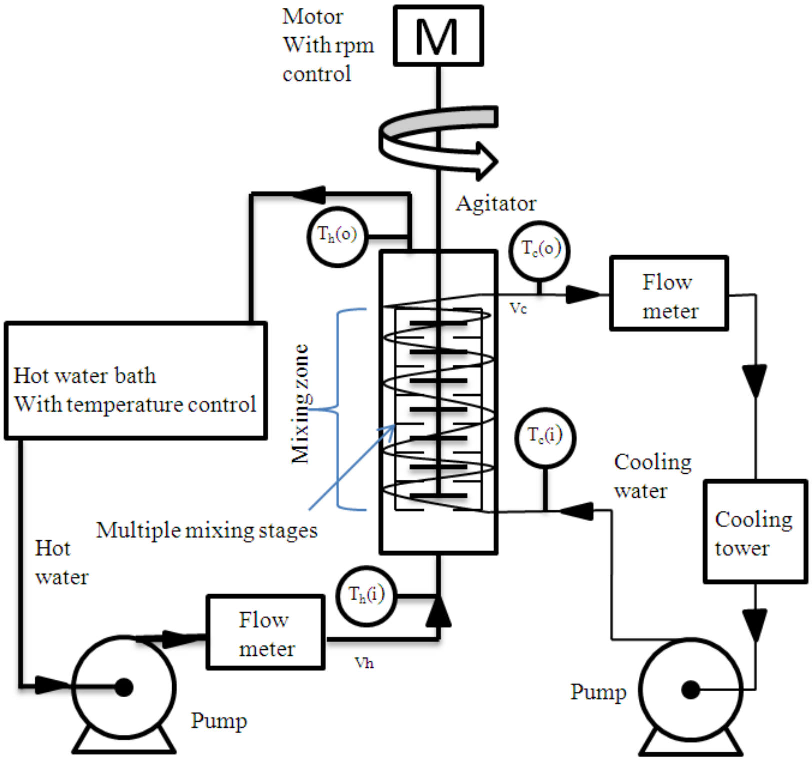

Fig. 5.2: Heat transfer studies in ABR: Experimental set-up for water-water system

Water was pumped to the ABR shell side and helical coil tube side with metering pumps at fixed flow rates through flow maters. Agitation speed control system consists of a motor connected to the agitating shaft of ABR with ‘rpm’ controller. ‘K’ type thermocouples were used for measuring inlet and outlet temperatures of two streams. Experiments were carried out by varying agitation speed and flow rates of hot water through shell side of ABR with constant cooling water flow rate. In various sets of experiments, the steady state temperatures were noted for given operating conditions.

Flow measurement error of water was 1% of flow rate. Measurement error of temperature was 0.2 % of reading.

5.4 Results and discussion:

5.4.1. Heat transfer experiments with water on both sides:

This study was a steady state heat transfer analysis. Steady state temperatures obtained from fifteen heat transfer experiments carried out at different agitation speeds and varying flow rates are given in Table 5.1. The agitation speeds were varied from 0 to 700 rpm for three volumetric flow rates of 0.88, 0.5 and 0.25 lpm respectively.

Table 5.1: Steady state temperatures achieved at different experimental conditions

Expt. No.	V_h, lpm	V_c, lpm	rpm	T_h(i), °C	T_h(o), °C	T_c(i), °C	T_c(o), °C
1	0.88	0.86	0	63.6	54.8	24.6	34.1
2	0.88	0.86	100	63.6	54.2	24.6	34.7
3	0.88	0.86	250	63.6	53.1	24.7	35.7
4	0.88	0.86	500	63.7	52.8	24.9	36.5
5	0.88	0.86	700	63.8	52.8	24.9	36.4
6	0.5	0.86	0	61.8	49.4	25.8	32.8
7	0.5	0.86	100	61.8	48	25.5	33.6
8	0.5	0.86	250	61.7	46.7	25.7	34.2
9	0.5	0.86	500	61.8	46.5	25.8	34.5
10	0.5	0.86	700	61.9	46.3	25.9	33.9
11	0.25	0.86	0	57.8	42	25.4	30.3
12	0.25	0.86	100	57.9	40.5	25.6	30.6
13	0.25	0.86	250	58	38.8	25.8	30.3
14	0.25	0.86	500	58.1	38.3	27.2	30.3
15	0.25	0.86	700	58.1	38.1	24.8	30.2

Heat energy gained by the cold fluid, Q_c and heat energy lost by the hot fluid, Q_h have been estimated using Equations (5.2) & (5.3). Theoretically Q_c and Q_h should be equal, but a maximum error of 8.5 % is observed due to experimental inaccuracy.

Plots of 'heat duty per unit logarithmic mean temperature difference', $Q/\Delta T_{LM}$ versus 'rpm' for different hot water flow rate, corresponding to the experiments in Table 5.1, are generated and shown in Fig. 5.3. It is observed that the heat duty of the reactor increases with agitation speed for a given heat transfer area as seen in Fig. 5.3. At 0.88 lpm hot water flow rate, $Q/\Delta T_{LM}$ increases from 19.33 W/K to 26.45 W/K with increase in agitation speed. Similar trend, for Q/ΔT_{LM} versus ‘rpm’, were observed at lower hot water flow rates. Heat duty per unit logarithmic mean temperature difference increased with increase in hot water flow rate for a given agitation speed as seen in Fig. 5.3. The data point of 0.25 lpm hot water flow at 500 rpm agitation speed, the Q/ΔT_{LM} value is an experimental error which has not been considered in analysis of data.

In this study, it is assumed that individual and overall heat transfer coefficients are constant throughout heat transfer interface. In separate tracer studies, internal flow pattern is understood and its repeatability is checked. Therefore a fully developed fluid flow is assumed in the reactor.

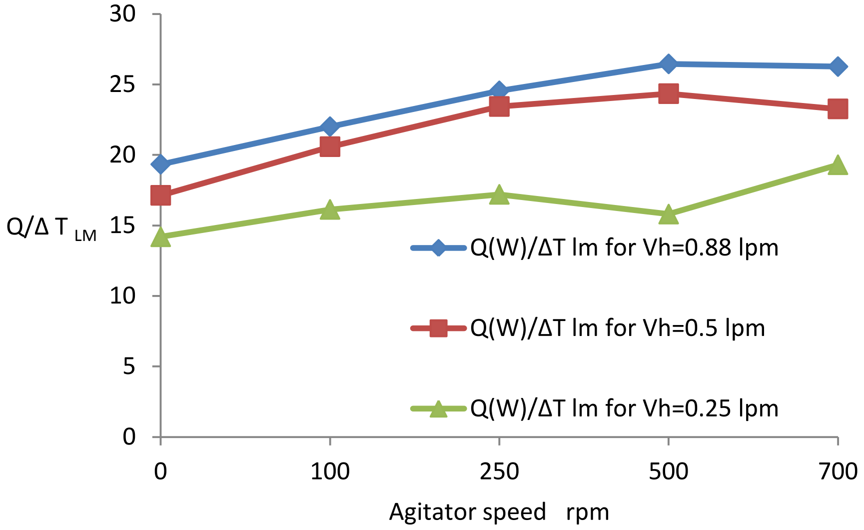

Fig. 5.3: Effect of ‘rpm’ on ‘heat duty per unit log mean temperature difference’ for different hot water flow rate

Enhancement in heat duty (Q/ΔT_{LM}) due to agitation has been captured in the external fluid flow correlation for helical coil heat exchanger by incorporating the effect of additional degree of turbulence due mixing, i.e. $Re_{impeller}$.

The overall heat transfer coefficient U_O has been calculated using Equation (5.4) by knowing the steady state temperature, heat duty, Q and heat transfer area, A_O. The heat transfer coefficient of cold fluid flowing inside a straight tube ‘h_i’ in Equation (5.5) is to be replaced by heat transfer coefficient of cold fluid flowing inside a helical coil tube 'h_{ic}' which was calculated using Equation (5.10) [167]. Using 'h_{ic}', resistance offered by the film in cold water side has been calculated. Knowing the thermal conductivity of material of tube, tube thickness and tube diameter, resistance offered by the wall has been calculated. These values have been substituted in Equation (5.4) and h_o is calculated. Using this 'h_o', Nusselt number, Nu_o (experimental) for the hot water side fluid has been calculated. Reynolds number for a flowing system, Re_{flow} and impeller Reynolds number $Re_{impeller}$ for an agitated system, are calculated using Equations (5.11) and (5.12) respectively.

$$h_{ic} = h_i\left(1 + 3.5\frac{d_i}{D_H}\right) \dots\dots\dots\dots\dots\dots\dots\dots\dots\dots\dots\dots\dots\dots. (5.10)$$

$$Re_{flow} = \frac{\rho VD}{\mu} \dots\dots\dots\dots\dots\dots\dots\dots\dots\dots\dots\dots\dots\dots\dots\dots\dots (5.11)$$

$$Re_{impeller} = \frac{Nd^2\rho}{\mu} \dots\dots\dots\dots\dots\dots\dots\dots\dots\dots\dots\dots\dots\dots\dots (5.12)$$

Prandtl numbers for these fluids, Pr_h and Pr_c, have been calculated at bulk temperatures of the fluids. There is negligible effect on results when the effects of temperature dependent fluid properties are considered. Nu_o for a flowing system has been calculated with flow Reynolds number ($50 \leq Re_{flow} \leq 10{,}000$) using Equation (5.6) as Nu_o (flow). It is observed that the values of Nusselt number, Nu_o (experimental) are much higher than Nu_o (flow). This increase is due to the mixing provided by the agitator. A power function of impeller Reynolds number captures this enhancement in heat transfer coefficient due to mixing. The exponent of 0.25 was obtained from the log-log plot of Figs 5.4, 5.5 and 5.6 for the entire range of experimentation. Thus the modified heat transfer correlation which accounts fluid flow as well as mixing in the reactor side/shell side of

ABR applicable for the investigated range of operating conditions is given in equation (5.13).

$$\frac{h_o D_e}{k} = 0.6 Re_{flow}^{0.5} {Pr_h}^{0.31} (1 + Re_{impeller})^{0.25} \ldots\ldots\ldots\ldots (5.13)$$

$$50 \leq Re_{flow} \leq 500$$

$$1500 \leq Re_{impeller} \leq 15{,}000$$

Nusselt number, Nu_o (model) calculated with the modified correlation is compared with experimental values for different hot water flow rate and is plotted against impeller Reynolds number in Figs. 5.4, 5.5, 5.6. The model predicts the experimental data points with good accuracy. The correlation is reasonably accurate in the range of 50 to 500 of flow Reynolds' number and in the range of 1,500 to 15,000 of impeller Reynolds' number.

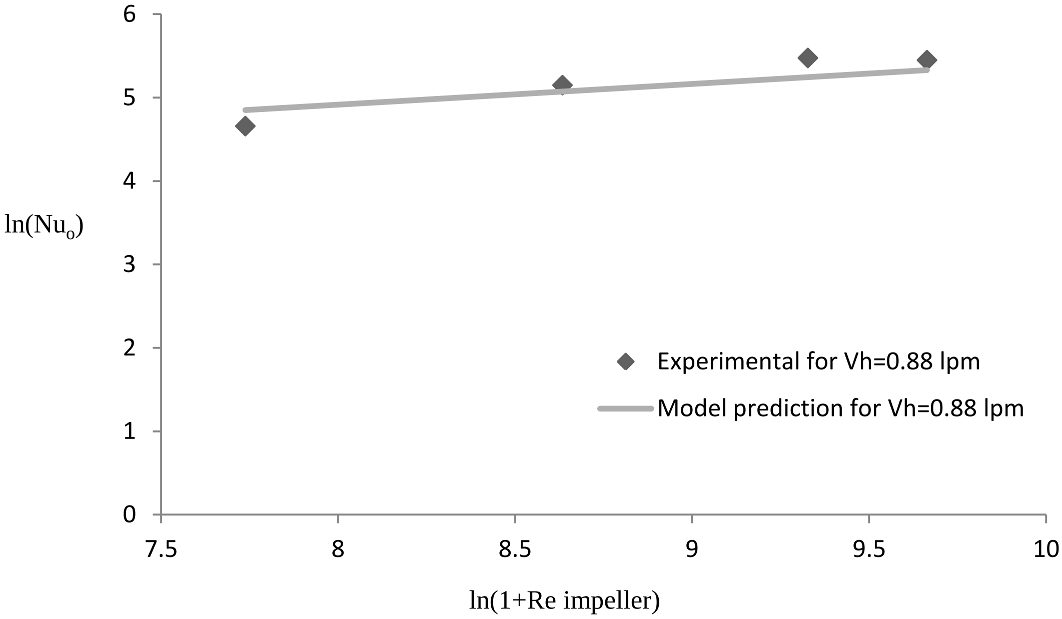

Fig. 5.4: Prediction of experimental data points, for V_h=0.88 *lpm* flow, with the modified correlation for ABR

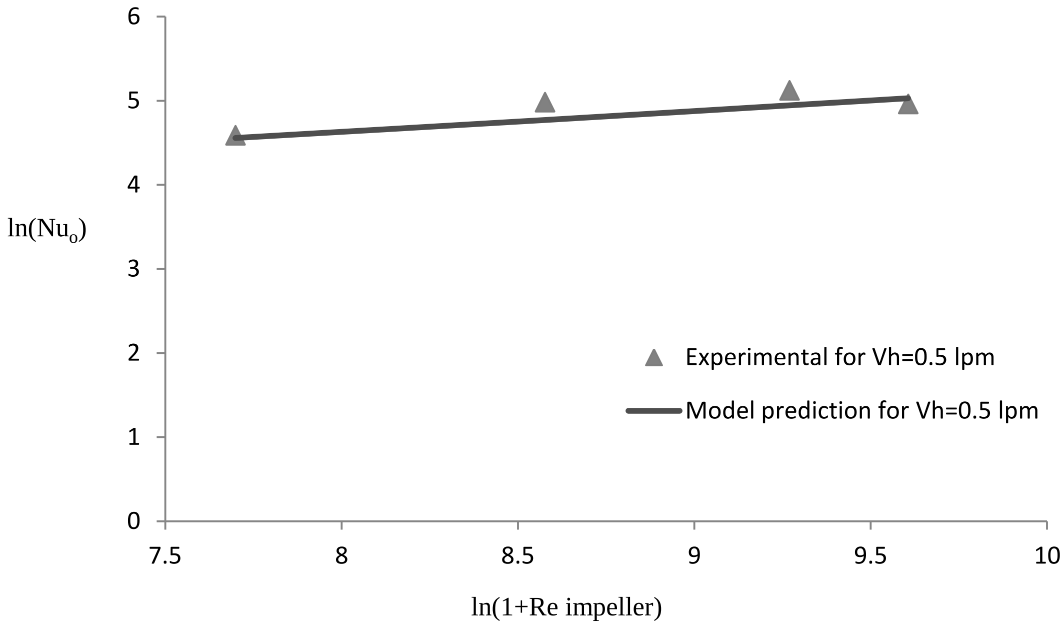

Fig. 5.5: Prediction of experimental data points, for V_h=0.5 *lpm* flow, with the modified correlation for ABR

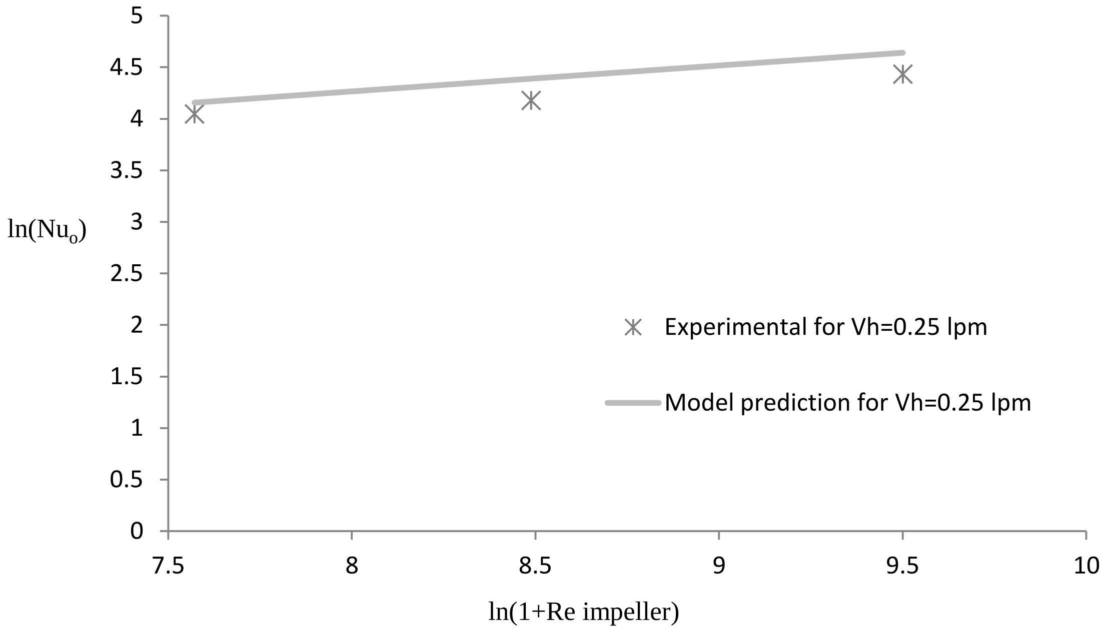

Fig. 5.6: Prediction of experimental data points, for V_h=0.25*lpm* flow, with the modified correlation for ABR

5.4.2. Heat transfer experiments with Bunsen reaction in ABR:

In ABR, Bunsen reaction has been carried out. The reactants, Iodine saturated hydriodic acid, water and Sulfur dioxide gas were passed through the reactor. The heat of reaction was removed by the cooling water flowing through the helical coil. Isothermal conditions were maintained in the reactor.

Taking into experimental conditions into account such as heat of reaction, flow rates of reactants were chosen. Experiments were carried out with flow rates 51mlpm of Iodine saturated hydriodic acid and 10 mlpm of water. Flow of sulfur dioxide and agitator speed were changed in the experiments with the experimental parameters as shown in Table 5.2.

Table 5.2: Steady state temperature data during Bunsen reaction at various experimental conditions

Sr No	SO_2 flow gps	Agitator speed rpm	Reactor temperature ^{O}C	Cooing water flow mlpm	Cooling water in temperature ^{O}C	Cooling water out temperature ^{O}C	Overall heat transfer coefficient W/m^2 K		Error %
							Experimental	Calculated	
1	0.015	150	29.3	185	27.5	28.3	106	116	9.14
2	0.05	200	30.5	185	27.8	29.1	119	122	2.63

For the first experiment, the overall heat transfer coefficient calculated using the correlation Equation 13. It is within 10% of the experimentally obtained value. For the second experiment with increased SO_2 flow (thereby increase in heat of reaction) and increased agitator speed, experimentally obtained overall heat transfer coefficient has increased. This enhancement in heat transfer, also well predicted by Equation (5.13) is within 3% error.

At increased SO_2 flow, gas bubbles flow in reactor enhances heat transfer to some extent. This effect is not considered in developed correlation. Therefore there is a higher value for experimental overall heat transfer coefficient at higher SO_2 flow.

Uncertainty estimate in the overall heat transfer coefficient is around +/- 4 %.

Thus the applicability of heat transfer correlation, developed with water-water heat transfer study, is validated for the actual Bunsen reaction system in ABR, where in density of reactants is around 2.5 times of that of water and the viscosity around 1.5 times of water.

5.5 Conclusion:

Heat transfer study in Agitated Bunsen Reactor is required for reactor sizing with effective heat removal. In the agitated Bunsen reactor heat removal can be more efficient by increasing the agitation speed and/or cooling water flow rate through the coil. Study has been conducted for water as well as Bunsen reaction by varying the flow rates through the reactor side at different agitation speeds. Modified heat transfer correlation for the reactor side / shell side, which accounts both fluid flow as well as mixing, has been obtained. The correlation is reasonably accurate in the range of 50 to 500 of flow Reynolds' number and in the range of 1,500 to 15,000 of impeller Reynolds' number.

Chapter VI

Phase Separation Studies

in

Agitated Bunsen Reactor

6.1. Introduction:

In Bunsen reaction with chemicals, sulfur dioxide and iodine, water is split to form two acids viz. hydriodic and sulfuric acid. Separation of acids produced [132,169] is the key step, after the reaction. Separation studies [143,170,171] have been carried out in batch apparatus and effect of different compositions on layer formation was studied.

In ABR simultaneous reaction and phase separation is envisaged. For removing the light phase from top section of reactor, there has to be separation between the light and heavy phases. This demarcation is the interphase. The study of interphase thickness i.e. mixed phase thickness where both phases are present, is important from operational point. The interphase thickness has to be less, such that it can be easily detected by instruments. So that interphase layer can be maintained at a particular height and thereby withdrawal of light and heavy phase can be adjusted. When interphase thickness is more, the heavy phase gets entrained in the light phase, leading to increased impurity in the light phase. Thus, twin objective of reaction and phase separation in single reactor gets defeated.

6.2. Experimental:

The experimental setup (Figure 6.1) consists of agitated Bunsen reactor assembly, volumetric flow meters, pumps for feeding the two phases and sample ports.

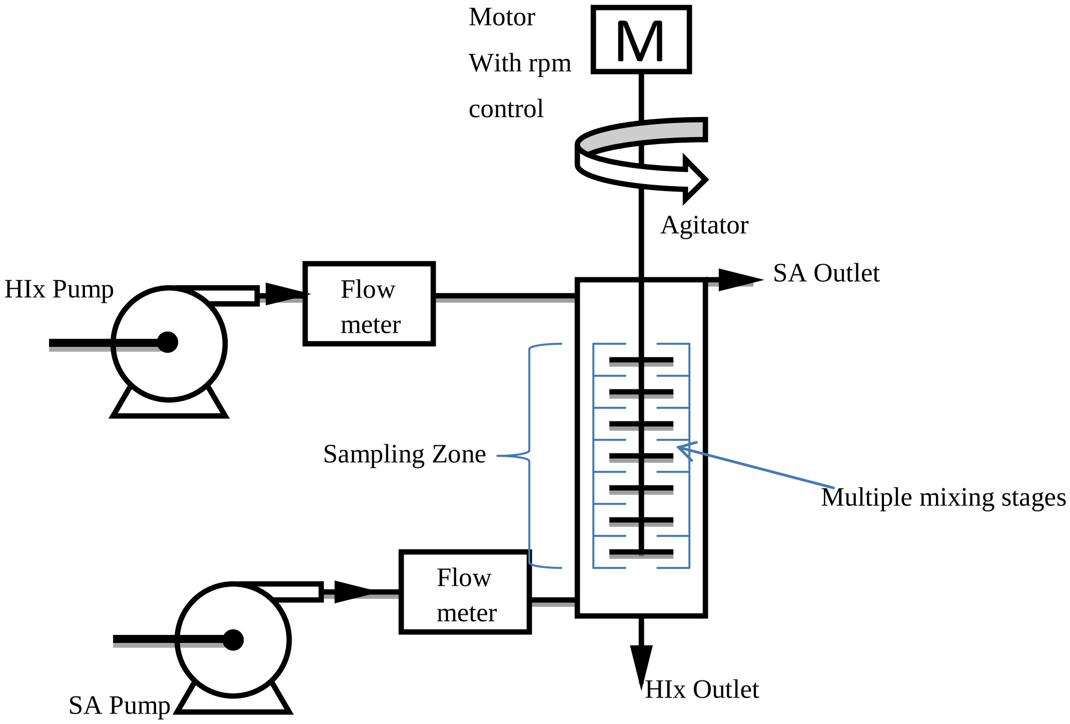

Figure 6.1: Schematic of experimental setup

To study phase separation in ABR two different pairs of chemicals have been used.

6.2.1. Case A: Water and kerosene

Water and kerosene were chosen for the study. Water was fed from the top which was a heavy phase and kerosene which was a light phase was fed from the bottom, samples were collected at different points along the axial direction as shown in Figure 6.2. The flow rates were fixed 200 mlpm for water and 50 mlpm for kerosene. The agitation speeds were 370, 450, and 530 rpm. Experiments were carried out at standard atmospheric conditions.

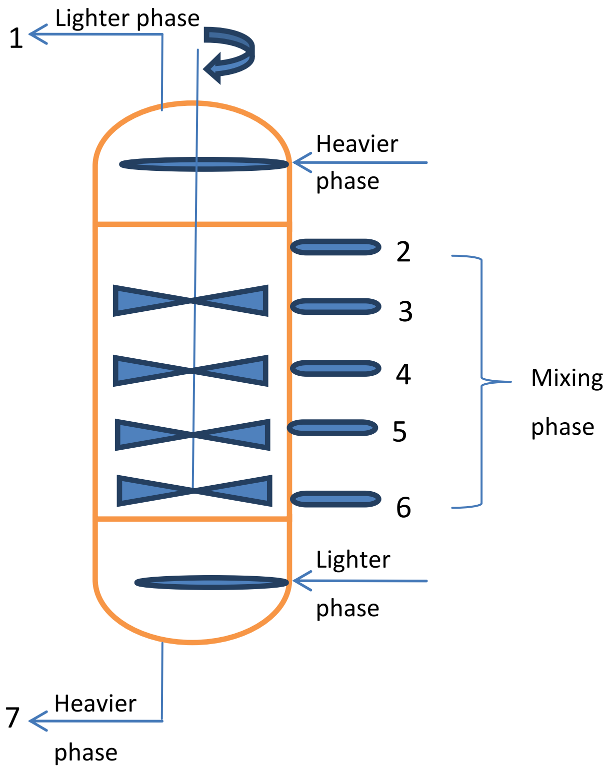

Figure 6.2: Sample drawing location for water & kerosene experiments

6.2.2. Case B: Hydriodic acid and sulfuric acid

Bunsen reaction products viz. hydriodic acid and sulfuric acid were chosen for the study. The flow rates of SA (sulfuric acid) phase (light) and HIx (heavy phase) were in the range of 40-50 millilitre per minute (mlpm) and 160-200 mlpm respectively. The experiments were carried out in the lowest to the highest ranges of flow rates i.e. 40 mlpm & 160 mlpm of light and heavy phase respectively and 50 mlpm & 200 mlpm of light and heavy phase respectively. This ratio of flow rates was chosen as during Bunsen reaction the product composition of sulfuric acid and hydriodic acid is around 1:4. Experiments were carried out at standard atmospheric conditions and at 240, 350 & 500 rpm of stirrer speed. Experiments were carried out without conducting Bunsen reaction. The composition of SA was 50 wt% and in HIx phase Iodine was 7.2 mol/l in 57 wt% HI solution. When these acids were mixed together in a test tube and allowed to settle, clear phase separation was observed.

From top inlet heavy phase HIx was fed and from the bottom inlet light phase sulfuric acid was fed by pumps. From top outlet separated sulfuric acid was collected and from bottom outlet separated HIx was collected and samples were collected at different points along the axial direction as shown in Figure 6.3.

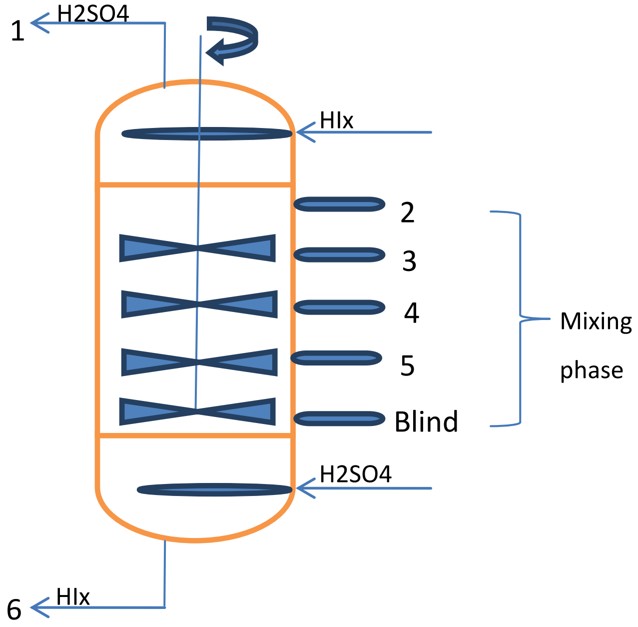

Figure 6.3: Schematic of Reactor with sample drawing location for SA & HIx experiments

6.3. Results and discussions:

6.3.1. Case A: Water and kerosene experiments

Tables 6.1, 6.2 and 6.3 show percentage of kerosene and water in samples at different agitation speed.

Figures 6.4, 6.5 and 6.6 show the volume (%) vs. sample location profiles at 370, 450, 530 rpm respectively. Water and kerosene separation was instantaneous in all the cases. As soon as the kerosene entered the bottom; droplets coalesce to form larger droplets and move upward by buoyancy forces. There was a significant concentration difference in the radial direction (visual observation during experiments) i.e. as the two liquids travel in radial direction there was phase separation; precisely this was the reason for very less or negligible quantities of either phases in the sample collection. This was due to very less mixing (even at the highest agitation speed of 530 rpm) in individual compartments which results in the phase separation in the radial direction also. The interplay between breakage and coalescence process, which depends on the agitation intensity, physical properties of two liquids (especially the interfacial tension) determines the mean drop diameters and drop size distribution and local dispersed-phase hold-up. Conversely, high agitation levels lead to strong drop breakage, consequently to very small drops and large interfacial areas, but too small drops lead to entrainment losses, excessive axial mixing, and higher local hold-ups, potentially also leading to the flooding of the column.

Table 6.1: kerosene and water separation data at 370 rpm

Sample Port No	Agitation (rpm)	Total volume sample (ml)	kerosene volume (ml) in sample	water volume (ml) in sample	% kerosene	% water
1	370	14.6	14.6	0	100.0	0.0
2		18.5	0.2	18.3	1.1	98.9
3		20.6	0.05	20.55	0.2	99.8
4		30.3	0	30.3	0.0	100.0
5		22.3	0	22.3	0.0	100.0
6		20.4	0	20.4	0.0	100.0
7		22.8	0	22.8	0.0	100.0

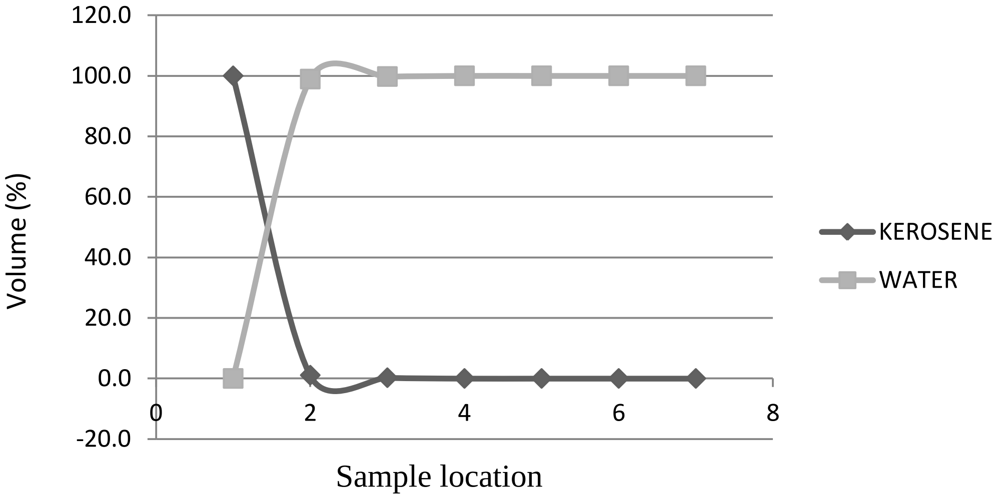

Fig 6.4: volume (%) vs sample location number of water and kerosene, at 370 rpm

Table 6.2: kerosene and water separation data at 450 rpm

Sample Port No	Agitation (rpm)	Total volume sample (ml)	kerosene volume (ml) in sample	water volume (ml) in sample	% kerosene	% water
1	450	24.7	24.07	0	97.4	0.0
2		19.5	0.05	19.45	0.3	99.7
3		17.5	0.01	17.5	0.1	100.0
4		25.4	0	25.4	0.0	100.0
5		22.8	0	22.8	0.0	100.0
6		26.7	0	26.7	0.0	100.0
7		23.4	0	23.4	0.0	100.0

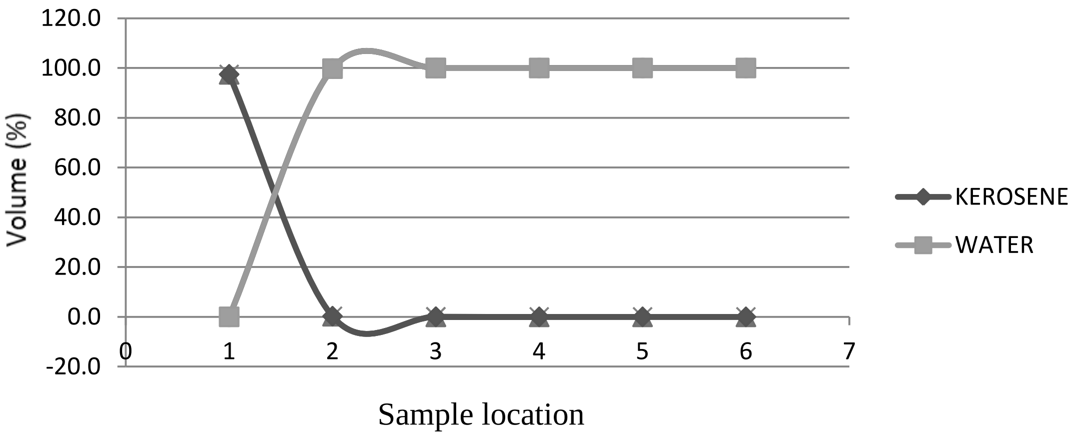

Fig 6.5: volume (%) vs sample location number of water and kerosene, at 450 rpm

Table 6.3: kerosene and water separation data at 530 rpm

Sample Port No	Agitation (rpm)	Total volume sample (ml)	kerosene volume (ml) in sample	water volume (ml) in sample	% kerosene	% water
1	530	28.1	28.1	0	100.0	0.0
2		26.9	0.05	26.85	0.2	99.8
3		21.5	0.1	21.4	0.5	99.5
4		22.5	0.15	22.35	0.7	99.3
5		23.3	0.1	23.2	0.4	99.6
6		34.1	0	34.1	0.0	100.0
7		28.3	0	28.3	0.0	100.0

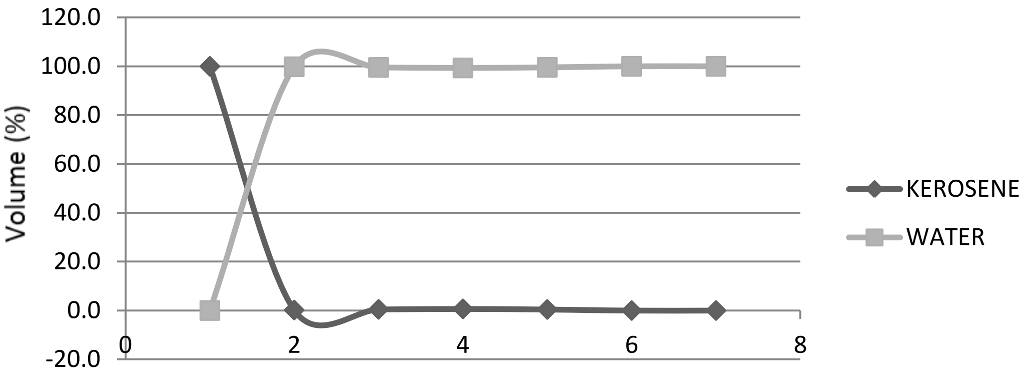

Fig 6.6: volume (%) vs sample location number of water and kerosene, at 530 rpm

6.3.2. Case B: Sulfuric acid and HIx phase experiments

The results are shown in the Tables 6.4 & 6.5 for different set of experiments at different agitation speeds and different flow rates of two phases. The separation was the best when there was no agitation which is a reasonable result as shown in Figures 6.7 & 6.8. Agitation enhances the inter mixing of the two phases which in turn increases the impurity levels in the phases. But agitation is required during Bunsen reaction, to remove the exothermic heat and maintain the desired reactor temperature and high mass transfer rates between the reactants. As the agitation was increased up to 350 rpm the variation in the phase separation (Figure 6.9 & 6.10) behavior was not drastic but at 500 rpm phase impurities increased significantly (Figure 6.11). The other observation was, as the agitation speed was increased the interphase layer which was maintained above the HIx feed point, broadened as shown in Table 6.6 which again was undesirable.

The inter-phase layer broadening leads to the entrainment of HIx in the sulfuric acid phase which in-turn can choke the lines in sulfuric acid section and also corrosion of material in that section. It is desirable to operate the Bunsen reactor under agitation speed such that good mass and heat transfer characteristics are achieved but agitation speed should not be high enough that leads to disruption in phase separation.

Results show that the agitation speed up to 240 rpm is suitable for the better separation.

Table 6.4: SA (50 mlpm) and HIx (200 mlpm) phase separation data at different rpm

Sample Port No	Agitation rpm	H_2SO_4 (mol/l)	HI (mol/l)
1	Nil	3.30	0.60
2		0.15	2.84
3		0.20	2.76
4		0.18	2.86
5		0.26	2.84
1	240	3.26	0.60
2		0.12	2.86
3		0.09	2.91
4		0.29	2.73
5		0.19	2.77
1	350	3.18	0.60
2		0.15	2.76
3		0.12	2.82
4		0.16	2.77
5		0.22	2.73
1	500	0.60	2.66
2		0.21	2.70
3		0.17	2.81
4		0.19	2.75
5		0.25	2.68

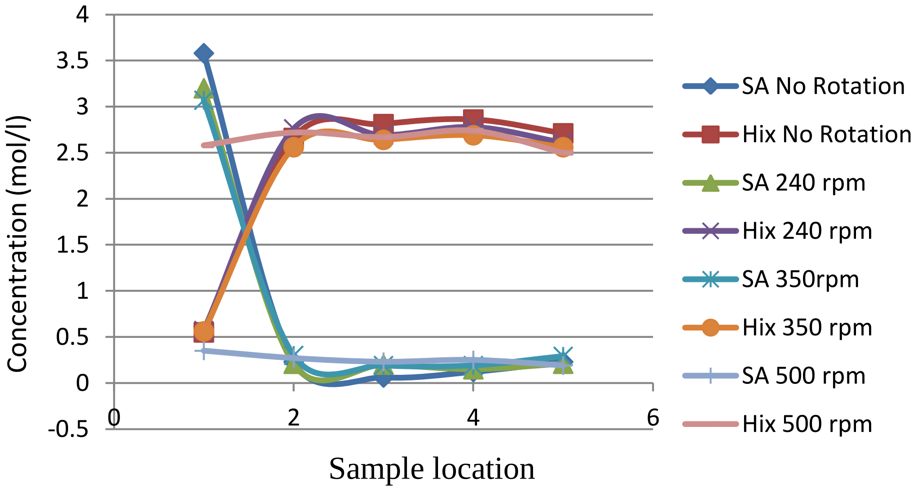

Fig 6.7: Concentration (mol/l) vs sample location number of 50 mlpm SA and 200 mlpm HIx

Table 6.5: SA (40 mlpm) and HIx (160 mlpm) phase separation data at different rpm

Sample port No	Agitation rpm	H_2SO_4 (mol/l)	HI (mol/l)
1	Nil	3.58	0.55
2		0.23	2.66
3		0.06	2.81
4		0.12	2.86
5		0.23	2.71
1	240	3.20	0.57
2		0.21	2.76
3		0.20	2.69
4		0.15	2.78
5		0.21	2.61
1	350	3.07	0.56
2		0.30	2.56
3		0.19	2.64
4		0.19	2.69
5		0.29	2.56
1	500	0.35	2.58
2		0.27	2.72
3		0.23	2.67
4		0.25	2.74
5		0.19	2.50

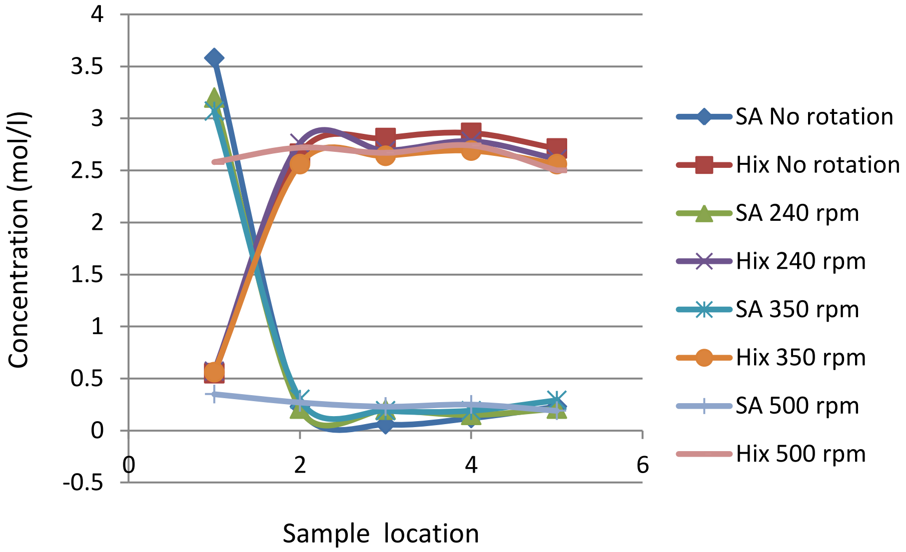

Fig 6.8: Concentration (mol/l) vs sample location number of 40 mlpm SA and 160 mlpm HIx

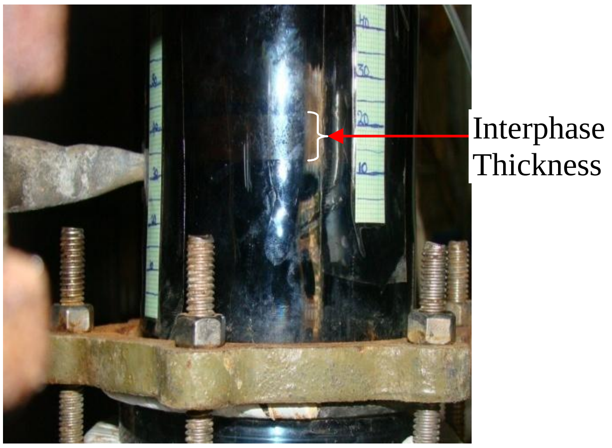

Fig 6.9: Interphase thickness of ~9 mm at 240 rpm

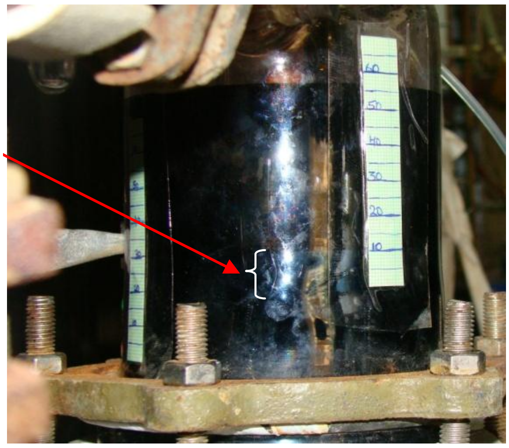

Fig 6.10: Interphase thickness of ~15mm at 350 rpm

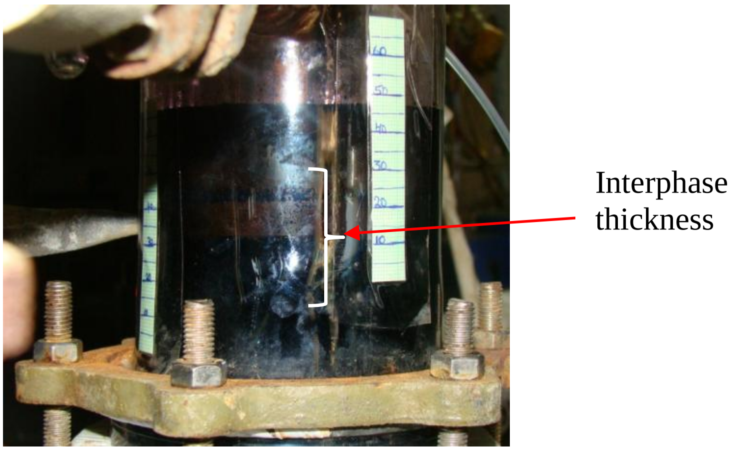

Fig 6.11: Interphase thickness of >25 mm at 500 rpm

Table 6.6: Inter phase layer at different agitation speed at 50 mlpm SA and 200 mlpm HIx

Agitation Speed (rpm)	Interphase layer thickness (mm)
Nil	< 1
240	~ 9
350	~ 15
500	>25

When these two acids, SA and HIx were mixed and left in sample bottle, within few minutes distinct interface in the form of a line could be seen.

But the result in Table 6.6 for no agitation shows, < 1 mm as interphase thickness, this was due to the fact that the two acid phases were in constant motion with continuous input and output which led to disturbance and hence variation from distinct line of interphase was observed. For the case of 500 rpm, it was observed that the interphase layer got entrained into sulfuric acid phase outlet.

6.4. Conclusions:

Bunsen reaction products mixture phase separation behavior was studied in a counter-current flow reactor at different flow rates and different agitation speeds. It was observed that the best phase separation was achieved when there was no agitation and higher agitation intensities were leading to undesirable scenarios such as broadening of the interphase layer, cross contamination of the two phases. Lower agitation intensities were desirable as it gave stable interphase layer.

From the studies, it was concluded that process integration of Bunsen reaction and separation of phases in single equipment is feasible.

Chapter VII

Reaction and Layer Separation Studies in Agitated Bunsen Reactor

7.1. Introduction:

In this chapter obervations of counter-current Bunsen reaction experiments and layer separation are discussed.

7.2. Experimental:

Experimental set-up consisted of Bunsen reactor (ABR) along with hot/cold water system feeding to internal helical coils, feeding systems for gaseous reactant (sulfur dioxide), nitrogen, iodine & water and scrubbing system for un-reacted sulfur dioxide as shown in Fig. 2.3 in chapter II. The heating/cooling water system maintained the temperature of the reactor such that isothermal operation was achieved.

Experiments were carried out in ABR in continuous counter-current mode. Reaction liquid was brought to the desired temperature with the hot/cold water flowing through the helical coil of the reactor. SO_2 gas (pure SO_2 or SO_2 diluted with nitrogen) was bubbled from bottom portion of the reactor. Iodine dissolved in hydriodic acid solution was fed from the top portion of the reactor and water was fed in the middle portion of the reactor. Iodine & water were in large excess. Their concentrations varied slightly for different experiments. Agitator speed was set at 200 rpm for all experiments. At this agitator speed & in the experimental range of flows, near to plug flow conditions were achieved in the reactor. This has been established separately by carrying out RTD (residence time distribution) studies and arriving at vessel dispersion number, which is indicative of extent of axial dispersion.

The product sulfuric acid was withdrawn from the topmost portion whereas hydriodic acid containing iodine was withdrawn from the bottommost portion of reactor as shown in the block diagram of experimental set-up in figure 2.3 of chapter II. Un-reacted SO_2 was scrubbed continuously in scrubbing system containing potassium hydroxide and samples were taken at different time intervals for analysis. Experiments were carried out by varying the operating parameters in combination such as temperature (22°C to 39°C), SO_2 flow ($2.3438X10^{-4}$, $7.8125X10^{-4}$ & $15.625X10^{-4}$ moles/s) and SO_2 partial pressure (1, 0.814, 0.665, 0.399 bar(a)). As reaction rate and conversion information was not available even for room temperature, the above mentioned temperatures were chosen to generate data. Maximum flow rate of SO_2 was chosen considering the maximum heat removal capacity of ABR for the given conditions which was obtained during heat transfer studies. SO_2 partial pressures range chosen was around the expected partial pressure when SO_2 is recycled to Bunsen reactor from sulfuric acid section.

7.3. Results and Discussion:

Table 7.1 shows operating conditions for 12 number of experiments carried-out at different temperatures by varying SO_2 flow rate and SO_2 partial pressure with various combinations.

Table 7.1: Experimental operating conditions

Experiment no.	Operating condition			
	Reactor Temp. (°C)	SO_2 flow $X10^4$ (moles/s)	N_2 flow $X10^4$ (moles/s)	SO_2 partial pressure (atm (a))
1	29.3	2.3438	0.000	1
2	30.5	7.8125	0.000	1
3	31.1	15.625	0.000	1
4	22.3	7.8125	0.000	1
5	38.9	7.8125	0.000	1
6	29.8	2.3438	1.0714	0.665
7	29.9	7.8125	1.7857	0.814
8	29.9	7.8125	3.9286	0.665
9	29.5	7.8125	11.786	0.399
10	29.5	15.625	7.8571	0.665
11	23.6	7.8125	3.9286	0.665
12	36.1	7.8125	3.9286	0.665

Table 7.2 shows steady state composition (mole fraction) of the ABR top phase (H_2SO_4) and bottom phase (HI_X) for 12 numbers of experiments. Weight % of the acids reported in further description was calculated considering only water solvation i.e. weight % of the sulfuric acid is calculated by considering H_2SO_4 & H_2O, neglecting the HI & I_2 impurities in the top phase separated out. Similarly, weight% of the hydriodic acid is calculated by considering HI & H_2O, neglecting the I_2 solvation as well as H_2SO_4 impurity in the bottom phase separated out.

Table 7.2: Steady state phase composition at different operating conditions

Ex pt. No.	Phase composition (Mole fractionX10^2)								Global Mixture (Devoid of HI & H_2O in I_2 feed)(Mole fractionX10^2)			
	H_2SO_4 phase				HI_X phase							
	H_2SO_4	H_2O	HI	I_2	H_2SO_4	H_2O	HI	I_2	H_2SO_4	H_2O	HI	I_2
1	0.616	74.3	10.8	14.2	0.765	72.3	11.7	15.3	5.35	69.9	10.7	14.1
2	1.42	67.7	12.5	18.5	1.42	72.9	10.6	15.1	5.53	67.4	11.06	16.06
3	2.10	67.0	12.6	18.3	0.959	72.3	11.7	15.0	5.81	66.63	11.62	15.94
4	0.320	78.2	9.61	11.9	0.862	76.3	9.25	13.6	4.53	74.19	9.06	12.23
5	10.3	87.7	1.50	0.390	0.682	70.8	11.8	16.7	Phase separation observed			
6	0.121	78.2	9.38	12.4	0.260	83.4	7.54	8.78	4.07	77.65	8.13	10.15
7	6.46	88.8	3.55	1.17	1.33	71.3	10.9	16.5	Phase separation observed			
8	10.9	86.7	2.65	0.322	0.946	75.8	9.48	13.7	Phase separation observed			
9	11.1	85.7	2.22	1.03	0.772	75.9	9.52	13.8	Phase separation observed			
10	16.2	81.3	1.20	1.26	0.903	74.7	9.41	15.0	Phase separation observed			
11	0.903	76.2	9.76	13.2	0.861	79.3	8.41	11.5	4.38	74.97	8.76	11.9
12	10.1	86.9	2.08	0.887	0.849	75.3	9.91	13.9	Phase separation observed			

7.3.1. Experiments with pure SO_2:

Experiments nos. 1 to 5, were carried out with pure SO_2 by varying SO_2 flow rate at different temperatures. Effects of flow rate and temperature on acid separation are described below.

a) **Effect of SO_2 flow rate:**

Layer separation of acids produced; was not observed for varying SO_2 flow experiments carried out at room temperatures as seen in Table 7.2 (Experiment numbers 1, 2 & 3). In these sets of experiments iodine to water mole ratio in the product system were found to be inadequate for phase separation to occur. Density of produced homogenous Bunsen reaction acid product was found to be approximately 2.3 g/ml. Effect of SO_2 flow on layer separation could not be studied due to homogeneous Bunsen reaction product.

b) **Effect of reactor temperature:**

Layer separation was not observed for the experiments carried out at low temperatures 22.3°C & 30.5 °C (Experiment nos. 4 & 2). In these two sets of experiments iodine to water mole ratio in the product system was found to be inadequate for phase separation to occur. Density of the homogenous product solution was found to be around 2.3 g/ml.

Layer separation of the Bunsen reaction product acids was observed for the Experiment no. 5, carried out at 38.9 °C. H_2SO_4 (39 weight %) along with other impurities was separated out at the top of ABR and HI (54.3 weight %) along with iodine and sulfuric acid impurity was separated out at the bottom of ABR.

7.3.2. Experiments with dilute SO_2:

Experiment nos. 6 to 12, were carried out with diluted SO_2 feed (gas mixture of SO_2 & N_2) by varying SO_2 flow rate, SO_2 partial pressure and temperature. Effects of flow rate, partial pressure and temperature on acid separation are described below.

a. Effect of SO_2 flow rate:

Layer separation was not seen for the experiment no. 6 carried out at very low SO_2 flow and low N_2 flow because of insufficient iodine to water mole ratio in the product system. Density of the top sample collected was found to be 2.3 g/ml and that of bottom sample was 2.4 g/ml.

Layer separation was observed for the experiments carried out at increased gas flows (Experiments nos. 8 &10).

Mole fraction or concentration of produced sulfuric acid in the top phase increases with increase in SO_2 flow rate for the experiment nos. 8 & 10, carried out at room temperature and 0.665 atm (a) SO_2 partial pressure. H_2SO_4 (40 weight %) was produced along with other impurities and hydriodic acid (47 weight%) was produced along with iodine and sulfuric acid impurity for an increased SO_2 flow rate of 7.8125E-4 moles/s. H_2SO_4 (52 weight %) is produced along with other impurities and hydriodic acid (40 weight%) was produced along with iodine and sulfuric acid impurity at 15.625E-4 moles/s SO_2 flow rate.

b. Effect of SO_2 partial pressure:

Distinct layer separation of produced acids was observed for the room temperature experiments carried out at constant SO_2 feed flow rate at different SO_2 partial pressure (Experiment nos. 7, 8 & 9). It’s observed that the concentration/mole fraction of sulfuric acid in the top phase increases with decrease in partial pressure of SO_2 and concentration/mole fraction of sulfuric acid in the bottom phase decreases with decrease in partial pressure of SO_2. This is due to the enhancement in upward movement of produced H_2SO_4 molecules with increase in upward bubble population flow of nitrogen gas. A thorough study on effect of N_2 flow on layer separation characteristics has to be studied for further detailed understanding. Similarly variation of other components in top phase as well as bottom phase at different SO_2 partial pressure is shown in Fig. 7.1. Weight % of the acids produced (H_2SO_4-H_2O system & HI-H_2O system) are tabulated in Table 7.3. There is an increase in H_2SO_4 weight % from 28 to 40 with a decrease in SO_2 partial pressure (0.814 to 0.665 atm (a)) which is due to the enhanced upward flow of produced H_2SO_4 molecules with increase in N_2 partial pressure. This effect is negligible at low SO_2 partial pressures (between 0.665 & 0.399 atm (a)). Decrese in weight% of HI at lower SO_2 partial pressure was due to decrease in production rate of HI because of decrease in Bunsen reaction rate.

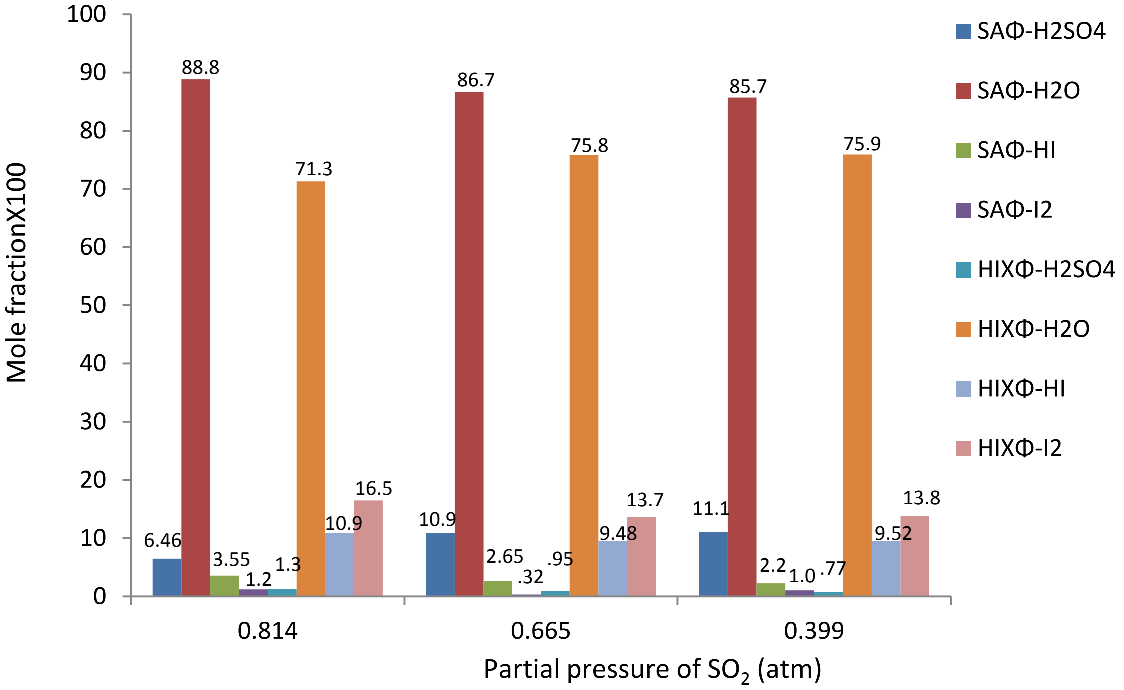

Fig 7.1: Effect of SO_2 partial pressure on layer separated acid solution’s composition

Table 7.3: Produced acid weight % at different SO_2 partial pressures

Experiment No.	H_2SO_4 phase wt%	HIx phase wt%
7	28	52
8	40	47
9	41	47

c. Effect of reactor temperature:

Layer separation of produced acids was not observed for experiment no. 11, carried out at 23.6 °C because of the less I_2/H_2O ratio in the product solution. Density of the top sample collected was 2.3 g/ml and that of bottom sample was 2.4 g/ml. Produced acids got separated out for the experiments carried out at 29.9 °C and 36.1°C (Experiment nos. 8 & 12). Decrease in sulfuric acid concentration/mole fraction was observed in top phase as well as bottom phase with increase in reactor temperature. This was due to the decrease in SO_2 conversion or acid production at increased temperature. Similarly, variation of other components in top phase as well as bottom phase at different reactor temperature is shown in Fig. 7.2.

H_2SO_4 (40 weight %) along with other impurities was separated out at the top of ABR and HI (47 weight %) along with iodine and sulfuric acid impurity was separated out at the bottom of ABR for the experiment carried out at 29.9 °C. H_2SO_4 (38 weight %) along with other impurities was separated out at the top of ABR and HI (48 weight %) along with iodine and sulfuric acid impurity was separated out at the bottom of ABR for the experiment carried out at 36.1 °C.

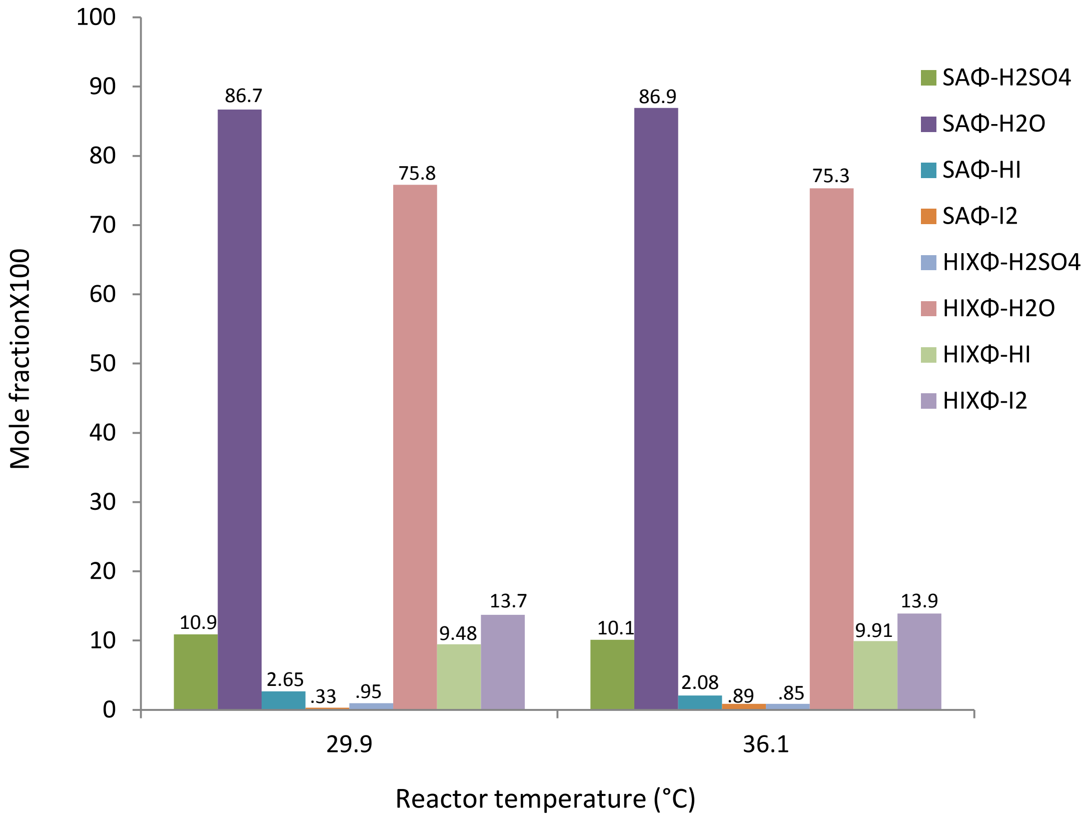

Fig 7.2: Effect of reactor temperature on layer separated acid solution's composition

7.3.3. Density of top phase (H_2SO_4 phase) and bottom phase (HIx phase) at different experimental condition:

Density of top H_2SO_4 phase and bottom HIx phase obtained from the analysis at different experimental conditions are shown in Fig. 7.3 Homogenous Bunsen reaction acid product was collected at top as well as at bottom for the experiments carried out at low temperatures and/or pure SO_2 feed (Experiment nos. 1 to 4, 6 & 11). For the experiments carried out at elevated temperatures (Experiment nos. 5 & 12) and/or with diluted SO_2 (Experiment nos. 7 to 10), acids got separated out based on difference in density. It was observed that the density of the bottom heavy HIx phase was unchanged irrespective of different experimental conditions and that of top light sulfuric acid phase varied between 1.2 g/ml and 1.6 g/ml.

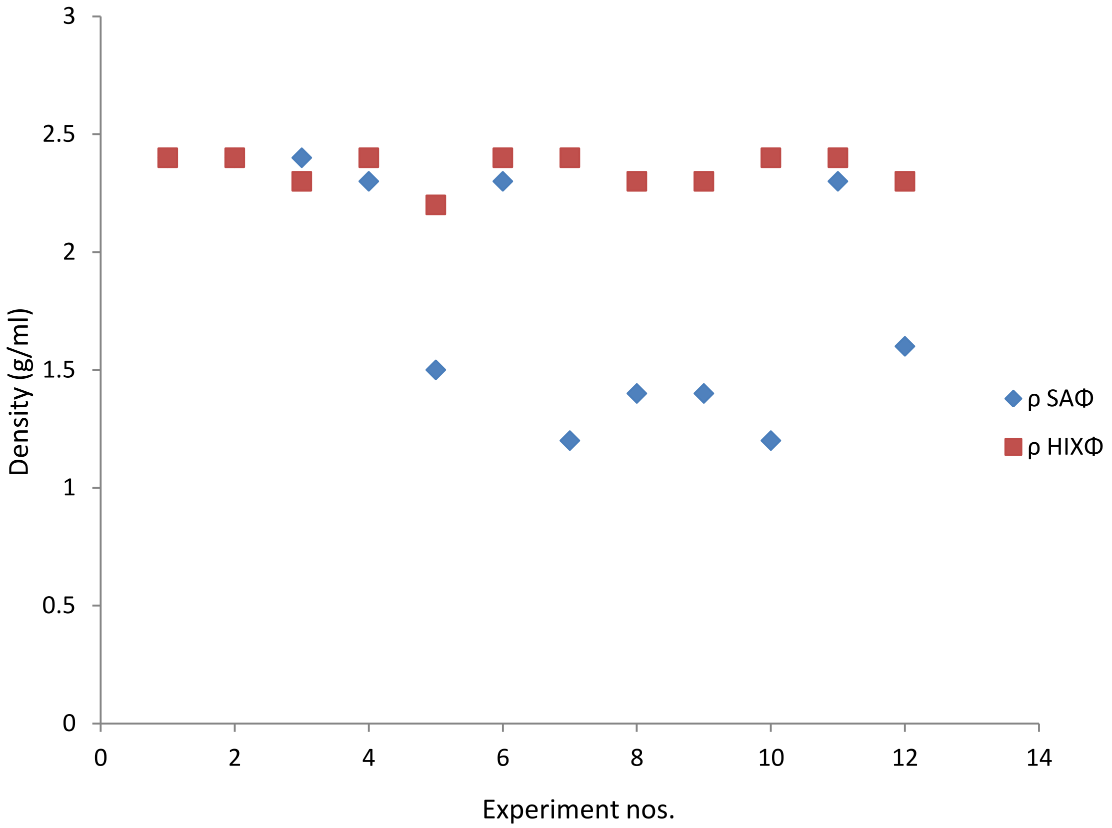

Fig 7.3: Density of top & bottom phase obtained for different experimental conditions studied

7.4. Conclusions:

For Iodine-Sulfur thermo-chemical cycle, a detailed study of heterogeneous Bunsen reaction was been carried out in agitated Bunsen reactor (ABR) in continuous counter-current mode of operation. Continuous Bunsen reaction and layer separation was carried out in ABR and feasibility of steady state, stable operation of ABR in continuous counter-current mode has been established. Layer separation of acids was not observed for experiments where I_2/H_2O ratio in the product system was less than or equal to 0.3. Decrease in the mole fraction of sulfuric acid in the top phase as well as in the bottom phase was observed with increase in temperature for experiments carried out with diluted SO_2. Increase in sulfuric acid mole fraction in the top phase and decrease in sulfuric acid mole fraction in the bottom phase was observed with decrease in SO_2 partial pressure. Density of layer separated bottom heavy phase was less affected by different experimental condition but the density of the layer separated top light phase was significantly affected by different experimental condition.

Chapter VIII

Modeling and Validation

of

Agitated Bunsen Reactor

8.1. Introduction:

In this chapter a model is proposed for ABR. The experimental results vis a vis model predictions have been compared.

8.2. Modeling of reaction system:

‘Tanks-in-series’ model, one of the non ideal reactor models has been chosen to represent ABR reaction system, in order to extract the reactor performance. ABR is a complicated reaction system where heat transfer, mass transfer and chemical reaction take place simultaneously. Ideal CSTR has been considered in each mixing zone in ABR. There are six such mixing zones in reactor which are considered as six numbers of CSTR in series.

Near to plug flow condition (ideal CSTRs in series) has been obtained at 200 rpm agitation speed at the desired flow rate. This was identified by conducting residence time distribution (RTD) study in ABR in separate experimental study (Chapter VI).

Following were the assumptions for considering non-ideal reactor model for ABR:

1. The flow of liquid and the flow of SO_2 gas through the reactor in plug flow mode. (Gas and liquid assumed to be well mixed in radial direction due to the presence of agitation in each mixing stage. Axial dispersion was found very less in the RTD (residence time distribution) studies carried out earlier on the studied ABR.)
2. The reaction liquid at uniform temperature.
   (As helical coils were immersed in the reaction liquid, the exothermic reaction heat was removed instantaneously from reaction zone.)
3. The first order reaction with respect to SO_2 in presence of excess iodine and water. (The concentration of iodine and water was maintained very high compared to the stoichiometric reaction requirement.)
4. The reactor could be modeled using ‘Tanks-in-series’ model.
   (As the reactor had six mixing stages/zones with agitator one above the other, six number of ideal continuous stirred tank reactors (CSTRs) [162-164] in series have been considered in the model.)

Let the mixing zones be CSTR 1, 2, 3 ….6 with reaction rate per unit volume of each CSTR ($-r_A''''$) as r_1, $-r_2$, $-r_3$…..$-r_6$ as shown in Fig. 8.1. F_{Ain} & F_{Aout} are the molar flow rate of SO_2 in and out of ABR, F_{N2} is the molar flow rate of nitrogen gas, $F_{Total\ in}$ & $F_{Total\ out}$ are the total molar flow rate of gas in and out of the reactor and P_{Ain} & P_{Aout} are the partial pressure of SO_2 gas at inlet and outlet of reactor. Let V_r be the volume of each CSTR, then

$$\text{Loss of A from the gas in volume element}, V_r = (F_{Ain} - F_{Aout}) = -r_A''''V_r \quad (8.1)$$

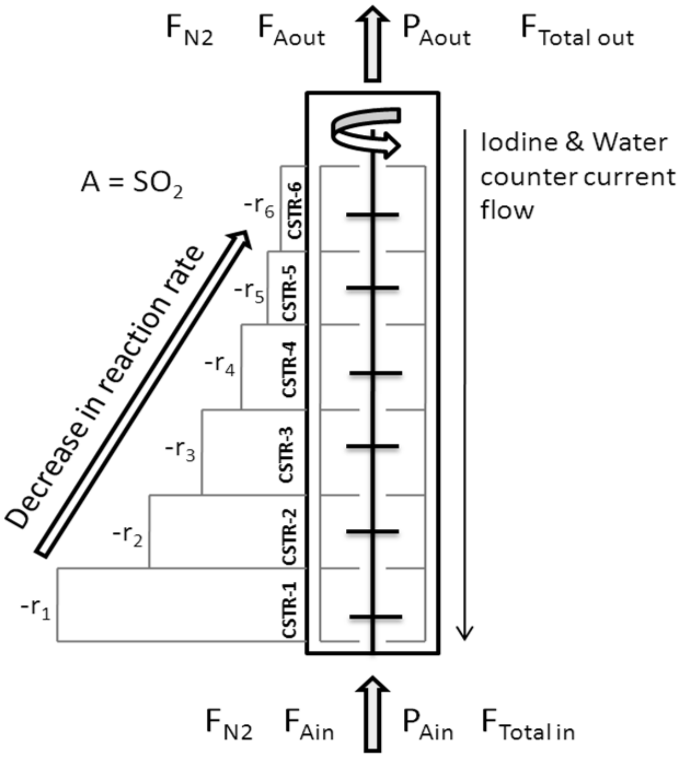

Fig. 8.1: ‘Tanks in series’ model for ABR

The heterogeneous reaction in each CSTR is described based on two film theory wherein the absorption of a diluted gaseous reactant (SO_2 + nitrogen) is taking place in an excess liquid reactant (H_2O) and getting reacted in liquid phase. Here three resistances are in series; first one is the gas film resistance second one is the liquid film resistance and third is the reaction resistance. Thus the solubility of the gaseous reactant and mass transfer effect from liquid film to the reaction plane should be accounted [159-161].

Reaction rate ($-r_A''''$) for the heterogeneous reaction system accounting all three resistances [162] is given by

$$-r_A'''' = \frac{P_A}{\left(\frac{1}{K_{Ag}a} + \frac{H_A}{K_{Al}aE} + \frac{H_A}{kf_l}\right)} \quad (8.2)$$

where P_A is the partial pressure of SO_2 gas at any location in the reactor, H_A is the phase distribution coefficient or Henry’s law constant for the gas phase system, K_{Ag} & K_{Al}

are the mass transfer coefficients for the gas phase and liquid phase respectively, 'a' is the gas-liquid interfacial area per unit volume of contactor, 'E' is enhancement factor for mass transfer with reaction, 'k' is reaction rate constant and 'f_l' is the liquid holdup. Value of 'k' reaction rate constant lies between $10^2 – 10^3$ s^{-1} [124] and value on lower side i.e. 10^2 s^{-1} has been considered for calculations. Dependent parameters in Equation (8.2) such as K_{Ag}, K_{Al} , 'a' , E and H_A are calculated by choosing appropriate standard equations and empirical correlations which are given in Appendix 1.

Equations (8.1) & (8.2) describe the reaction system. Equation (8.1) is the material balance for the CSTR system and Equation (8.2) is the kinetic model of Bunsen reaction system which accounts for both reaction kinetics as well as mass transfer kinetics. F_{Aout} from each CSTR was calculated from Equation (8.1) & (8.2), which was the F_{Ain} for the next CSTR. Sulfur dioxide (pure or diluted) enters at the bottom of CSTR 1, where the reaction rate, $-r_1$ is supposed to be the highest as represented in Fig. 8.2. The effect of partial pressure, temperature and velocity of SO_2 gas or $SO_2 + N_2$ gas mixture considered here; were the three independent parameters of the system.

8.3. Results and Discussion:

Table 8.1 shows the experiments carried out at different temperatures by varying sulfur dioxide flow rate and SO_2 partial pressure with various combinations. Experiment nos. 1, 2 and 3 have been carried out at room temperature (around 30°C) with different flow rates of pure SO_2 in order to study its effect on reactor performance. Experiment nos. 2, 4 and 5 were carried out at constant SO_2 flow rate with varying temperature to study its effect on reaction system. Experiment nos. 6, 8 and 10 were carried out at room temperature (around 30°C) at different SO_2 flow rate with a constant partial pressure of 0.665 atm (a) in order to study the effect of SO_2 gas flow rate on the reactor performance. Effect of SO_2 partial pressure on reactor performance has been studied in experiment nos.

7, 8 and 9, which were carried out at room temperature (around 30°C) and at a constant SO_2 flow rate by varying SO_2 partial pressure. Experiment nos. 8, 11 and 12 were carried out at constant SO_2 flow rate and constant SO_2 partial pressure with varying temperature to study its effect on reaction system.

Efforts have been made to maintain temperatures at desired value (say room temperature ~ 30°C). Due to much dynamicity of complex heterogeneous Bunsen reaction system, final steady state temperatures achieved (29.3°C, 30.5°C, 31.1°C etc. shown in Table 8.1) were not exactly at desired value but not far from desired value. Slight deviation of steady state temperature from the desired value is acceptable for the present study.

Table 8.1: Range of experiments carried out at different operating conditions

Experiment no.	Operating condition			
	Reactor Temp. (°C)	SO_2 flow $X10^4$ (moles/s)	N_2 flow $X10^4$ (moles/s)	SO_2 partial pressure (atm(a))
1	29.3	2.3438	0.000	1
2	30.5	7.8125	0.000	1
3	31.1	15.625	0.000	1
4	22.3	7.8125	0.000	1
5	38.9	7.8125	0.000	1
6	29.8	2.3438	1.0714	0.665
7	29.9	7.8125	1.7857	0.814
8	29.9	7.8125	3.9286	0.665
9	29.5	7.8125	11.786	0.399
10	29.5	15.625	7.8571	0.665
11	23.6	7.8125	3.9286	0.665
12	36.1	7.8125	3.9286	0.665

Average reaction rate $(-r_A''''V_r)$ in ‘moles/s’ was calculated experimentally with feed flow rate and scrubbing rate of SO_2. Average reaction rate in model was calculated as the sum of the products of rates in individual CSTR and corresponding CSTR volumes, i.e $\sum -r_i''''V_i$.

Experimental sulfur dioxide conversion was found out by subtracting the amount of sulfur dioxide scrubbed in KOH scrubber from the total sulfur dioxide fed to the ABR in the given experimental time. Model conversion was calculated from flow rate of SO_2 at the inlet of first CSTR and that at the outlet of last CSTR.

Model results are compared with experimental results for various combinations and discussed below.

8.3.1. Experiments with pure SO_2:

a) Varying SO_2 flow and constant temperature

Table 8.2 and Fig. 8.2 show the effect of sulfur dioxide flow rate on the average reaction rate and conversion at constant reactor temperature in pure SO_2 experiments. From the table and graph, it is seen that both experimental and model predicted average reaction rate increase with increase in SO_2 flow rate. Experimental conversion and model conversion for all 3 different cases are 100%, which shows the presence of other reactants (H_2O & I_2) in excess and thereby pseudo first order kinetics of Bunsen reaction with respect to SO_2.

Table 8.2: Effect of pure SO_2 flow rate on average reaction rate and conversion at room temperature

Expt No.	SO_2 flow $X10^4$ *(moles/s)*	Avg. rate*Vol.$X10^4$ (moles/s)			Conversion (%)		
		Experiment $-r_A''''V_r$	Model $\sum -r_i''''V_i$	Error (%)	Experimental	Model	Error
1	2.3438	2.3	2.3	0	100	100	0
2	7.8125	7.8	7.8	0	100	100	0
3	15.625	15.6	15.6	0	100	100	0

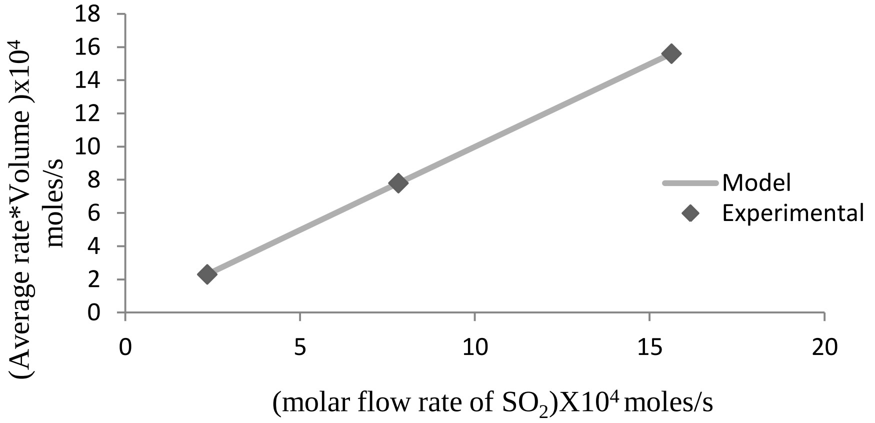

Fig 8.2: Effect of pure SO_2 flow rate on average reaction rate at constant reactor temperature

b) Varying temperature and constant sulfur dioxide flow

Table 8.3 and Fig. 8.3 show the effect of reactor temperature on the average reaction rate and conversion at constant sulfur dioxide flow rate in pure SO_2 experiments. This flow rate chosen is half of the maximum flow rate of SO_2 depending upon the maximum heat removal capacity of ABR for the given conditions. It is seen that both experimental and model predicted average reaction rate decrease with increase in reactor temperature. As the reaction is exothermic, increase in temperature also contributes to decrease in conversion.. Also increase in 'phase distribution coefficient' at higher temperatures decreases the solubility of SO_2 in the gas-liquid interphase resulting in decrease in conversion. Experimental and model conversions were 100% for 22.3 °C & 30.5 °C experiments, which shows the availability of reaction volume / reactor volume for complete SO_2 conversion even though there is a decrease in gas solubility for a temperature rise of 8.2 °C. At 38.9 °C, decrease in SO_2 gas solubility is predominant and there is a decrease in reaction rate and hence SO_2 conversion. This decrease in conversion predicted by the model is within 2.1% error with respect to experimental conversion. The errors in model prediction for average reaction rates are within 3% with respect to experimental values.

Table 8.3: Effect of reactor temperature on average reaction rate and conversion at constant pure SO_2 flow rate @$7.8125X10^{-4}$ *moles/s*

Expt No.	Reactor temperature (°C)	Avg. rate*Vol.$X10^4$ (moles/s)			Conversion (%)		
		Experiment $-r_A''''V_r$	Model $\sum -r_i''''V_i$	Error (%)	Experimental	Model	Error
4	22.3	7.8	7.8	0	100	100	0
2	30.5	7.8	7.8	0	100	100	0
5	38.9	7.4	7.6	+2.7	95	97	+2.1

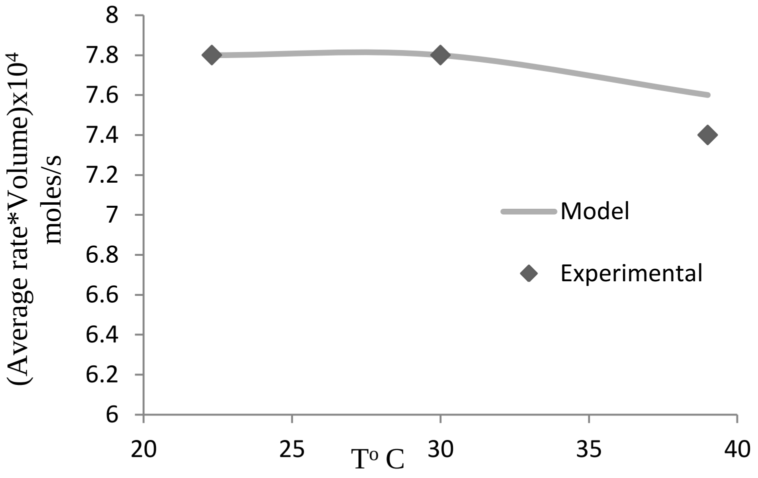

Fig 8.3: Effect of reactor temperature on average reaction rate for pure SO_2 at constant flow rate

8.3.2. Experiments with dilute SO_2:

a. Varying (SO_2 + N_2) flow at constant temperature and same partial pressure

Table 8.4 and Fig. 8.4 show the effect of sulfur dioxide flow rate on average reaction rate and conversion at constant reactor temperature and a fixed inlet SO_2 partial pressure in diluted (with N_2) SO_2 experiments. The criteria for choosing 0.665 atm (a) partial pressure is that when SO_2 is recycled from sulfuric acid section to Bunsen reactor, this is the expected partial pressure. From the table and graph, it is seen that both experimental average reaction rate and model predicted average reaction rate increase with increase in SO_2 flow rate.

Experimental conversion and also model conversion increase with increase in flow of SO_2. With increase in flow of SO_2 + nitrogen, mass transfer coefficient increases. Also increase in total flow increases interfacial area. The increase in interfacial area is more predominant compared to increase in mass transfer coefficient.The errors in model prediction for reaction rate and conversion are within 11% with respect to experimental values.

It was observed that the average reaction rates and conversions achieved for diluted SO_2 experiments (diluted with N_2 gas) were lesser compared to that of pure SO_2 experiments (Table 8.2). This was due to lesser SO_2 partial pressure in the reactor and increased film resistance (gas film & liquid film) at the inlet of the reactor.

Table 8.4: Effect of SO_2 flow rate on average reaction rate and conversion for a constant inlet SO_2 partial pressure 0.665*atm (a)* and reactor temperature

Expt No.	SO_2 flowX10^4 *(moles/s)*	N_2 flow X10^4 *(moles/s)*	Avg. rate*Vol.X10^4 (moles/s)			Conversion (%)		
			Experiment $-r_A''''V_r$	Model $\sum -r_i''''V_i$	Error (%)	Experimental	Model	Error
6	2.3438	1.0714	1.8	1.7	-5.6	75	73	-2.7
8	7.8125	3.9286	6.3	5.8	-9.8	81	74	-8.6
10	15.625	7.8571	13.2	11.9	-9.8	85	76	-10.6

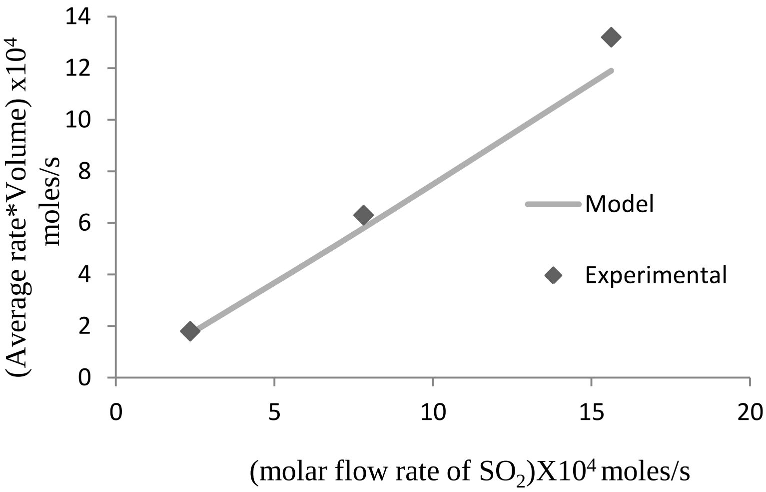

Fig 8.4: Effect of SO_2 flow rate on average reaction rate for a constant inlet SO_2 partial pressure and reactor temperature

b. Varying partial pressure at constant temperature with same sulfur dioxide flow

Table 8.5 and Fig. 8.5 show the effect of partial pressure of sulfur dioxide on average reaction rate and conversion at constant reactor temperature and a fixed SO_2 flow in diluted (with N_2) SO_2 experiments. It was observed that both experimental average reaction rate and model predicted average reaction rate decrease with decrease in SO_2 partial pressure. Experimental conversion and model predicted conversion decrease with decrease in sulfur dioxide partial pressure. The decrease in rate and decrease in conversion were due to decrease in SO_2 partial pressure in the reactor. The errors in model prediction for reaction rate and conversion are within 10% with respect to experimental values.

Table 8.5: Effect of inlet partial pressure of SO_2 on average reaction rate and conversion for a fixed SO_2 flow 7.8125X10^{-4} *moles/s* and at room temperature

Expt No.	N_2 flow X10^4 *(moles/s)*	SO_2 partial pressure *(atm(a))*	Avg. rate*Vol.X10^4 (moles/s)			Conversion (%)		
			Experiment $-r_A''''V_r$	Model $\sum -r_i''''V_i$	Error (%)	Experimental	Model	Error
7	1.7857	0.814	6.6	6.1	-7.6	84	78	-7.1
8	3.9286	0.665	6.3	5.8	-9.8	81	74	-8.6
9	11.786	0.399	6.1	5.6	-7.9	78	71	-9.0

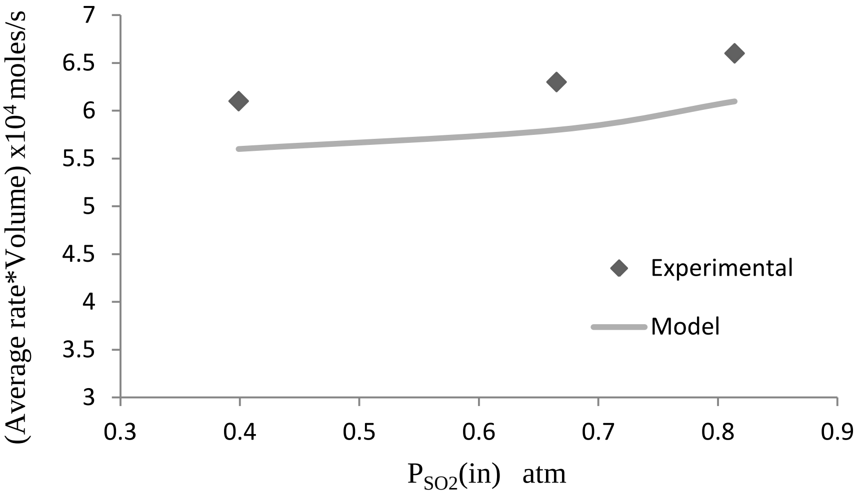

Fig 8.5: Effect of inlet partial pressure of SO_2 on average reaction rate for a fixed SO_2 flow rate at fixed reactor temperature

c Varying temperature with constant partial pressure and sulfur dioxide flow

Table 8.6 and Fig. 8.6 show the effect of reactor temperature on average reaction rate and conversion at constant sulfur dioxide flow rate and a fixed inlet partial pressure of SO_2 in diluted SO_2 experiments. From the table and graph, it is seen that both experimental average reaction rate and model predicted average reaction rate decrease with increase in reactor temperature. This decrease in average reaction rate is due to the increase in ‘phase distribution coefficient’ at higher temperatures and thereby limiting the solubility of SO_2 at the gas liquid interphase. Experimental conversion and model predicted conversion also decrease with increase in reactor temperature. The errors in model predicted average reaction rate and conversion are within 10% with respect to experimental values.

Table 8.6: Effect of reactor temperature on average reaction rate and conversion for a constant inlet SO_2 partial pressure 0.665 *atm(a)* and flow rate 7.8125X10^{-4} *moles/s* SO_2 & 3.9286X10^{-4} *moles/s* N_2

Expt No.	Reactor temperature (°C)	Avg. rate*Vol.X10^4 (moles/s)			Conversion (%)		
		Experiment $-r_A^{''''}V_r$	Model $\sum -r_i^{''''}V_i$	Error (%)	Experimental	Model	Error
8	23.6	6.5	6.0	-7.7	84	77	-8.3
11	29.9	6.3	5.8	-9.8	81	74	-8.6
12	36.1	6.2	5.6	-9.7	79	72	-8.9

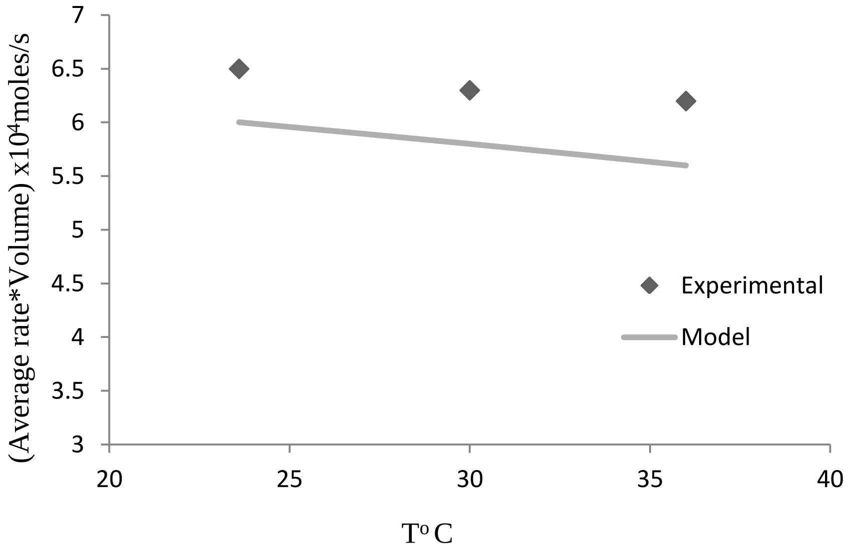

Fig 8.6: Effect of reactor temperature on average reaction rate for a constant inlet SO_2 partial pressure and flow rate

Both experimental as well as model predicted average reaction rate show increase in average reaction rate with increase in sulfur dioxide flow rate for pure SO_2 and diluted SO_2 (0.665 atm(a) partial pressure) at room temperature (Table 8.2 & 8.4). The rate of increase with unit rise in feed flow rate is comparatively higher for pure SO_2 experiments compared to diluted ones.

Experimental and model predicted average reaction rate show decrease with respect to increase in reactor temperature for pure as well as diluted SO_2 experiments (Table 8.3 & 8.6).

There is a significant drop in average reaction rate for 0.814 atm (a) SO_2 partial pressure experiment (6.6 moles/s Experimental / 6.1 moles/s Model) compared to pure SO_2 (partial pressure is 1 atm (a)) experiment (7.8 moles/s Experimental / 7.8 moles/s Model) keeping all other parameters same which is due to the combined effect of introduction of additional gas film resistance and decreased SO_2 partial pressures in reactor.

The decrease in average reaction rate for decrease in SO_2 partial pressure from 0.814 to 0.399 atm (a) is not so significant (Table 8.5).

As model prediction is within 11 % for all the cases studied, it can be safely concluded that the assumptions are valid and are applicable to the studied reactor.

Theoretical prediction is lower for average reaction rate and conversion in all the cases of diluted sulfur dioxide experiments. Decreased theoretical prediction is dominated in Table nos. 8.5 & 8.6, in which; trend in error seems to be systematic. This can be assigned to unaccounted variable volume zone between SO_2 feeding nozzle and the first CSTR, where substantial SO_2 conversion is possible. Theoretical predication can be further improved by accounting this variable volume zone between SO_2 feeding nozzle and the first CSTR compartment for the calculation of reaction rate and conversion or by keeping SO_2 feed nozzle very close to the first CSTR, thus eliminating this volume.

8.4. Conclusions:

For Iodine-Sulfur thermo-chemical cycle, a detailed study of heterogeneous Bunsen reaction has been carried out in agitated Bunsen reactor (ABR) in continuous counter-current mode of operation. It is found that, Bunsen reaction rate increases with increase in sulfur dioxide flow rate, increase in partial pressure of sulfur dioxide and decrease in reactor temperature. There is a significant drop in average reaction rate for 0.814 atm (a) SO_2 partial pressure experiment (6.6 moles/s Experimental / 6.1 moles/s Model) compared to pure SO_2 (partial pressure is 1 atm(a)) experiment (7.8 moles/s Experimental / 7.8 moles/s Model) keeping all other parameters same.

Theoretical predictions are within 11 % compared to experimental results for all the cases studied. It can be safely concluded that the assumptions are valid and the proposed non-ideal reactor model, ‘Tanks-in-series’ model along with the empirical correlations used, describe the reactor performance. This approach can be useful for the design and scale-up of agitated reactor.

Chapter IX

Conclusions

and

Recommendations

Energy requirement is increasing day by day. The search for renewable energy is on and hydrogen is envisaged as the future energy carrier. For production of hydrogen by splitting of water, thermochemical processes are being studied. Among others, iodine-sulfur thermochemical process is being studied world wide.

Water is split by means of Bunsen reaction, producing hydriodic acid and sulfuric acid as two phases, in presence of excess iodine.

The reactor in which reaction as well as acids separation can be carried out was proposed. The agitated Bunsen reactor (ABR) was studied.

1) ABR had been sized taking into consideration mixing of reactants, stages for mixing, size and type of impeller blades, cooling coil located inside the reactor and provision for input and output of reactants and products.
2) RTD studies have been carried out and range of agitator speed was found out, to operate the reactor near plug flow conditions, for the studied flow range.
3) The efficacy of cooling coil and effect of agitator speed on heat transfer performance has been studied and the existing heat transfer co-relation has been modified. The modified co-relation was validated for the Bunsen reaction experiments.
4) Phase separation of hydriodic acid and sulfuric acid flowing in counter-current direction was studied to establish feasibility of acids separation with agitating conditions.
5) The reaction and acids separation experiments have been carried out successfully. Experiments were carried out in continuous counter-current fashion. The feasibility of Bunsen reaction as well as acids separation in single equipment was established.

6) The mathematical model has been proposed for Bunsen reaction system and model has been validated with the experimental results.

The proposed Agitated Bunsen reactor with rotating blades on the axial shaft can be used as integrated equipment in iodine-sulfur thermochemical process for combining Bunsen reaction as well as acids separation. The proposed mathematical model can be used for scale up of reactor.

This work was carried out in two parts. High pressure and high temperature experiments in semi-batch mode in metallic reactor have been carried out. In glass agitated reactor, continuous counter-current mode Bunsen reaction and acids separation was carried out at atmospheric pressure and moderate temperatures.

Recommended future works are:

1) High pressure, high temperature experiments in metallic Agitated Bunsen reactor and validating/improving the proposed model.
2) Mixing of reactants in each stage and flow behaviour can be understood using CFD (computational fluid dynamics) software for better understanding of inside of the reactor.

Annexure 1

Equations used for the Modeling of Bunsen reaction system:

$$\mathrm{K_{Ag}} = 2\mathrm{D_{AB}}/\mathrm{d_b} \tag{A.1}$$

$$D_{AB} = \frac{10^{-3}\, T^{1.75} [\frac{M_A + M_B}{M_A M_B}]^{0.5}}{P[(\Sigma v)_A^{\frac{1}{3}} + (\Sigma v)_B^{\frac{1}{3}}]^2} \tag{A.2}$$

$$\mathrm{d_b} = \sqrt{\left(\frac{\sigma_L}{\rho_L} C \left(\frac{u_{SG}}{\{\sqrt[4]{[(\sigma_L g)/\rho_L]}\}}\right)^{\left(-\frac{1}{2}\right)} \left(\frac{\rho_L \sigma_L^3}{g \mu_L^4}\right)^{\left(-\frac{1}{8}\right)}\right)} \tag{A.3}$$

$$\varepsilon = 1.2 * \left(\frac{\mu_L u_{SG}}{\sigma_L}\right)^{\left(\frac{1}{4}\right)} \left(\frac{u_{SG}}{\left[\frac{\sigma_L g}{\rho_L}\right]^{\left(\frac{1}{4}\right)}}\right)^{\left(\frac{1}{2}\right)} \tag{A.4}$$

$$\mathrm{a} = \frac{6\varepsilon}{\mathrm{d_b}} \tag{A.5}$$

$$\ln \mathrm{H} = \mathrm{A} + \frac{\mathrm{B}}{\mathrm{T}} + \mathrm{C} * \ln \mathrm{T} \tag{A.6}$$

$$\mathrm{D} = 1.1728 * 10^{-16} * \frac{\mathrm{T} * (\varphi_B \mathrm{M_B})^{\left(\frac{1}{2}\right)}}{(\mu_B \mathrm{V_A^{0.6}})} \tag{A.7}$$

$$\mathrm{K_{Al}} = 0.42 \sqrt[3]{\frac{\mu_L g}{\rho_L}} \sqrt{\frac{\rho_L \mathrm{D_A}}{\mu_L}} \tag{A.8}$$

$$\mathrm{M_H} = \frac{\sqrt{\mathrm{D_A} k}}{\mathrm{K_{al}}} \tag{A.9}$$

$$\mathrm{E_i} = 1 + \frac{\mathrm{D_B C_B H_A}}{\mathrm{b D_A P_{Ai}}} \tag{A.10}$$

$$\mathrm{E} = \mathrm{f}(\mathrm{M_H} \& \mathrm{E_i}) \tag{A.11}$$

Equation (A.1) is the empirical co-relation to calculate gas phase mass transfer coefficient [172]. Equation (A.2) is to estimate diffusion coefficient for a binary mixture of gases [172]. Equation (A.3) is the correlation to calculate bubble diameter, d_b and Equation (A.4) is the correlation for gas hold up. The Gas-Liquid interfacial area, 'a' is given by Equation (A.5). Equations (A.3), (A.4) and (A.5) are applicable for heterogeneous gas-liquid reaction system in an agitated reactor in which gaseous reactant is continuously bubbling [173]. Here, plug flow reaction system is modeled as an infinite number of CSTR units in series. So above mentioned equations are applicable to individual CSTR system. Equation (A.6) is the empirical correlation for Henry's law constant for SO_2 reaction system applicable for the range of operating conditions in which A, B and C are the parameters [174]. Equation (A.7) is the correlation to calculate the gas diffusivity in liquid for dilute dissolved gas [172] and Equation (A.8) is the empirical correlation to calculate liquid phase mass transfer coefficient for completely mixed systems [175]. Equation (A.9) is to calculate the Hatta Number [162]. Expression for Enhancement factor for infinitely fast reaction, E_i is given by Equation (A.10) and Equation (A.11) shows the dependency of Enhancement factor on Hatta Number and E_i [162]. For evaluation of $E = f(M_H \& E_i)$, refer 'Enhancement factor for fluid-fluid reactions' in [162].

REFERENCES

1. REN21–Renewable Energy Policy Network for the 21st Century, Renewables 2012–Global Status Report, 2012
2. The Social impacts of energy development on national parks: final report By, United States National Park Service, University of Denver. Center for Community Change. The National Park Service, U.S. Dept. of the Interior, 1984.
3. Assessment of Energy Resource Development Impact on Water Quality, Volume 1. By Susan M. Melancon, Terry S. Michaud, Robert William Thomas. Environmental Monitoring and Support Laboratory, 1979.
4. Resources for the twenty-first century: proceedings of the international centennial symposium of the United States Geological Survey, held at Reston, Virginia, October 14–19, 1979. By Frank C. Whitmore, Mary Ellen Williams, U.S. Geological Survey.
5. The Homeowner's Guide to Renewable Energy: Achieving Energy Independence. By Dan Chiras. New Society Publishers, July 5, 2011.
6. Renewable Energy Sources for Sustainable Development. By Narendra Singh Rathore, N. L. Panwar. New India Publishing, January 1, 2007
7. Renewable Energy Sources and Climate Change Mitigation: Summary for Policymakers and Technical Summary: Special Report of the Intergovernmental Panel on Climate Change. Cambridge University Press, 2011.
8. Solar Energy and Nonfossil Fuel Research. By United States Cooperative State Research Service, Smithsonian Science Information Exchange. The Department, 1981.
9. Final Report of the Task Force on the Availability of Federally Owned Mineral Lands, Volumes 1-2. By United States. Task Force on the Availability of Federally Owned Mineral Lands.

10. eia.gov–U.S. Energy Information Administration International Energy Statistics
11. International Energy Agency: Key World Energy Statistics 2007. S. 6
12. Intergovernmental Panel on Climate Change (2007): IPCC Fourth Assessment Report - Working Group I Report on "The Physical Science Basis".
13. 'How much electricity does a typical nuclear power plant generate?' - FAQ - U.S. Energy Information Administration (EIA)
14. "Environmental impacts of coal power: air pollution". Union of Concerned Scientists. 18 August 2005. Retrieved 18 January 2008.
15. NRDC: There Is No Such Thing as "Clean Coal"
16. "Nuclear Energy". Energy Education is an interactive curriculum supplement for secondary-school science students, funded by the U. S. Department of Energy and the Texas State Energy Conservation Office (SECO). U. S. Department of Energy and the Texas State Energy Conservation Office (SECO). July 2010. Retrieved 2010-07-10.
17. "Key World Energy Statistics 2012" (PDF). International Energy Agency. 2012. Retrieved 2012-12-17.
18. "PRIS - Home". Iaea.org. Retrieved 2013-06-14.
19. "World Nuclear Power Reactors 2007-08 and Uranium Requirements". World Nuclear Association. 2008-06-09. Archived from the original on March 3, 2008. Retrieved 2008-06-21.
20. 'Japan approves two reactor restarts'. Taipei Times 2013-06-07. Retrieved 2013-06-14.
21. "Collectively, life cycle assessment literature shows that nuclear power is similar to other renewable and much lower than fossil fuel in total life cycle GHG emissions." Nrel.gov. 2013-01-24. Retrieved2013-06-22.

22. Ipsos (23 June 2011), Global Citizen Reaction to the Fukushima Nuclear Plant Disaster (theme: environment / climate) Ipsos Global @dvisor. Survey website: Ipsos MORI: Poll: Strong global opposition towards nuclear power.
23. "The myth of renewable energy | Bulletin of the Atomic Scientists". Thebulletin.org. 2011-11-22. Retrieved 2013-10-03.
24. REN21 (2010). Renewables 2010 Global Status Report p. 15.
25. http://www.iea.org/publications/freepublications/publication/cooking.pdf
26. REN21 (2011). "Renewables 2011: Global Status Report". pp. 17, 18.
27. REN21 (2013). "Renewables global futures report 2013".
28. International Energy Agency (2012). "Energy Technology Perspectives 2012".
29. United Nations Environment Programme Global Trends in Sustainable Energy Investment 2007: Analysis of Trends and Issues in the Financing of Renewable Energy and Energy Efficiency in OECD and Developing Countries (PDF), p. 3.
30. World Energy Assessment (2001). Renewable energy technologies, p. 221.
31. Steve Leone (25 August 2011). "U.N. Secretary-General: Renewables Can End Energy Poverty".Renewable Energy World.
32. Worldwatch Institute (January 2012). "Use and Capacity of Global Hydropower Increases".
33. Renewables 2011 Global Status Report, page 25, Hydropower, REN21, published 2011, accessed 2011-11-7.
34. The World Wind Energy Association (2014). 2014 Half-year Report. WWEA pp.1–8.
35. "Solar Energy Perspectives: Executive Summary" (PDF). International Energy Agency. 2011. Archived from the original on 2011-12-03.

36. Solar Fuels and Artificial Photosynthesis. Royal Society of Chemistry 2012 http://www.rsc.org/ScienceAndTechnology/Policy/Documents/solar-fuels.asp (accessed 11 March 2013)
37. European Photovoltaic Industry Association (2013). "Global Market Outlook for Photovoltaics 2013-2017".
38. European Photovoltaic Industry Association (2012). "Market Report 2011".
39. Global Solar PV installed Capacity crosses 100GW Mark. renewindians.com (11 February 2013).
40. "Technology Roadmap, Biofuels for Transport". 2011.
41. How geothermal energy works. Ucsusa.org. Retrieved on 2013-04-24.
42. "Geothermal capacity | About BP | BP Global". Bp.com. Retrieved 2013-10-05.
43. Fridleifsson, Ingvar B.; Bertani, Ruggero; Huenges, Ernst; Lund, John W.; Ragnarsson, Arni; Rybach, Ladislaus (2008-02-11), O. Hohmeyer and T. Trittin, ed., The possible role and contribution of geothermal energy to the mitigation of climate change (pdf), IPCC Scoping Meeting on Renewable Energy Sources, Luebeck, Germany, pp. 59–80, retrieved 2009-04-06
44. Glassley, William E. (2010). Geothermal Energy: Renewable Energy and the Environment, CRC Press, ISBN 9781420075700.
45. World energy consumption outlook from the International Energy Outlook, published by the U.S. DOE Energy Information Administration
46. Source: Energy Information Administration – International Energy Outlook 2004
47. National Hydrogen Association; United States Department of Energy. "The History of Hydrogen".hydrogenassociation.org. National Hydrogen Association. p. 1. Retrieved 17 December 2010.

48. Carmo, M; Fritz D; Mergel J; Stolten D (2013). "A comprehensive review on PEM water electrolysis". Journal of Hydrogen Energy. doi:10.1016/j.ijhydene.2013.01.151.
49. National Academy of Engineering (2004). The Hydrogen Economy: Opportunities, Costs, Barriers, and R&D Needs. Washington, D.C.: The National Academies Press. ISBN 0-309-53068-7. Retrieved17 December 2010.
50. BMW Group Clean Energy ZEV Symposium. September 2006, p. 12
51. "Integrated Hydrogen Production, Purification and Compression System; DOE Hydrogen Program FY 2008 Annual Progress Report" (PDF). United States Department of Energy. Retrieved 2009-09-19.
52. Badwal, Sukhvinder P.S.; Giddey, Sarbjit; Munnings, Christopher. "Hydrogen production via solid electrolytic routes". Wiley Interdisciplinary Reviews: Energy and Environment **2** (5): 473–487.doi:10.1002/wene.50.
53. "Global Hydrogen Production". Hydrogenassociation.org. 2004-08-13. Retrieved 2010-07-05.
54. "Vehicle Technologies Program: Fact #205: February 25, 2002 Hydrogen Cost and Worldwide Production". .eere.energy.gov. Retrieved 2009-09-19.
55. "Bellona-HydrogenReport". Interstatetraveler.us. Retrieved 2010-07-05.
56. 'Hydrogen production from organic solid matter'. Biohydrogen.nl.Retrieved 2010-07-05.
57. Badwal, SPS (2014). "Emerging electrochemical energy conversion and storage technologies". Frontiers in Chemistry. doi:10.3389/fchem.2014.00079.
58. Werner Zittel; Reinhold Wurster (1996-07-08). "Chapter 3: Production of Hydrogen. Part 4: Production from electricity by means of electrolysis". HyWeb: Knowledge - Hydrogen in the Energy Sector. Ludwig-Bölkow-Systemtechnik GmbH.
59. Bjørnar Kruse; Sondre Grinna; Cato Buch (2002-02-13). "Hydrogen—Status and Possibilities"(PDF). The Bellona Foundation. Archived from the original on 2002-

02-13. Efficiency factors for PEM electrolysers up to 94% are predicted, but this is only theoretical at this time.

60. Crabtree, George W.; Mildred S. Dresselhaus; Michelle V. Buchanan (December 2004). "The Hydrogen Economy". Physics Today. pp. 39. Retrieved 2008-05-09.

61. "Steam heat: researchers gear up for full-scale hydrogen plant" (Press release). Science Daily. 2008-09-18. Retrieved 2008-09-19.

62. "Nuclear Hydrogen R&D Plan" (PDF). U.S. Dept. of Energy. March 2004. Retrieved 2008-05-09.

63. William Ayers, US Patent 4,466,869 Photolytic Production of Hydrogen

64. del Valle, F. et al; Álvarez Galván, M. Consuelo; Del Valle, F.; Villoria De La Mano, José A.; Fierro, José L. G. (Jun 2009). "Water Splitting on Semiconductor Catalysts under Visible-Light Irradiation".*Chemsuschem* (WILEY-VCH Verlag GmbH & Co. KGaA, Weinheim) **2** (6): 471–485. doi:10.1002/cssc.200900018. PMID 19536754.

65. del Valle, F. et al; Del Valle, F.; Villoria De La Mano, J.A.; Álvarez-Galván, M.C.; Fierro, J.L.G. (2009). "Photocatalytic water splitting under visible Light: concept and materials requirements". *Advances in Chemical Engineering* (Academic Press) **36**: 111–143. doi:10.1016/S0065-2377(09)00404-9.

66. "Water Splitting by Visible Light: A Nanophotocathode for Hydrogen Production - Nann - 2010 - Angewandte Chemie International Edition - Wiley Online Library". .interscience.wiley.com. Retrieved2011-12-13.

67. "353 Thermochemical cycles" (PDF). Retrieved 2010-07-05.

68. Funk, J.E., Reinstrom, R.M., 1966. Energy requirements in the production of hydrogen from water. I&EC Process Design and Development 5(3):336-342.

69. Shinnar, R., Shapira, D., Zakai, S., 1981. Thermochemical and hybrid cycles for hydrogen production. A differential economic comparison with electrolysis. I&EC Process Design and Development 20(4):581-593.

70. Funk, J.E., 2001. Thermochemical hydrogen production: past and present. International Journal of Hydrogen Energy 26(3):185:190.

71. Steinfeld, A., 2005. Solar thermochemical production of hydrogen - a review. Solar Energy 78(5):603-615

72. Lédé, J., Lapicque, F., Villermaux, J., Cales, B., Ounalli, A., Baumard, J.F., Anthony, A.M., 1982. Production of hydrogen by direct thermal decomposition of water: preliminary investigations. International Journal of Hydrogen Energy 7(12):939-950.

73. Kogan, A., 1998. Direct solar thermal splitting of water and on-site separation of the products - II. Experimental feasibility study. International Journal of Hydrogen Energy 23(9):89-98.

74. Abraham, B.M., Schreiner, F., 1974. General principles underlying chemical cycles which thermally decompose water into elements. I&EC Fundamentals 13(4):305-310.

75. Roeb, M., Neises, M., Säck, J.P., Rietbrock, P., Monnerie, N.; Dersch, J., Schmitz, S., Sattler, C., 2009. Operational strategy of a two-step thermochemical process for solar hydrogen production. International Journal of Hydrogen Energy 34(10):4537-4545.

76. Schunk, L.O., Lipinski, W., Steinfeld, A., 2009. Heat transfer model of a solar receiver-reactor for the thermal dissociation of ZnO – Experimental validation at 10 kW and scale-up to 1 MW. Chemical Engineering Journal 150(2-3):502-508.

77. Glandt, E.D., Myers, A.L., 1976. Hydrogen production from water by means of chemical cycles. I&EC Process Design and Development 15(1):100-108.

78. Russel, J.L., Porter, J.T., 1975. A search for thermochemical water-splitting cycles. Verziroglu, T.N., Hydrogen Energy, 517-529, Plenum

79. Chao, R.E., 1974. Thermochemical water decomposition processes. I&EC Product Research Development 13(2):94-101.

80. Ota K., Conger, W.L., 1977. Thermochemical hydrogen production via a cycle using barium and sulfur: reaction between barium sulfide and water. International Journal of Hydrogen Energy 2(2):101:106.

81. Soliman, M.A., Conger, W.L., Carty, R.H., Funk, J.E., Cox, K.E., 1976. Hydrogen production via thermochemical cycles based on sulfur chemistry. International Journal of Hydrogen Energy 1(3):265-270.

82. Mason, C.F.m 1977. The reduction of hydrogen bromide using transition metal compounds. International Journal of hydrogen energy 1(4):427-434.

83. Schulten, R.m Knoche, K.F., Erzeugung von Wasserstoff und Sauerstoff aus Wasser mit Hilfe von Wärme. German Patent #2 257 103, December, the 26th, 1974

84. Yoshida, K., Kameyama, H., Toguchi, K., 1975. Proceeding of the U.S. Japan Joint Seminar Publication Office Ohta's Laboratory Yokohama National University, Tokyo, 20–23 June

85. Kameyama, H., Yoshida, K., Kunii, D., 1976. A method for screening possible thermochemical decomposition processes for water using deltaG-T diagrams. The Chemical Engineering Journal 11(3):223-229.

86. Besenbruch, G. 1982. General Atomic sulfur iodine thermochemical water-splitting process. Proceedings of the American Chemical Society, Div. Pet. Chem., 27(1):48-53.

87. Sheffe, Jonathan; Jianhua Li; Alan W. Weimer (2010). "A spinel ferrite/hercynite water-splitting redox cycle". International Journal of Hydrogen Energy **35** (8): 3333–3340. doi:10.1016/j.ijhydene.2010.01.140.

88. Rosen, M.A., Naterer, G.F., Sadhankar, R., Suppiah, S., "Nuclear-Based Hydrogen Production with a Thermochemical Copper-Chlorine Cycle and Supercritical Water Reactor", Canadian Hydrogen Association Workshop, Quebec, October 19 – 20, 2006. (PDF).

89. Lewis, M. and Masin, J., "An Assessment of the Efficiency of the Hybrid Copper-Chloride Thermochemical Cycle", Argonne National Laboratory, University of Chicago, 2 November 2005. (PDF).

90. Naterer, G. F.; et al. (2009). "Recent Canadian Advances in Nuclear-Based Hydrogen Production and the Thermochemical Cu-Cl Cycle". International Journal of Hydrogen Energy **34** (7): 2901–2917.doi:10.1016/j.ijhydene.2009.01.090.

91. Dokiya, M.; Kotera, Y. (1976). "Hybrid Cycle with Electrolysis Using Cu-Cl System". International Journal of Hydrogen Energy **1** (2): 117–121. doi:10.1016/0360-3199(76)90064-1.

92. Chukwu, C., Naterer, G. F., Rosen, M. A., "Process Simulation of Nuclear-Produced Hydrogen with a Cu-Cl Cycle", 29th Conference of the Canadian Nuclear Society, Toronto, Ontario, Canada, June 1–4, 2008.

93. Hydrogen Website of UOIT (University of Ontario Institute of Technology)

94. Lee E. Brecher and Christopher K. Wu, “Electrolytic decomposition of water”, Westinghouse Electric Corp., Patent 3,888,750, June 10, 1975.

95. Maximilian B. Gorensek & William A. Summers. Hybrid Sulfur flow sheets using PEM electrolysis and a bayonet decomposition reactor. International Journal of Hydrogen Energy. 2008;34(9):4097–4114. doi:10.1016/j.ijhydene.2008.06.049.

96. Maximilian B. Gorensek, John A. Staser, Thomas G. Stanford & John W. Weidner. A thermodynamic analysis of the SO_2/H_2SO_4 system in SO_2-depolarized

electrolysis. International Journal of Hydrogen Energy. 2009; 34(15):6089–6095.doi:10.1016/j.ijhydene.2009.06.020.

97. Sakurai M., Bilgen E., Tsutsumi A., Yoshida K., Adiabatic UT-3 Thermochemical process for hydrogen production, International Journal of Hydrogen Energy, Vol. 21, No. 10, 865-870, 1996.

98. L.C. Brown, G.E. Besenbruck, K.R. Schultz, S.K. Showalter, A.C. Marshall, P S. Pickard, and J.F. Funk, High efficiency generation of Hydrogen fuels using thermochemical cycles and nuclear power, GA-A24326, March 2002.

99. Sakurai M., Bilgen E., Tsutsumi A., Yoshida K., Solar UT-3 thermochemical cycle for hydrogen production, Solar Energy, 57,No. 1, 51-58, 1996.

100. Kameyama H., and K. Yoshida K., Reactor design for the UT-3 thermochemical hydrogen production process, International Journal of Hydrogen Energy, 1981, 6, (6), Pages 567-575.

101. Kameyama H, TominoY, Sato T, Amir R, Orihara A, Aihara M, and Yoshida K, Process simulation of “mascot” plant using the UT-3 thermochemical cycle for hydrogen production, International Journal of Hydrogen Energy, Vol 14, N°5, 1989.

102. Aihara M, Umida H, Tsutsumi A, Yoshida K. Kinetic study of UT-3 thermochemical hydrogen production process. International Journal of Hydrogen Energy 1990;15(1):7–11.

103. Lemort F., Lafon C., Dedryvère R., Gonbeau D., Physicochemical and thermodynamic investigation of the UT-3 hydrogen production cycle: A new technological assessment, International Journal of Hydrogen Energy, 31, (2006), Pages 906-918.

104. Tadokoro Y., Kajiyama T., Yamaguchi T., Sakai N., Kameyama H., Yoshida K., Technical evaluation of UT-3 thermochemical hydrogen production process for an

industrial scale plant, International Journal of Hydrogen Energy, 1997, vol 22, n°1, Pages 49-56.

105. Man Su Lee, Yogi Goswami D., Stefanakos Elias. K. Immobilization of calcium oxide solid reactant on an yttria fabric and thermodynamic analysis of UT-3 thermochemical hydrogen production cycle, International Journal of Hydrogen Energy, (2008), Pages 1-8.

106. Morooka, S., Kim, S.S. , Yan, S. , Kusakabe, K., Watanabe, M., Separation of hydrogen from an H2-H2O-HBr system with an SiO2 membrane formed in macropores of an a-alumina support tube. International Journal of Hydrogen Energy 1996, 21, (3), 183-188.

107. Ohya, H., Nakajima, H., Togami, N., Ohashi, H., Aihara, M., Tanisho, S., Negishi Y., Hydrogen purification using zirconia-silica composite membranes for thermochemical process. International Journal of Hydrogen Energy 1997, 22, (5), 509-515.

108. Teo E.D., B. N. P., Vos E., Kramer G.J., A critical pathway energy efficiency analysis of the thermochemical UT-3 cycle. International Journal of Hydrogen Energy 2005, 30, (5), 55

109. Besenbruch, G. 1982. General Atomic sulfur iodine thermochemical water-splitting process. Proceedings of the American Chemical Society, Div. Pet. Chem., 27(1):48-53.

110. Paul M. Mathias and Lloyd C. Brown "Thermodynamics of the Sulfur-Iodine Cycle for Thermochemical Hydrogen Production", presented at the 68 th Annual Meeting of the Society of Chemical Engineers, Japan 23 March 2003. (PDF).

111. Atsuhiko TERADA; Jin IWATSUKI, Shuichi ISHIKURA, Hiroki NOGUCHI, Shinji KUBO, Hiroyuki OKUDA, Seiji KASAHARA, Nobuyuki TANAKA, Hiroyuki

OTA, Kaoru ONUKI and Ryutaro HINO, "Development of Hydrogen Production Technology by Thermochemical Water Splitting IS Process Pilot Test Plan", Journal of Nuclear Science and Technology, Vol.44, No.3, p. 477–482 (2007).(PDF).

112. Paul Pickard, Sulfur-Iodine Thermochemical Cycle 2005 DOE Hydrogen Program Review

113. Wonga, B.; Buckingham, R. T.; Brown, L. C.; Russ, B. E.; Besenbruch, G. E.; Kaiparambil, A.; Santhanakrishnan, R.; Roy, Ajit (2007). "Construction materials development in sulfur–iodine thermochemical water-splitting process for hydrogen production". International Journal of Hydrogen Energy **32** (4): 497–504. doi:10.1016/j.ijhydene.2006.06.058.

114. T. Drake, B. E. Russ, L. Brown, G. Besenbruch, "Tantalum Applications For Use In Scale Sulfur-Iodine Experiments", AIChE 2007 Fall Annual Meeting, 566a.

115. Dokiya M., Kameyama T., Fukuda K. Thermochemical hydrogen preparation-Part V. A feasibility study of the Sulfur-Iodine cycle [1-4]. International Journal of Hydrogen Energy 1979; Vol 4, 267-277.

116. O'Keefe D., Allen C., Besenbruch G., Brown L., Norman J., sharp R., McCorkle K. Preliminary results from bench-scale testing of a sulfur-iodine thermochemical Water- Splitting cycle. International Journal of Hydrogen Energy 1982; Vol 7, No. 5, 381-392.

117. Norman J. H., Mysels K. J., Sharp R., Williamson D. Studies of the Sulfur-Iodine thermochemical water –splitting cycle. International Journal of Hydrogen Energy 1982; Vol 7, No. 7, 545-556.

118. Ilie Fishtik, Ravindra Datta. Systematic generation of thermochemical cycles for water splitting. Computers and Chemical Engineering 2008; 32: 1625-1634.

119. Rahul R Bhosale, Rajesh V Shende, Jan A Puszynski. Thermochemical water-splitting for H_2 generation using sol-gel derived Mn-ferrite in a packed bed reactor. International Journal of Hydrogen Energy 2012; 37: 2924-2934.
120. Xinxin Wu, Kaoru Onuki. Thermochemical Water Splitting for Hydrogen Production Utilizing Nuclear Heat from an HTGR. Tsinghua Science & Technology 2005; 10: 270-276.
121. Charles W Forsberg. Hydrogen, nuclear energy, and the advance high-temperature reactor. International Journal of Hydrogen Energy 2003; 28: 1073-1081.
122. Herranz L E, Linares J I, Moratilla B Y. Power cycle assessment of nuclear high temperature gas-cooled reactors. Applied Thermal Engineering 2009; 29: 1759-1765.
123. Rachael Elder, Ray Allen. Nuclear heat for hydrogen production: Coupling a very high temperature reactor to a hydrogen production plant. Progress in Nuclear Energy 2009; 51: 500-525.
124. IS process for thermochemical hydrogen production. JAERI-Review 94-006.
125. Leybros J, Carles P, Jean-Marc Borgard. Countercurrent reactor design and flowsheet for sulfur-iodine thermochemical water splitting process. International Journal of Hydrogen Energy 2009; 34, 9060-9075.
126. Patrice Charvin, Abanades Stephane, Lemort Florent, Flamaqnt Gilles. Analysis of solar chemical processes for hydrogen production form water splitting thermochemical cycles. Energy Conversion and Management 2008; 49: 1547-1556.
127. Xavier Vitart, Philippe Carles, Pascal Anzieu. A general survey of the potential and the main issues associated with the sulfur-iodine thermochemical cycle for hydrogen production using nuclear heat. Progress in Nuclear Energy 2008; 50: 402-410.

128. Zhang P, Chen S Z., Wang L J., Yao T Y, Xu J M. Study on a lab-scale hydrogen production by closed cycle thermo-chemical iodine sulfur process. International Journal of Hydrogen Energy 2010; 35: 10166-10172.

129. Seiji Kasahara, Shinji Kubo, Ryutaro Hino, Kaoru Onuki, Mikihiro Nomura, Shin-inchi Nakao. Flowsheet study of the thermochemical water-splitting iodine-sulfur process for effective hydrogen production. International Journal of Hydrogen Energy 2007; 32: 489-496.

130. Shinji Kubo, Hayato Nakajima, Seiji Kasahara, Syunichi Higashi, Tomoo Masaki, Hiroyoshi Abe, Kaoru Onuki. A demonstration study on a closed-cycle hydrogen production by the thermochemical water-splitting iodine-sulfur process. Nuclear Engineering and Design 2004; 233: 347-354.

131. Saeed Dehghani, Hoseyn Sayyaadi. Energy and exergetic evaluations of Bunsen section of the sulfur-iodine thermochemical hydrogen production plant. International Journal of Hydrogen Energy 2013; 38: 9074-9084.

132. Giaconia A, Caputo G, Ceroli A, Diamanti M, Barbarossa V, Tarquini P, Sau S. Experimental study of two phase separation in the Bunsen section of the sulfur-iodine thermochemical cycle. International Journal of Hydrogen Energy 2007; 32: 531-536.

133. Barbarossa V, Brutti S, Diamanti M, Sau S, De Maria G. Catalytic thermal decomposition of sulfuric acid in sulfur-iodine cycle for hydrogen production. International Journal of Hydrogen Energy 2006; 31: 883-890.

134. Banerjee A M, Pai M R, Bhattacharya K, Tripathi A K, Kamble V S, Bharadwaj S R, Kulshreshtha S K. Catalytic decomposition of sulfuric acid on mixed Cr/Fe oxide samples and its application in sulfur-iodine cycle for hydrogen production. International Journal of Hydrogen Energy 2008; 33: 319-326.

135. Cunping Huang, Ali T-Raissi. Analysis of sulfur-iodine thermochemical cycle for solar hydrogen production. Part I: decomposition of sulfuric acid. Solar Energy 2005; 78: 632-646.
136. Laijun Wang, Daocai Li, Ping Zhang, Songzhe Chen, Jingming Xu. The HI catalytic decomposition for the lab-scale H_2 producing apparatus for the iodine-sulfur thermochemical cycle. International Journal of Hydrogen Energy 2012; 37: 6415-6421.
137. Daniel M, Ginosar, Lucia M, Petkovic, Kyle C, Burch. Commercial activated carbon for the catalytic production of hydrogen via the sulfur-iodine thermochemical water splitting cycle. International Journal of Hydrogen Energy 2011; 36: 8908-8914.
138. Qiaoqiao Zhu, Yanwei Zhang, Zhi Ying, Shujie Wang, Zhihua Wang, Junhu Zhou, Kefa Cen. Kinetic and thermodynamic studies of the Bunsen reaction in the sulfur-iodine thermochemical process. International Journal of Hydrogen Energy 2013; 38: 8617-8624.
139. Mohamed Kamel Hadj-Kali, Vincent Gerbaud, Patrick Lovera, Olivier Baudouin, Pascal Floquet, Xavier Joulia, Jean-Marc Borgard, Philippe Carles. Bunsen section thermodynamic model for hydrogen production by the sulfur-iodine cycle. International Journal of Hydrogen Energy 2009; 34: 6625-6635.

140. Lee BJ, No HC, Yoon Hj, Kim SJ, Kim ES. An optimal operating window for the Bunsen process in the I-S thermochemical cycle. International Journal of Hydrogen Energy 2008; 33:2200-10.
141. Colete-Maatouk s, Brijou-Mokrani N, Tabarant M, Fleche JL, Carles P. Study of the miscibility gap in H_2SO_4/HI/ I_2 / H_2o mixtures produces by the Bunsen reaction –part I : preliminary results at 308 K. International Journal of Hydrogen Energy 2009;37:7155-61.

142. Guo H, Zhang P, Lan S, Chen s, Wan L, Xu J. Study on the phase separation characteristics of HI_-I_2 - $H_2SO_{4-}H_2O$ mixtures at 20^0 C. Fluid Phase Equilibria 2012;324:33-40.

143. Sakurai M, Nakajima H, Onuki K, Shimizu S. Investigation of 2 liquid phase separation characteristics on the Iodine-Sulfur thermochemical hydrogen production process. International Journal of Hydrogen Energy 2000; 25:605-11.

144. Zhu QQ Zhang YW, Zhou C, Wang ZH, Zhou JH, Cen KF, Optimization of liquid – liquid phase separation characterstics in the Bunsen section of the sulfur – iodine hydrogen production process International Journal of Hydrogen Energy 2012;37:6407-14.

145. Hadj-Kali MK, Gerbaud V, Lovera P, Baudouin O, Floquet P, Joulia X, et al. Bunsen section thermodynamic model for hydrogen production by the sulfur-iodine cycle. International Journal of Hydrogen Energy 2009; 34:6625-35.

146. Sau S, Giaconia A, Caputo G, Prosini PP. Decrease the rate of recycling agents in the sulfur-iodine cycle by solid phase separation. International Journal of Hydrogen Energy 2008; 33:6439-44

147. Giaconia A, Caputo G, Sau S, Prosini PP, Pozio A, De Francesco M, et al. Survey of Bunsen reaction routes to improve the sulfur-iodine thermochemical water-splitting cycle. International Journal of Hydrogen Energy 2009; 34:4041-8.

148. Sakurai M, Nakajima H, Amir R, Onuki K, Shimizu S. Experimental study on side-reaction occurance condition in the iodine-sulfur thermochemical hydrogen production process. International Journal of Hydrogen Energy 2000; 25:613-619.

149. Nomura Nakao SI, Okuda H, Fujiwara S, Kasahara S, Ikenoya K, et al. Development of an electrochemical cell for efficient hydrogen production through the IS process. AICHE J 2004; 50;1991-8.

150. Nomura M, Fujiwara S, Ikenoya K, Kasahara S, Nkajima H, Kubo S, et al. Application of an electrochemical membrane reactor to the thermojchemical water splitting IS process for hydrogen production Journal of Membrane Science 2004;240:221-226.

151. V. Immanuel, K. U. Gokul, Anupam Shukla. Membrane electrolysis of Bunsen reaction in the iodine-sulfur process for hydrogen production. International Journal of Hydrogen Energy 2012; 37: 3595-3601.

152. Zhi Ying, Yanwei Zhang, Qiaoqiao Zhu, Pingan Peng, Zhihua Wang, Junhu Zhou, Jianzhong Liu, Kefa Cen. Electro chemical investigation of the Bunsen reaction in the sulfur-iodine cycle. International Journal of Hydrogen Energy 2013; 38: 1-11.

153. Leybros J, T. Gilardi, Saturnin A., Mansilla C., Carles P. Plant sizing and evaluation of hydrogen production costs from advanced processes coupled to a nuclear heat source. Part I: Sulfur-iodine cycle. International Journal of Hydrogen Energy 2010; 35, 1008-1018.

154. Hyo Sub Kim, Young Ho Kim, Sang Jin Han, Chu Sik Park, Ki Kwang Bae, Jong Gyu Lee. Continuous Bunsen reaction and simultaneous separation using a counter-current flow reactor for the sulfur-iodine hydrogen production process. International Journal of Hydrogen Energy 2010; 35, 1008-1018.

155. Young-Ho Kim, Hyo-Sub Kim, Sang-Jin Han, Chu-Sik Park, Ki-Kwang Bae and Jong-Gyu Lee. Bunsen Reaction using a counter-current flow reactor in Sulfur-Iodine hydrogen production process: Effects of reactor shape and temperature. Advanced Materials Research Vols, 347-353 (2012) pp 3238-3241

156. C. S. R. Prasad, H. Z. Fani, S. B. Menon, “Heterogeneous Bunsen reaction analysis & experimental study of chemical absorption of sulfur dioxide and dissolution of iodine into aqueous reacting system”. IAEA-CN-152-18 (2007) held in Japan.

157. Rober C. Moore ‘Design options for a Bunsen reactor’ Sandia Report, SAND2012-9318.

158. Jayong Hur, J.P. O’Connell, Ki-Kwang Bae, Kyung-Soo Kang, Jeong Won Kang. Measurements and correlation of solid-liquid equilibria of the HI + I_2 + H_2O system. International Journal of Hydrogen Energy 2011; 36: 8187-8191

159. Satish J, Parulekar, Nor Aishah Saidina Amin. Gas-liquid reactions in well-mixed reactors- A fresh perspective. Chemical Engineering Science 1996; 51: 4561-4577.

160. Benoit Haut, Veronique Halloin. Mass transfer in gas-liquid contactors: a new technique for the numerical solution of the film equations. Chemical Engineering and Processing: Process Intensification 2004; 43: 1339-1346.

161. Oinas P, Wild G, Midoux N, Haario H. Identification of mass-transfer parameters in cases of simultaneous gas absorption and chemical reaction. Chemical Engineering and Processing: Process Intensification 1995; 34: 503-513.

162. Levenspiel O. Chemical Reaction Engineering (third edition). Wiley India (P) Ltd 2010.

163. Minye Liu. Age distribution and the degree of mixing in continuous flow stirred tank reactors. Chemical Engineering Science 2012; 69: 382-393.

164. Fogler H. S. Elements of Chemical Reaction Engineering (Fourth edition). PHI Learning (P) Ltd. 2010.

165. Sujeesh S. “Study of Bunsen reaction at elevated temperature and high pressure” M. Tech. Thesis, HBNI, Mumbai, India, August 2013

166. Coats, J., and Pressburg, B. S. Heat transfer to moving fluids. Chem. Eng., 1959: pp. 67-72.

167. Kern, D. Q., “Process heat transfer” McGraw-Hill, New York, 1950: pp 103, 137, 549, 721, 834.

168. Dostal, M., Petera, K., Rieger, F. Measurement of heat transfer coefficients in an agitated vessel with tube baffles. ACTA POLYTECHNICA 2010; Vol. 50, No. 2.
169. Vincenzo Barbarossa et al., Chemically Enhanced Separation of H_2SO_4/HI mixtures from the Bunsen Reaction in the Sulfur-Iodine Thermochemical Cycle., Ind. Eng. Chem. Res. 2009, 48, 9040-9044.
170. R. H. Elder, G. H. Priestman, B. C. Ewan and R. W.K. Allen .The separation of HIx in the sulphur-iodine thermo chemical cycle for sustainable Hydrogen Production. Institution of Chemical Engineers, Trans IchemE Part B, July 2005
171. Sonia Colette Maatouk et al., Study of the miscibility gap in H_2SO_4/HI/I_2/H_2O mixtures produced by the Bunsen reaction – Part I: Preliminary results at 308 K, International Journal of Hydrogen Energy, 2009, 34 (17), 7155-7161.
172. Perry R.H. and Green D. W., “Chemical Engineers Handbook” 8th Edition, McGraw-Hill (1997).
173. Van Dierendonck, L. L. Vegrotingregels voor gasbelwassers, Ph. D Thesis, Twente University, Netherlands (1970).
174. Edwards, T. J., G. Maurer, J. Newman and J. M. Prausnitz, “Vapor-Liquid Equilibria in Multicomponent Aqueous Solutions of Volatile Weak Electrolytes”, AIChE Journal, 24 (1978).
175. Calderbank P. H., “The chemical engineer”, No. 212, CE209 (1967).